Single-Molecule Insights into PcrA-Driven Disruption of RecA Filaments

by

Matthew Vincent Fagerburg

B.S., B.A. University of Pittsburgh, 2003

Submitted to the Graduate Faculty of

School of Medicine in partial fulfillment

of the requirements for the degree of

Doctor of Philosophy

University of Pittsburgh

2011

UNIVERSITY OF PITTSBURGH

School of Medicine

This dissertation was presented

by

Matthew V. Fagerburg

It was defended on

December 9, 2011

and approved by

Patricia Opresko, Assistant Professor, Department of Environmental and Occupational Health

Richard Steinman, Associate Professor, Department of Medicine

Bennett Van Houten, Professor, Department of Pharmacology and Chemical Biology

Dissertation Advisor: Sanford H. Leuba, Associate Professor, Department of Cell Biology

Single-Molecule Insights into PcrA-Driven Disruption of RecA Filaments

Matthew V. Fagerburg, PhD

University of Pittsburgh, 2011

Homologous recombination (HR) plays a critical role in many important cellular processes, including the resolution of stalled replication forks. HR must be highly regulated within the cell because aberrant recombination can introduce gene deletions as well as structural barriers to genetic replication and repair; various families of proteins have evolved in different organisms to achieve this regulation.

The bacterial DNA-binding protein RecA is one such prototypical agent that promotes HR. It forms helical nucleoprotein filaments on single-stranded DNA (ssDNA) that act as HR loci. The assembly and disassembly of RecA filaments are dynamic, and depend on the ATPase cycle of the protein. Both processes are subject to modulation and regulation by other factors. RecA filaments can be actively removed from DNA by non-replicative helicases such as PcrA (present in Gram-positive bacteria such as *Staphylococcus aureus* and *Streptococcus pneumoniae*) and UvrD (present in Gram-negative bacteria such as *Escherichia coli* and *Pseudomonas aeruginosa*), and deletion of either of these leads to dysregulation of HR, which suggests that they play an important role in regulating HR via the removal of RecA filaments. We used single-molecule FRET (smFRET) to further investigate this removal and discovered that the ATPase activity of RecA is required for it to occur. The exquisite sensitivity of the single molecule technique allowed us to observe individual, short RecA filaments on ssDNA, as well as how PcrA disrupts them.

The work described in this dissertation highlights a novel mechanistic component in the regulation of RecA, namely the crucial role that its ATPase activity plays in filament removal by PcrA.

...the soul at dawn is like darkened water that slowly
begins to say Thank you, thank you…

-Rumi

ACKNOWLEDGEMENTS

The work described here could not have been done without the help and support of many people to whom I am deeply grateful. I would first like to thank my advisor Dr. Sanford Leuba, who accepted me into his lab and granted me the freedom to explore the projects I was most interested in. My experiences in the Leuba lab have shaped my thinking about Science from the nano-scale to the national policy level, while also providing me an opportunity to reflect upon and develop my habits connecting thought and action. Thank you, Sanford for giving me such an opportunity!

I would also like to thank the members of my thesis committee, each of whom has given me guidance, scientific and otherwise, and each of whom has helped me to better understand what it means to be a Scientist.

Gratitude is due to the many colleagues and friends made in various labs, universities, and countries that I have had the privilege to work with. I have come to understand that the most profound aspect of research is the social nature of the endeavor, and the power it has to draw people together in a common pursuit. It invites us all to share in the awe of our world, and the connections of understanding it fosters are paralleled by the bonds of friendship it builds.

I want to specifically thank my friend and lab mate Grant Schauer for his good ideas, conversation, scientific criticism, taste in music, and above all good company as we sat together in the endless darkness searching for tiny points of light. Thank you Sir, may you always be able to find a sound stock of green chiles, no matter where you are. I also offer my heartfelt thanks to my research partner Dr. Syam Anand, who is a true inspiration and friend. Without his collaboration and guidance, this journey could not have been made. I lift my glass to you, Sir!

Finally, I would like to offer my deepest thanks to my family of Fagerburgs and Friedrichses, for their unwavering love and support throughout the years. I am thankful to bursting for having such a wonderful family in my life. And to my wife jes and son indy, thank you endlessly for your love and patience; I dedicate the best parts of this work to you.

TABLE OF CONTENTS

LIST OF TABLES

LIST OF FIGURES

All figures were composed by the author; in cases where the content of a figure was adapted from a published source, this source has been cited.

ABBREVIATIONS

ALEX	Alternating laser excitation
APD	Avalanche photodiode
ADP	Adenosine diphosphate
ATP	Adenosine triphosphate
ATPγS	Adenosine 5′-O-(3-thio)triphosphate
CCD	Charge-coupled device
DSB	dsDNA break
dsDNA	double-stranded DNA
EMCCD	Electron-multiplying CCD
FOV	Field of view
FRET	Förster resonant energy transfer
G4	G-quadruplex DNA
HJ	Holliday junction
HR	Homologous recombination
PcrA	Plasmid copy reduced protein
PIFE	Protein induced fluorescence enhancement
Rad51	Radiation-resistance protein
RecA	Recombination protein A

RecBCD	Complex of recombination proteins RecB, RecC, RecD
RecFOR	Complex of recombination proteins RecF, RecO, RecR
Rep	Replication protein (bacteriophage)
smFRET	Single Molecule Förster resonant energy transfer
Srs2	Suppressor of radiation sensitivity protein
ssDNA	single-stranded DNA
SSB	ssDNA binding protein
TIRF	Total internal reflection fluorescence
UvrD	UV-resistance ‘D’ protein

1.0 INTRODUCTION

1.1 BACTERIAL RECOMBINATION

Homologous recombination (HR) is a process by which stretches of DNA that are similar, though not necessarily identical in sequence, are exchanged within a genome (Kowalczykowski et al. 1994). Mechanisms and molecular machineries that support this process are conserved across all kingdoms of life, as well as viruses (Kowalczykowski et al., 1994). Paradoxically, HR is important for both generating genetic diversity (by enabling large-scale rearrangement, copying, and deletion of genetic sequences) and also for maintaining the genomic integrity; this latter function is achieved by HR's role in both DNA repair and replication restart pathways (Lusetti and Cox 2002). Evidence highlighting HR's roles *in vivo* comes from experiments showing: (1) bacterial mutants lacking HR components accumulate DNA damage, (2) HR-compromised organisms are unable to complete meiotic divisions and sexually reproduce, and (3) the development of cancers in multicellular organisms with defects in HR pathways (Opresko et al., 2003; Wu and Hickson, 2006; Bachrati and Hickson, 2008; Martinez-Perez and Colaiácovo, 2009; Yanowitz, 2010; Ayora et al., 2011).

One of the two basic models for HR was proposed by Robert Holliday in 1964 (Holliday, 1964) to explain inheritance patterns that did not conform to Mendelian rules. In Holliday's original model one of a pair of homologous DNA molecules having a single-strand nick displaces the nicked strand on the sister dsDNA molecule, giving rise to a dynamic crossover structure called a Holliday junction (HJ, Figure 1-1). It is possible for this HJ to migrate many hundreds or thousands of base pairs (Panyutin and Hsieh, 1994; Palets et al., 2010) before another set of single stranded nicks terminates the process, resulting in the swap of a continuous stretch of genetic sequence (Figure 1-1: Holliday model for HR featuring a HJ intermediate.). *In vivo*, such a swap may be permanently incorporated into the organism's genome through the

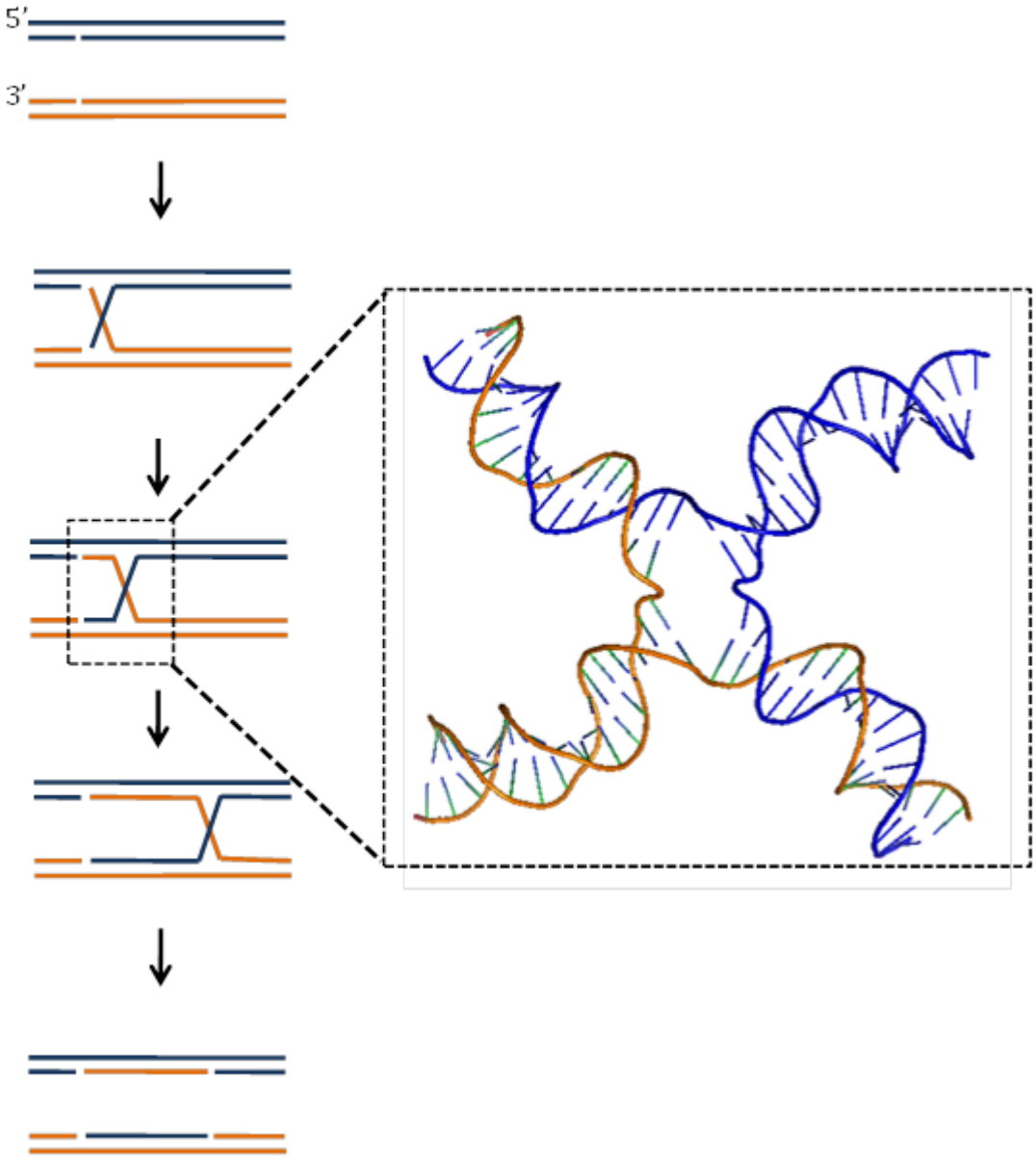

Figure 1-1: Holliday model for HR featuring a HJ intermediate.

Robert Holliday's proposed model for HR begins with two homologous dsDNA molecules: one with a nick in its 5' strand, and the other with a nick in its 3' strand. These nicks allow each ssDNA strand to cross-over and invade the opposite dsDNA, displacing the original (homologous) template strand and creating a mobile HJ structure (shown in box; PDB 3CRX (Gopaul et al., 1998). This HJ can migrate along the dsDNA substrates, causing further strand

displacement in the dsDNAs. Ultimately, the HJ is resolved, resulting in the exchange of homologous sequence (figure based on (Kowalczykowski et al., 1994)).

actions of the cellular genetic repair machinery (West, 1997).

It is useful to consider the process of HR to be divided into four discrete steps: initiation, homologous pairing/strand exchange, heteroduplex extension, and resolution (Kowalczykowski et al., 1994; Heyer, 2007). The phases of homology search and exchange of DNA strands during the recombination reaction are reconstituted in vitro by adding RecA or Rad51 to DNA substrates that harbor sequence homology and following the physical swapping of one of strands from one substrate for its complementary strand derived from another substrate molecule (Kowalczykowski et al., 1994). *In vitro* DNA strand exchange reactions mediated by RecA have been helpful in identifying the biochemical activities of RecA that are essential for supporting this reaction and also for investigating the regulation of the strand exchange activity of RecA by other proteins (Cox and Lehman, 1981; DasGupta et al., 1981; Lindsley and Cox, 1990; Rosselli and Stasiak, 1991; Kim et al., 1992; Kowalczykowski and Krupp, 1995; Veaute et al., 2005; Anand et al., 2007; Cox, 2007b; Singh et al., 2010). For example, it has been shown that helicases such as PcrA and UvrD can inhibit DNA strand exchange mediated by RecA *in vitro* (Veaute et al., 2005; Anand et al., 2007; Park et al., 2010; Singh et al., 2010).

1.1.1 Rescue of Stalled Bacterial Replication Forks via Double Strand Break Repair

From the earliest experiments leading to the discovery of RecA, it has been clear that recombination machinery plays a role in resistance to UV DNA damage (Clark and Margulies 1965). Further research in the past decades has demonstrated that one of the major cellular functions of homologous recombination is to support replication restart (Lusetti and Cox, 2002). The process of DNA replication is complex; it is coordinated by many different proteins that assemble a replisome at a dynamic structure called a replication fork (Figure 1-2), (Benkovic et

al., 2001). In bacteria, replicative helicases like DnaB unwind dsDNA at the forefront of the fork, allowing subsequent copying of the exposed ssDNA by polymerases. However, replication forks cannot progress uninterrupted through DNA lesions, resulting in a relatively high proportion of forks (10-20%) that are halted at some point (Lusetti and Cox, 2002). When such a stoppage occurs, it is the process of HR that rescues the stalled fork by assisting in the repair of the damage and allowing replication to resume (Lusetti and Cox, 2002).

Although the exact repair pathway that is followed depends on the nature of the DNA damage, in all cases the stalled fork must move through the four stages of HR in order to be rescued. For the sake of simplicity, the rescue of a fork in which a dsDNA break (DSB) is generated will be considered here (Figure 1-3). DSBs are generated by incident UV-radiation or attack by chemical radicals (Lusetti and Cox, 2002) and must be repaired if the cell is to remain viable. Such a scenario can result from a ssDNA nick in either the leading or lagging strand of the template DNA (Figure 1-3).

The HR repair of a DSB begins with the initiation stage, where the terminated fragment of the DSB is selectively degraded to produce a ssDNA overhang primed for homologous paring with a sister dsDNA molecule (Figure 1-3) (Lusetti and Cox, 2002). Thus prepared, strand exchange begins as the ssDNA undertakes a search for homologous dsDNA sequence and initiates a strand invasion once a suitable target is discovered. As the invading ssDNA displaces more and more sequence within the duplex, a Holliday junction is created; the migration of this HJ extends the heteroduplex regions in each dsDNA. At some point, the HJ is resolved, and the HR process reaches its conclusion. At this point a replication fork can be restarted, as the initial DNA lesion has been resolved.

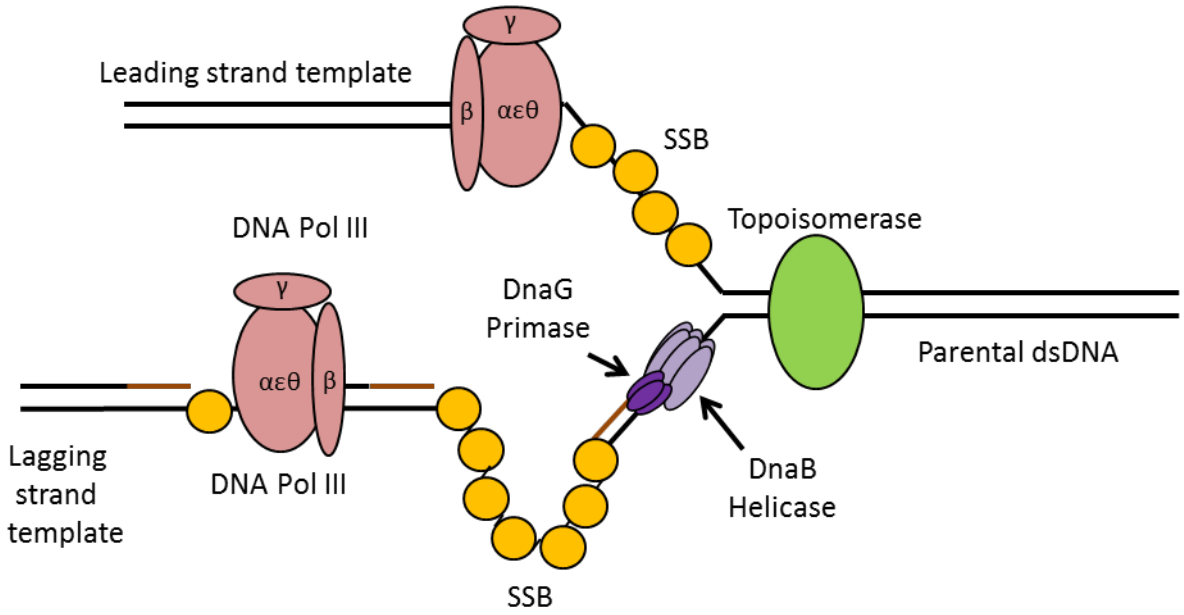

Figure 1-2: A simplified model replication fork.

The bacterial replication fork is a complicated and dynamic structure involving the coordination of many different protein machineries. Shown here is a simplified model fork showcasing some of the key proteins required for DNA replication (figure based on (Johnson and O'Donnell, 2005)). Topoisomerases ahead of the fork relieve torsional stress produced by the helicases responsible for unwinding the dsDNA at the fork. As the dsDNA is unwound for replication, the resulting ssDNA templates are protected by SSB protein until they are copied by DNA Pol III complexes. Not shown are the many additional proteins that play a role in assembling, maintaining and regulating an active replication fork.

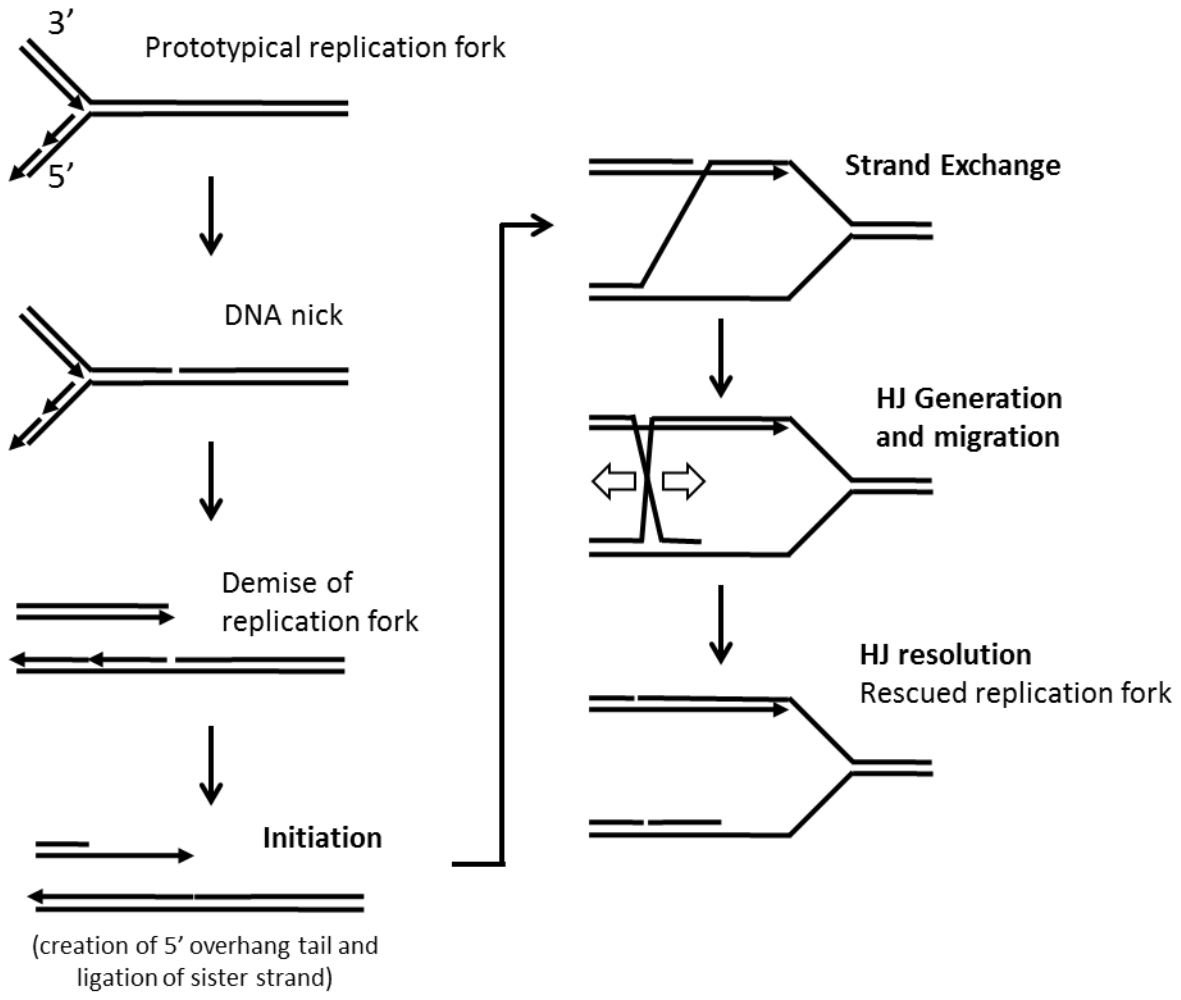

Figure 1-3: Proposed pathway for the repair of a replication fork compromised by a nick in the leading template strand.

Such a nick produces a DSB, arresting replication. The terminated DNA is processed to a 5’ ssDNA overhang which can then participate in HR via strand exchange with the sister molecule. After branch migration and resolution of the HJ, the replication fork can reassemble and continue its progress (figure based on (Lusetti and Cox, 2002)).

1.1.2 Mediators and Regulators of Bacterial Homologous Recombination

Every stage of HR is coordinated by multiple protein factors (Kowalczykowski et al., 1994); families of proteins with similar functions operate at each stage across the kingdoms of life (Table 1-1). In the bacterial (*E. coli*) system the most prominent players in HR are proteins of the Rec family (proteins isolated in screens for *rec*ombination deficiency), Ruv family (proteins isolated for screens for UV resistance), Single-stranded DNA binding protein (SSB), DNA polymerases and DNA ligases (Kowalczykowski et al., 1994). Among these proteins, members of the RecA/Rad51 family have the unique ability to search for sequence homology and physically exchange DNA strands by aligning homologous sequences within their active sites (Chen et al., 2008). The role of other proteins is to regulate the activity of RecA and complete the cascade of reactions by resolving the structures that arise from the activity of RecA. This involves various activities such as DNA unwinding (helicases), stabilization of ssDNA (SSB), nicking and closing of DNA (resolvases), synthesis of new DNA (polymerases) and sealing of nicks (ligases) (Kowalczykowski et al., 1994).

In the case of DSB repair by HR, the first task to be undertaken is the generation of a ssDNA template suitable for homologous pairing (Figure 1-3). RecBCD, a complex consisting of three proteins, possesses both helicase and nuclease activity capable of chewing up one strand from the end of the DSB; however, other proteins such as RecQ (a helicase) and RecE (a nuclease) can achieve the same result. RecA then binds and rapidly polymerizes on the ssDNA template, forming a presynaptic filament complex that is capable of rapidly and efficiently searching for sequence homology (Figure 1-4) (Kowalczykowski et al., 1994). The binding of RecA is influenced by other proteins, notably the RecFOR complex, which appears to target

Table 1-1: Comparison of some homologous recombination proteins across several species.

(adapted from (Heyer, 2007))

Stage	*E. coli*	*S. cerevisiae*	*H. sapien*
Initiation	RecBCD	-	-
	RecQ	Sgs1	RecQL, RecQ4, recQ5, BLM, WRN
	UvrD, PcrA	Srs2	Fbh1(?)
Homologous pairing and DNA strand exchange	RecA	Rad51, Dmc1	Rad51, Dmc1
	SSB	RPA	RPA
	RecF(R)	Rad55-Rad57	Xrcc3-Rad51C
	RecO(R)	Rad52	Rad52
DNA Heteroduplex extension	RuvAB	Rad54	Rad54
	RecQ	Sgs1	RecQL, RecQ4, RecQ5, BLM, WRN
Resolution	RuvC	-	Resolvase A
	RecQ-TopoIII	Sgs1-TopoIII-Rmi1	BLM-TopoIIIalpha-BLAP75

RecA binding to ssDNA [(Umezu et al., 1993; Bork et al., 2001; Morimatsu and Kowalczykowski, 2003). RecA nucleoprotein filaments drive HR and branch migration (Cox, 2007a; Rossi et al., 2011); after facilitating the initial homology search, such a filament catalyzes homologous pairing through strand exchange by hydrolyzing ATP, driving forward the stages of homologous pairing and heteroduplex extension.

Once homologous pairing has been initiated, proteins such as RecG and the RuvAB complex can act to drive the extension of the heteroduplex region by directly affecting the branch migration of the HJ. RecA also plays a role in this stage, using the energy of ATP hydrolysis to drive the strand exchange reaction forward (Kim et al., 1992; Rehrauer and Kowalczykowski, 1993; Cox, 1994; Kowalczykowski and Krupp, 1995). It has also been shown to interact with and possibly affect the dynamics of HJs (Rossi et al., 2011). HR is terminated by the scission of the migrating HJ and subsequent religation of the resulting recombination products. Nucleases such as RuvC that specifically cleave HJ substrates play a key role at this stage (Kowalczykowski et al., 1994).

There are conflicting views about the relative contributions of the branch migration activity of RecA compared to that of RuvABC, another protein complex that plays an essential role in HR (West and Connolly, 1992; Cox, 2007a; Rossi et al., 2011). However, it is clear that considering the key role played by RecA in initiating HR, regulation of RecA's activities can have dramatic effect on the progression of HR. While some proteins (*e.g.*, RecFOR) promote RecA's activity, others such as RecX, DinI and PsiB negatively modulate its ability to bind ssDNA by different mechanisms [(Drees et al., 2004; Renzette et al., 2007; Cox, 2007b; Petrova et al., 2009). RecA can also be displaced from DNA by helicases such as UvrD and PcrA (Veaute et al. 2005; Syam P Anand et al. 2007; Centore and Sandler 2007).

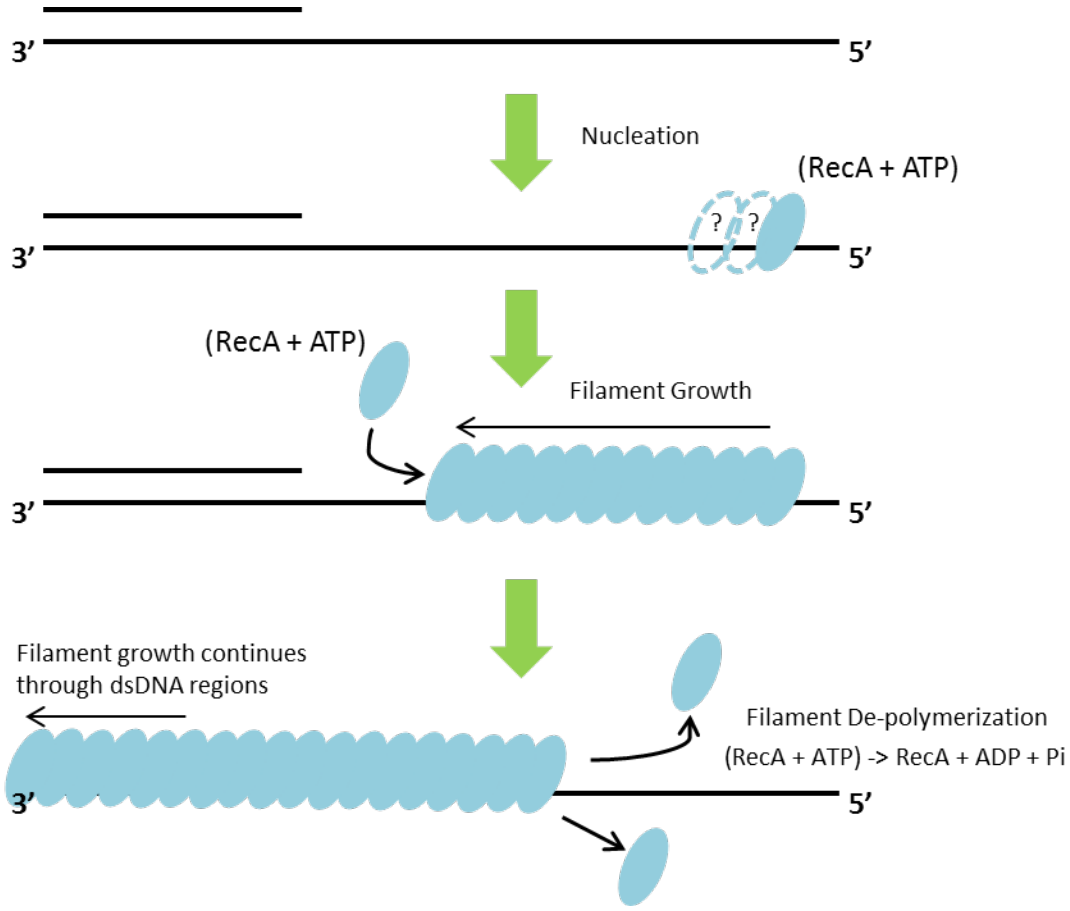

Figure 1-4: Model of RecA filament formation on duplex DNA.

After a slow nucleation step (possibly involving multiple RecA monomers), RecA filament polymerizes on DNA in a 5' -> 3' direction. Filament de-polymerization also occurs in a 5' -> 3' direction as terminal RecA monomers hydrolyze ATP (figure based on (Lusetti and Cox, 2002)).

1.1.3 Disruption of DNA-Bound Proteins and Barriers by Translocases

Translocases are motor proteins that use energy from NTP hydrolysis to track along DNA or RNA in a biased direction; helicases are effectively a subclass of translocases that also catalyze the separation of double-stranded nucleic acids (Matson et al., 1994; Lohman et al., 2008). Translocases are believed to play important roles in cellular processes, by removing barriers consisting of proteins bound to DNA/RNA and nucleic acid secondary structures like hairpins and G-quadruplex DNA (Yeruva and Raney, 2010). Such barriers are assumed to hinder processes like DNA replication and repair, transcription, and translation of mRNA (Lohman et al., 2008). In eukaryotes, where the majority of the genome is bound up in nucleosomes, many chromatin remodelers have been found to contain structural homology with translocase domains, which enables them to shift the positions of nucleosomes *in vivo* (Fyodorov and Kadonaga, 2001; Racki et al., 2009).

Although it may be naively assumed that translocases remove all such barriers by physical 'brute force' pushing, experiments suggest that a range of removal mechanisms are employed (Anand et al., 2007; Antony et al., 2009; Finkelstein et al., 2010; Singh et al., 2010; Ward et al., 2010). Interestingly, in some cases it appears that the removal of bound protein from DNA depends on species-specific protein interactions, suggesting that subtle mechanisms have been allosterically tuned by evolution for tight control (Singh et al., 2010).

Several of the components in RecA-mediated HR have been studied in terms of their ability to remove bound proteins (or to be removed themselves), revealing a diversity of removal mechanisms. Eric Green and coworkers studied the ability of RecBCD translocase to remove a variety of protein targets from DNA, and found that different models were required to explain the mechanism of barrier ejection, depending on what the barrier protein was (Finkelstein et al.,

2010). All of these studies involved barriers that were either single proteins or small complexes; an intriguing question is whether there is a limit to the amount of force that a given translocase can generate, and thus a limit on the types of barriers it could conceivably remove.

Of particular interest in this regard is the challenge involved in removing a nascent RecA filament, which may consist of many hundreds of polymerized RecA monomers bound to the DNA. It seems unlikely that a single translocase or even a serial train of translocases could generate enough force to dislodge such a formidable obstacle. One potential solution to this dilemma involves the translocase effecting a change in the target protein's DNA binding affinity, rendering it easier to displace. Studies on the eukaryotic Rad51/Srs2 suggest that the helicase Srs2 removes Rad51 filaments by stimulating their ATPase activity, which in turn destabilizes their DNA binding affinity (Antony et al., 2009).

1.2 THE RECA RECOMBINASE

RecA was identified in a screen for enzymatic components that support recombination in *E. coli* (Clark and Margulies, 1965). The basal level of RecA expression *in vivo* is estimated to be ~10k copies/cell; these levels are increased in response to DNA damage, with as many as 80k proteins estimated to be present post induction (Gudas and Pardee, 1976; Sommer et al., 1998; Cox, 2003). Further research has shown that RecA induction is a key player in a coordinated process called the SOS response that inhibits DNA synthesis and cell division until DNA damage is repaired (Witkin, 1991).

RecA is the prototypical bacterial recombinase protein, responsible for catalyzing the strand exchange activity that is the hallmark of HR (Howard-Flanders et al., 1984). RecA

homologs are present in all organisms (*e.g.*, Rad51 in yeast; (Shinohara et al., 1992)), and are also present in bacteriophages such as T4 (Table 1-1) (Kodadek et al., 1988; Beernink and Morrical, 1999). In addition to its strand exchange activity, RecA appears to have two additional functions *in vivo*: regulation of the SOS response (by promoting LexA proteolysis), as well as the mutagenic bypass of lesions during SOS (Witkin 1991; Pham et al. 2001; Gruenig et al. 2008; Long, Renzette, and Sandler 2009; Storz and Hengge-Aronis 2000).

RecA's strand exchange activity is dependent on its ability to form long, dynamic nucleoprotein filaments (Menetski et al., 1990; Rehrauer and Kowalczykowski, 1993; Kowalczykowski and Krupp, 1995). The formation and stability of these filaments are modulated by many other proteins, some of which are identified in section 1.1.2. Although much is known about the biochemical activity of RecA, there remain many unanswered questions concerning the details of its interaction with DNA and the exact role that its ATPase activity plays *in vivo* (Cox, 1994; Cox et al., 2005).

1.2.1 RecA Structure

RecA is a 37.8 kDa protein with three distinct structural domains (Figure 1-5) (Story and Steitz, 1992). It binds and hydrolyzes ATP, and the presence of DNA accelerates this activity dramatically (Menetski and Kowalczykowski, 1985; Bianco and Weinstock, 1996). A variety of RecA crystal structures have been solved containing different NTP analogs, and these exhibit significant structural variations that probably reflect active and inactive forms of the protein (Story and Steitz, 1992; Yu and Egelman, 1992; Xing and Bell, 2004). Recently, the co-crystal structure of RecA in complex with ssDNA and dsDNA substrates have been solved with high resolution giving us a unique glimpse into the unique chemical, physical and structural bases of

homology-search and strand exchange mediated by the scaffolding formed by polymers of RecA on DNA (Chen et al., 2008).

A single RecA monomer has a binding footprint of ~3 nucleotides, and filaments assemble in a 5' to 3' direction as a right-handed helix around DNA with six RecA monomers per turn (Yu et al., 2001; Chen et al., 2008). A deep groove spirals around the filament, and (in a ssDNA filament) this is where a target homologous DNA molecule is believed to bind. DNA within the filament is underwound and stretched by a factor of approximately 1.5 (Stasiak and Di Capua, 1982; Pugh et al., 1989); it has been suggested that this underwound state may facilitate homology search (Story and Steitz, 1992; Chen et al., 2008).

The core domain of RecA is the most highly conserved (Figure 1-5), and shares structural similarity with hexameric helicases and also F_1-ATPase (Story et al., 1993; Bird et al., 1998). It contains a Walker-A box motif that binds NTPs and NTP-analogs (Walker et al., 1982; Story et al., 1993). Also within this core domain are two disordered loops (L1 and L2, Figure 1-5) that have been shown to be involved in DNA binding (Malkov and Camerini-Otero, 1995).

The C-terminal domain exhibits considerably less sequence conservation across species, although it is generally rich in negatively-charged amino acids (Roca and Cox, 1997). It appears to play a distinct role in autoregulating RecA's activity *in vivo* (Lusetti and Cox, 2002). C-terminal deletion mutants have enhanced binding affinities for DNA, and are also able to more effectively compete with SSB for binding sites on ssDNA (Tateishi et al., 1992; Lusetti et al., 2003). In addition, RecA's non-recombinagenic functions are also enhanced by deletion of its C-terminal amino acids (Lusetti and Cox, 2002; Schlacher et al., 2006).

Comparatively less is known about the N-terminal domain of RecA, although there is evidence that it is involved in DNA binding (Lee and Wang, 2009). Due to its proximal location,

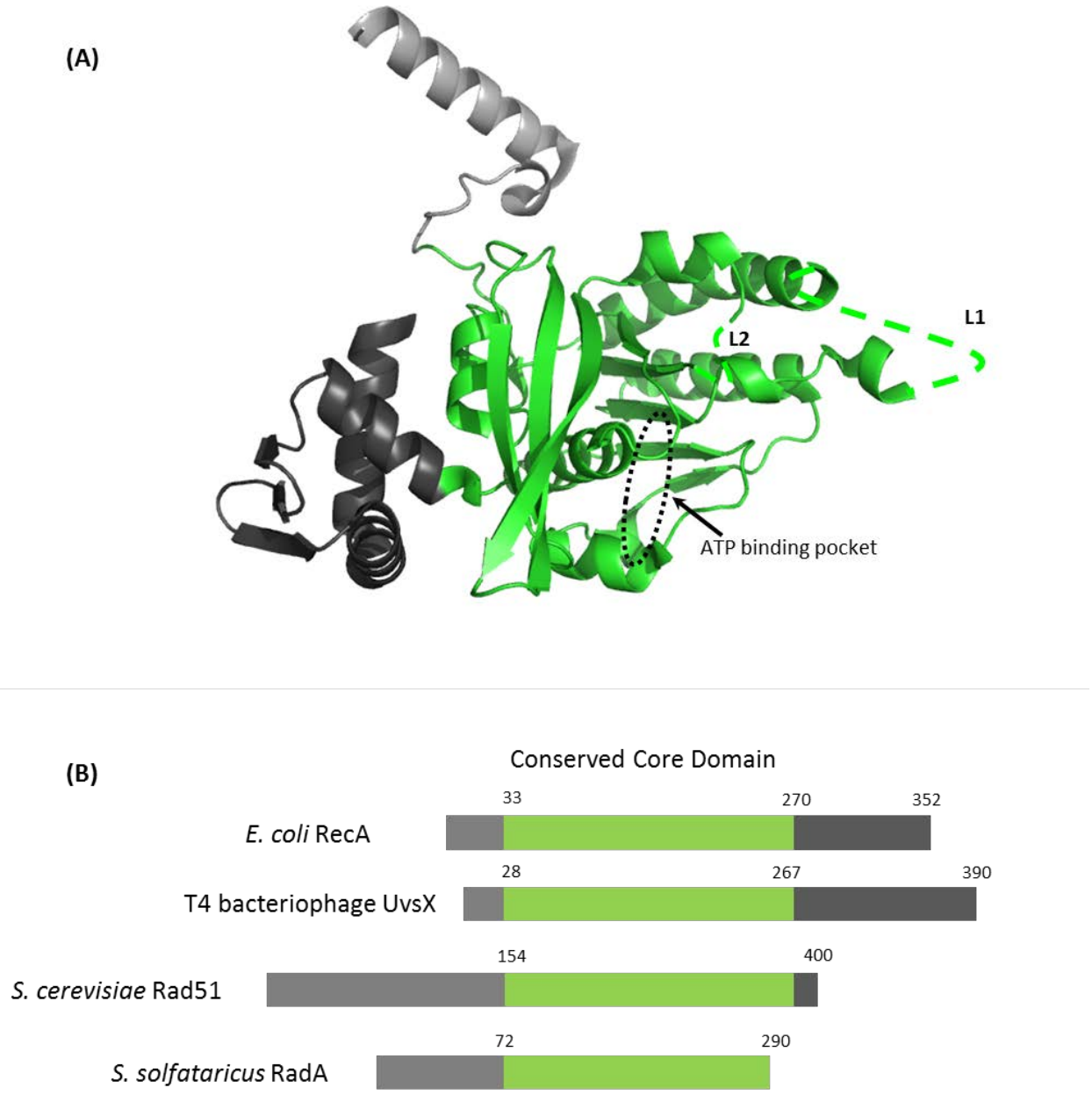

Figure 1-5: Crystal structure of *E. coli* RecA protein.

(A) *E. coli* RecA crystal structure with ATP binding pocket and DNA-binding loops L1 and L2 identified. Subsequent work has suggested that this is the conformation of the low-affinity DNA binding form of the protein. (Figure was constructed from the PDB file 2REB (Story and Steitz, 1992)). **(B)** Sequence comparisons among various RecA homologs showing highly conserved

central domain and varying lengths of both N- and C-terminal domains. (Figure based on (Lusetti and Cox, 2002)).

it is likely to be involved in monomer-monomer interactions within RecA filaments (Story and Steitz, 1992; Chen et al., 2008).

1.2.2 RecA Filaments and Activity

In order to catalyze strand exchange *in vivo*, RecA forms long nucleoprotein filaments on DNA that promote homologous sequence exchange in an ATP dependent reaction (Stasiak et al., 1981; Stasiak and Di Capua, 1982; Howard-Flanders et al., 1984). Although RecA filaments are formed on both ssDNA as well as dsDNA, initial binding occurs much faster on ssDNA (Menetski and Kowalczykowski, 1985; Kowalczykowski et al., 1987), and ssDNA filaments are likely the most important in HR (Chen et al., 2008). Once a ssDNA-RecA filament has formed, it searches out and pairs with a homologous dsDNA region and strand exchange ensues (Kowalczykowski et al., 1994). The strand exchange activity of RecA filaments is readily assayed *in vitro* using purified RecA and labeled DNA (Kowalczykowski et al., 1994).

RecA nucleofilaments are dynamic, and their assembly and disassembly are principally driven by the hydrolysis of ATP (Cox, 1994; Cox et al., 2005). RecA polymerizes on DNA primarily in the 5' -> 3' direction, and this is the same direction in which filaments disassemble (Figure 1-4) (Register and Griffith, 1985; Lindsley and Cox, 1990). Filament assembly begins with a relatively slow nucleation step, where one or a few monomers of RecA bind to DNA (Figure 1-4) (Kowalczykowski et al., 1987). Subsequent addition of RecA monomers to the filament is rapid and cooperative, and this cooperativity complicates the measurement of binding affinity values for RecA (Lusetti and Cox, 2002). There is a paucity of reported values for the rates of filament assembly, although values from recent single molecule experiments suggest a range of 2-7 monomers/s (Galletto et al., 2006; Joo et al., 2006). Filament disassembly occurs as

RecA molecules hydrolyze ATP and have been shown to be around 1 monomer/s on ssDNA (Arenson et al., 1999; Joo et al., 2006). The rates of polymerization on ssDNA and dsDNA differ as nucleation occurs more readily on ssDNA and often leads to multiple nucleation events (Joo et al., 2006). The rate of polymerization on dsDNA has been estimated to be 12 monomers/s (Shivashankar et al., 1999).

The overall stability of RecA filaments depends on the binding affinity of the RecA monomers for DNA, and this affinity is in turn affected by the state of RecA ATP hydrolysis within the protein (Menetski and Kowalczykowski, 1985). RecA with bound ATP has a significantly higher binding affinity for DNA than RecA with bound ADP; this suggests that the ATPase activity of RecA plays a central role in destabilizing filaments. When RecA binds the negligibly-hydrolyzed analog ATPγS, filament stability is dramatically enhanced (Menetski and Kowalczykowski, 1985; Joo et al., 2006). Similarly, RecA mutants that bind ATP but that exhibit compromised ATPase activity also yield exceptionally stable filaments (Rehrauer and Kowalczykowski, 1993; Campbell and Davis, 1999a). Such mutations inhibit strand exchange activity, but not joint molecule formation. It should be noted that ATP is hydrolyzed uniformly throughout the RecA filament (under ATP-saturating conditions the k_{cat} of RecA is ~30/min on ssDNA (Lusetti and Cox, 2002)); given such robust activity, why do RecA filaments remain stable at all? In general, RecA dissociation from a filament occurs only at the 5' end, suggesting that within the filament, RecA binding to the DNA is stabilized by monomer-monomer contacts (Story et al., 1992; Mikawa et al., 1998; Cox et al., 2005; Chen et al., 2008). The greater rate of filament assembly compared to disassembly also plays a role in filament longevity, and RecA monomers that dissociate can likely join the filament at its growing end, although this has not been experimentally demonstrated.

In addition to its effects on filament stability, RecA ATPase is also required for homologous strand exchange to take place, but its role in this process is not entirely clear (Cox, 1994, 2007a; Cox et al., 2005). Such activity appears to be necessary in order to surmount secondary structure barriers within the homologous DNA, including long regions of heterologous sequence (Rosselli and Stasiak, 1991; Kim et al., 1992). Various models have been proposed to explain the mechanism behind this requirement. Among the different models, the facilitated rotation model proposes that coordinated ATPase activity of RecA filaments help in the branch migration activity of RecA during DNA strand exchange reaction (Menetski et al., 1990; Cox, 2007a). However, definitive experiments to demonstrate rotation of DNA during strand exchange have yet to be performed. Recent single molecule experiments measured the strand exchange activity of RecA in real time. These studies demonstrated that the exchange occurs in 3 bp steps, an expectation arising from the structure of RecA filaments, where each monomer of RecA associates with 3 bases on the DNA (Ragunathan et al., 2011).

1.3 THE PCRA HELICASE

PcrA (Plasmid copy reduced) is a chromosomally encoded DNA helicase that was identified in a screen for genes that affected the rolling circle replication of plasmid pT181 (Iordanescu, 1993). Subsequent studies have revealed that PcrA is an essential helicase in Gram-positive bacteria such as *S. aureus* and *Streptococcus pneumoniaie* (Petit et al., 1998; Ruiz-Masó et al., 2006; Chaudhuri et al., 2009). Genome sequences of Gram-positive bacteria show the presence of a PcrA homolog (Yu et al., 2007). PcrA was shown to unwind plasmid pT181 in vitro and in *S. aureus* cell extracts and its unwinding action was shown to be essential for the

replication of plasmid pT181 (Petit et al., 1998; Chang et al., 2002; Anand et al., 2004, 2005). Studies in *B. subtilis* have shown that PcrA is involved in DNA UV repair and complements the UV repair phenotype of *E coli* mutants of UvrD (Petit et al., 1998). Cells expressing PcrA mutants exhibit hyper-recombinogenic phenotypes, and PcrA has been shown to block RecA-mediated strand exchange by displacing RecA, strongly suggesting that its role in HR involves mediation of RecA's function (Petit and Ehrlich, 2002; Anand et al., 2007).

1.3.1 PcrA Structure and Function

PcrA is a bacterial super-family 1 (SF1) helicase that shares homology with the *E. coli* helicases UvrD and Rep (Gorbalenya et al., 1989; Singleton and Wigley, 2002). Crystal structures of *Geobacillus stearothermophilus* PcrA reveal four distinct structural domains and also reveal its interaction with a partial DNA duplex structure (Figure 1-6) (Subramanya et al., 1996; Velankar et al., 1999). Domains 1A and 2A define the region that binds and hydrolyzes ATP, while domains 2B and 1B interact with the dsDNA and ssDNA, respectively (Figure 1-6) (Velankar et al., 1999). Coupled movements of these domains are believed to convert energy from ATP hydrolysis into translocase/helicase activity, and an 'inchworm model' has been proposed to describe monomeric PcrA's movement on DNA (Soultanas and Wigley, 2001).

Like its homologs Rep and UvrD, monomeric PcrA is an efficient and processive ssDNA translocase that travels in the 3' -> 5' direction, but that fails to exhibit any helicase activity *in vitro* (Niedziela-Majka et al., 2007). Curiously, deletion of the 2B domain activates a monomeric helicase activity in the homologous Rep helicase, suggesting that an interaction between this domain and dsDNA may be inhibitory (Brendza et al., 2005). At high concentrations of PcrA *in*

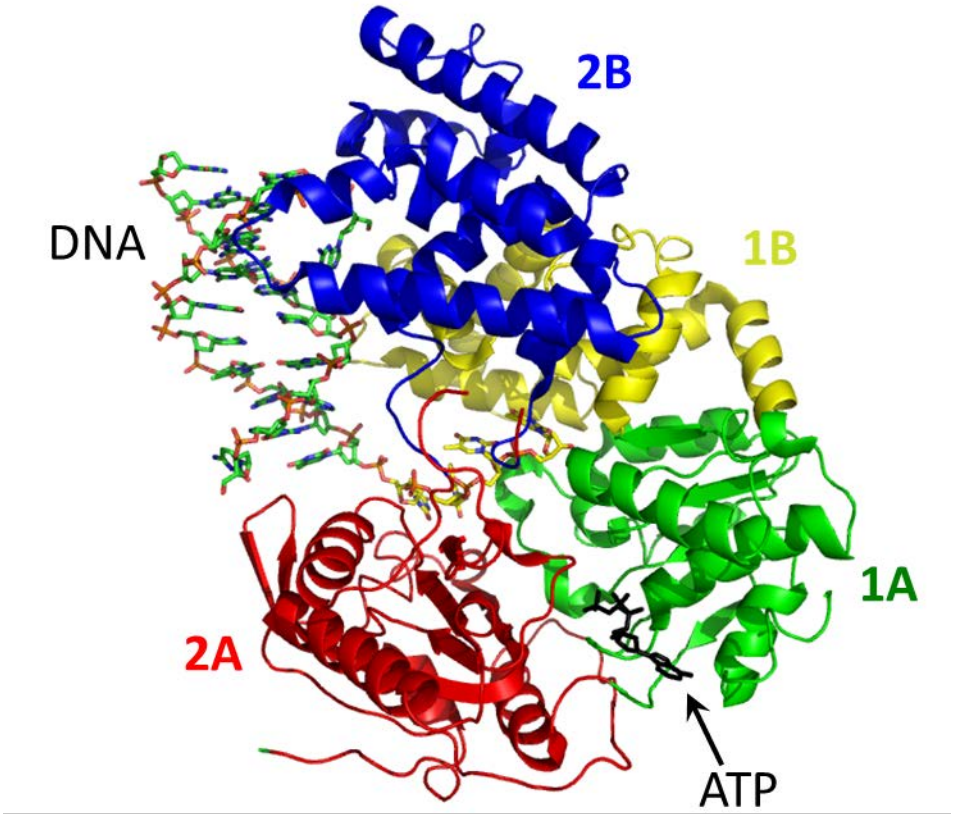

Figure 1-6: Crystal structure of Geobacillus stearothermophilus PcrA protein.

View of the PDB 3PJR structure; the four domains are labeled and color-coded according to (Velankar et al., 1999).

vitro, the protein exhibits robust helicase activity, suggesting that oligomerization of the protein is required for unwinding DNA (Niedziela-Majka et al., 2007; Yang et al., 2008).

In the absence of ATP, PcrA binds to a variety of DNA substrates, showing a preference for substrates that feature 5' ssDNA hairpin structures (Anand and Khan, 2004). Similar to Rep helicase, monomeric PcrA can also stably bind to a ss/dsDNA junction with a 5' ssDNA tail; when ATP is present, PcrA will repetitively process this tail through its 3' to 5' translocase activity (Park et al., 2010). PcrA binds to ss/ds junctions tightly with a well-defined footprint (Soultanas et al., 2000).

In vivo, suppressors of PcrA knock-out map to the *recFOR* cluster. These results suggest a role for PcrA in the regulation of RecA-mediated recombination (Petit and Ehrlich, 2002), and indeed, PcrA blocks RecA-mediated strand exchange *in vitro* (Anand et al., 2007). Like UvrD (but unlike its other close homolog, the Rep helicase), it has been shown to remove RecA from ssDNA (Veaute et al., 2005; Anand et al., 2007); curiously however, this activity persists even in PcrA mutants that lack ATPase activity (Anand et al., 2007). This calls into question a proposed model of PcrA-mediated RecA filament removal that suggests that PcrA's translocase activity is solely responsible for knocking RecA off of ssDNA (Park et al., 2010). Intriguingly, the eukaryotic homolog of PcrA, Srs2 has been shown to remove Rad51 filaments by stimulating the ATPase activity of Rad51, which results in destabilization of the filaments (Antony et al., 2009). It should be noted that like PcrA, Rad51's ATPase and helicase activities are dispensable for regulating its associated recombinase (Ward et al., 2010).

1.4 STATEMENT OF THE PROBLEM

Bacterial models of HR highlight the central importance of filaments formed by the recombinase proteins RecA/Rad51 and suggest that several HR regulation pathways target these recombinases. One mode of regulation that is employed in both prokaryotes and eukaryotes is the physical disassembly of RecA/Rad51 nucleoprotein filaments by helicases such as UvrD, PcrA and Srs2 (Krejci et al., 2003; Veaute et al., 2003, 2005; Anand et al., 2007; Antony et al., 2009).

The first study that reported PcrA-mediated displacement of RecA from DNA also showed that the ATPase and helicase activities of the protein are not essential for this activity (Anand et al., 2007). This study suggested a potential role for the affinity of RecA for DNA in PcrA-mediated RecA displacement because helicase mutants that disrupted RecA-ATP filaments did not disrupt RecA-dATP filaments efficiently. It is known that RecA-dATP filaments bind more tightly to the DNA compared to RecA-ATP filaments (Menetski and Kowalczykowski, 1989).

Since the nucleotide bound state of RecA determines the stability of RecA filaments, we tested the role of the ATPase activity of RecA in PcrA-mediated disruption of its filaments. We hypothesize that RecA's ATPase activity is required to produce the lower affinity ADP-bound state of the protein on DNA, which is then prone to displacement by PcrA. Recent spectroscopic studies of Rad51 filament removal by Srs2 suggest a similar role for the ATPase activity of Rad51, lending further support to this hypothesis (Antony et al., 2009).

Our first goal was to develop a total internal reflection microscope capable of single molecule measurement that can be used for helicase/recombinase studies. This involved the extensive rebuild of an existing system, including the incorporation of an additional laser path,

testing and characterization of this augmented instrument, and development of best practices for data analysis (Fagerburg and Leuba, 2011).

The second goal was to examine the mechanism of disruption RecA filaments by PcrA in more detail. Single molecule experiments were performed to determine whether RecA's ATPase activity is necessary for the disassembly of filaments by a translocating PcrA. We used an ATPase-mutant of RecA, as well as negligibly hydrolysable ATP analogs to directly probe PcrA-mediated disruption of RecA filaments.

2.0 SINGLE MOLECULE FRET

2.1 PRINCIPLES OF SINGLE MOLECULE FRET

Förster resonance energy transfer (FRET) is a physical process by which electronic excitation energy is transferred from one fluorophore to another, without the generation of a measurable photon (Förster, 1960; Lakowicz, 2006). The basic phenomenon is named after Dr. Theodor Förster, who published a complete mathematical description of this mechanism (Förster, 1948). It is a near-field optical phenomenon, taking place over length scales (typically 1 – 10 nm) that are considerably shorter than the excitation wavelengths involved (hundreds of nanometers for optical wavelengths) (Förster, 1960). The efficiency of FRET depends sensitively on the distance separating the two fluorophores as well as the orientation between them, and it can thus be employed as a 'molecular ruler' to optically measure distances well below the diffraction limit (Stryer and Haugland, 1967). Recent advances in single molecule detection and imaging have enabled the measurement of FRET between single, molecular fluorophore pairs (Ha et al., 1996; Ha, 2001), providing the opportunity to directly observe and measure the dynamics of individual bio-macromolecules (Weiss, 1999).

FRET can be explained using classical electromagnetic theory, and modeling each fluorophore as an electric dipole; typically, these fluorophores are small organic molecules (Figure 2-1) (Förster, 1960; Clegg, Robert M., 1992). One of these fluorophores, the 'donor', is stimulated (by absorbing a photon) into an excited state and, provided that certain conditions are met (see discussion below), can transfer this excitation energy to the second, 'acceptor' fluorophore via a long range electrostatic dipole-dipole interaction. It is this transfer of energy via interaction of the fluorophores' electric dipole moments that is called 'FRET.' FRET is only one of the mechanisms by which the donor can dissipate its excitation energy; other mechanisms include the emission of a photon, collisional quenching with other molecules, or quantum

mechanical mechanisms such as internal conversion and/or inter-systems crossing (Gell et al., 2006; Lakowicz, 2006). The amount of time that the donor spends in an excited state is related inversely to the sum of all of the rates at which these relaxation processes occur:

$$\tau_{DA}^{-1} = k_{IC} + k_{ISC} + k_Q + k_F + k_{FRET} \quad \textbf{2-1}$$

Here τ_{DA} is the life time (in seconds) of the donor molecule's excited state when it is in proximity to a suitable acceptor molecule and k's are the rates (in inverse seconds, or Hz) at which different relaxation processes occur, identified by their subscripts (IC = internal conversion, ISC = internal system conversion, Q = collisional quenching, F = emission of fluorescence photon, FRET = transfer of excitation by FRET mechanism).

The efficiency of FRET for a given donor-acceptor pair is defined as the ratio of the rate of the excited donor's relaxation via FRET relative to the sum of all of the relaxation rates involved in donor de-excitation:

$$E_{FRET} = \frac{k_{FRET}}{k_{IC} + k_{ISC} + k_Q + k_F + k_{FRET}} \quad \textbf{2-2}$$

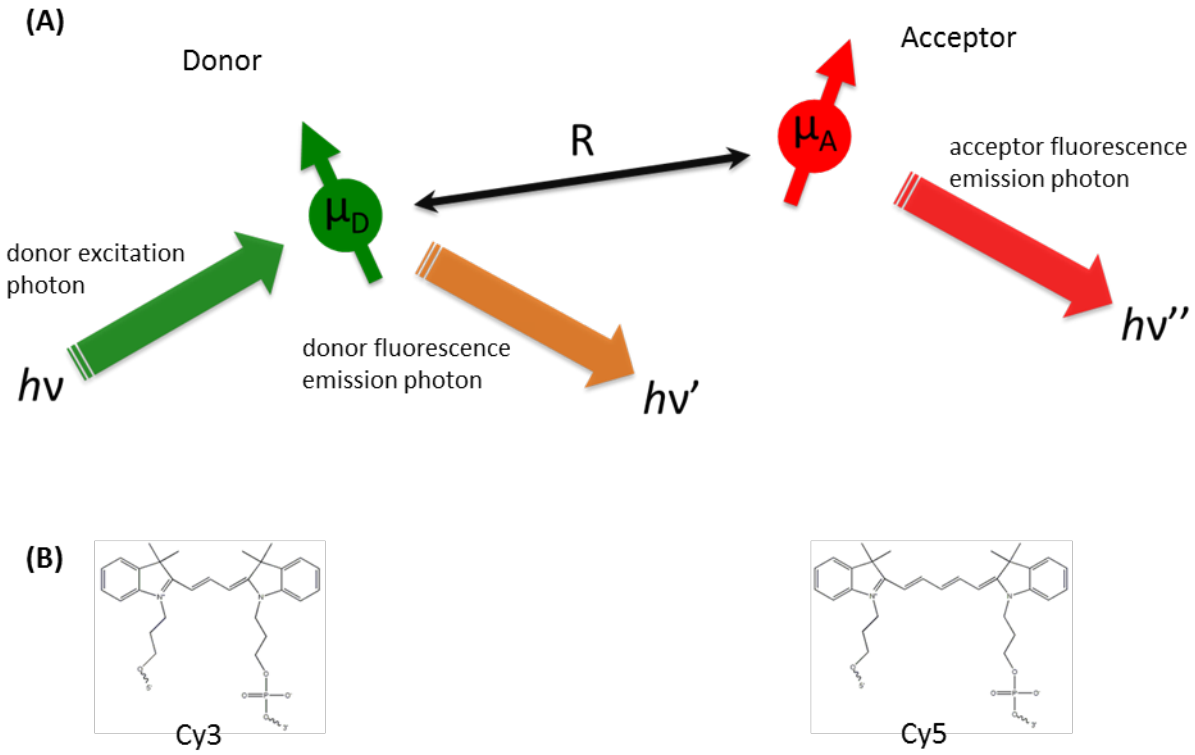

Figure 2-1: Schematic of a FRET pair.

(A) Donor and acceptor fluorophores, represented as electric dipoles with specific orientations and separation distance R. The donor is driven into an excited state by absorbing an excitation photon with energy hv. Two potential routes to donor de-excitation are via emission of a lower energy photon (fluorescence emission) with energy hv' < hv, or energy transfer via FRET to a nearby acceptor fluorophore. The latter process results in driving the acceptor fluorophore into an excited state, from which it can relax via emission of a photon with energy hv'' < hv' < hv. **(B)** Chemical structures for the commonly used donor/acceptor fluorophore pair Cy3/Cy5.

Experimentally, it is typically infeasible to measure relaxation rates directly, and a ratiometric method of defining E_{FRET} is used that involves only the fluorescence emission intensities of the donor and acceptor molecules (Dahan et al., 1999; Deniz et al., 2001):

$$E_{FRET}^{Exp} = \frac{I_A}{\gamma I_D + I_A} \quad \textbf{2-3}$$

Where I_A is the measured fluorescence intensity from the acceptor molecule, and I_D is the measured fluorescence intensity from the donor dye. γ is a correction factor to account for differences in detection efficiencies and quantum yields for the donor and acceptor; often such differences are insignificant enough that $\gamma \approx 1$ is assumed. It should be noted that E_{FRET}^{Exp} is usually assumed to be equivalent to E_{FRET} (Gell et al., 2006). Good quality data should show anti-correlated donor and acceptor fluorescence intensities (Figure 2-2); this is due to the fact that when E_{FRET} is high, the donor is transferring its excitation to the acceptor, rather than emitting fluorescence signal. Conversely, when E_{FRET} is low, the donor will preferentially emit a fluorescence signal, rather than participate in de-excitation via FRET.

One of Förster's foundational contributions to the study of FRET was his derivation of the expression for k_{FRET} in equation 2-2 (Lakowicz, 2006):

$$k_{FRET} = \frac{9000(\ln 10)\kappa^2 Q_D J}{128\pi^5 n^4 N_A \tau_D R^6} \quad \textbf{2-4}$$

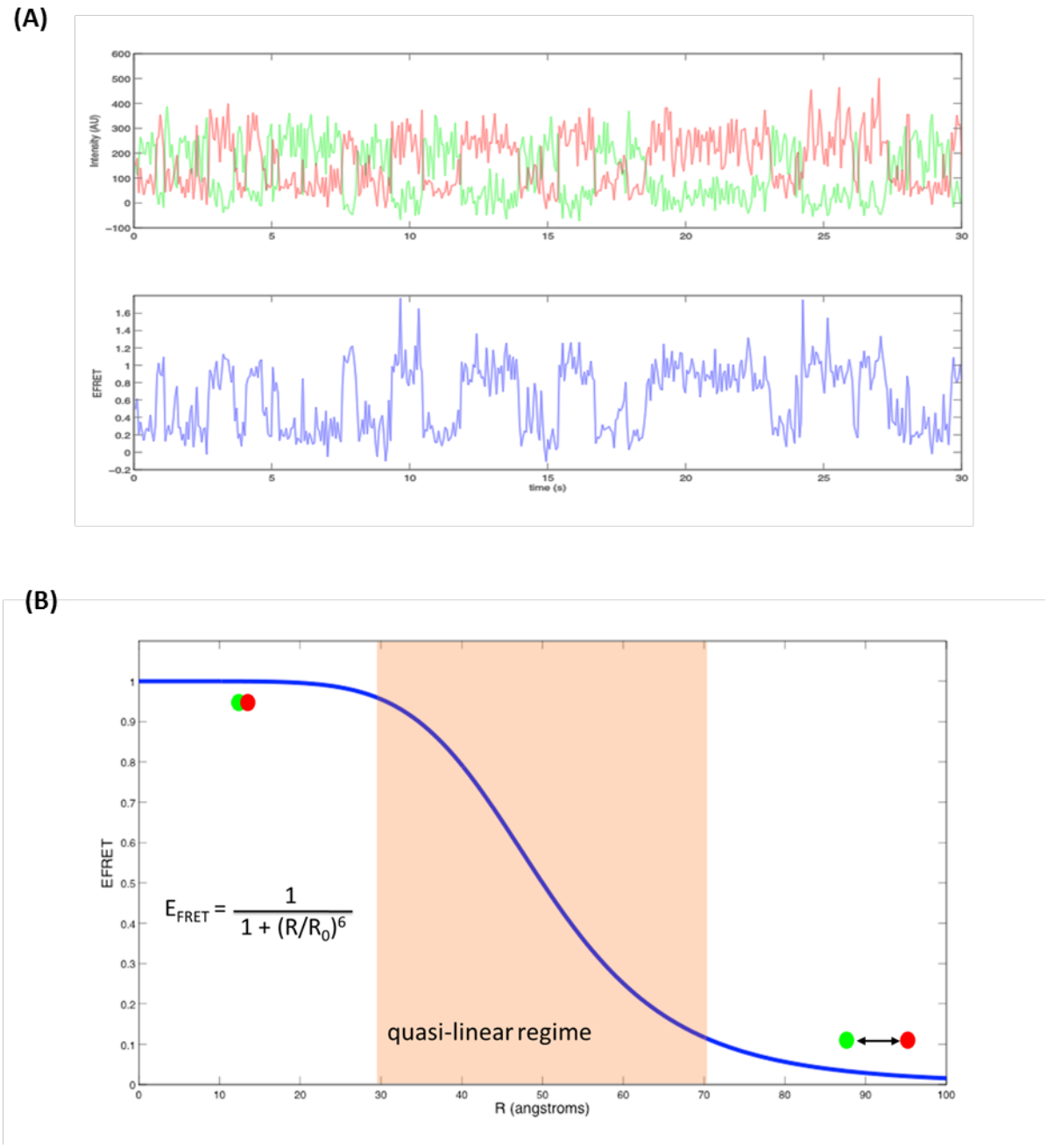

Figure 2-2: Example E_{FRET} trajectory and relationship between E_{FRET} and R.

(A) Example fluorescence signal trajectories for a donor (Cy3, green) and acceptor (Cy5, red) fluorophore pair. Note anti-correlated behavior of fluorescence signals. Also shown is the calculated $E_{FRET} = I_D/(I_D+I_A)$ (blue). As the separation between the fluorophores increases, the E_{FRET} signal decreases, and vice versa. **(B)** The relationship between E_{FRET} and R for a

hypothetical donor/acceptor pair with R_0 = 50 Å. The R^{-6} dependence results in a sigmoidal curve that reflects a quasi-linear region of FRET from ~0.5*R_0 to ~1.5*R_0. Measurements are most reliably made within this distance range.

where κ is the orientation factor between the donor and acceptor dipole moments (explained in more detail below), Q_D is the quantum yield of the donor dye, J is the spectral overlap between the donor and acceptor dye fluorescence spectra (explained in more detail below), n is the index of refraction of the media in between the donor and acceptor, N_A is Avogadro's number, τ_D is the excited-state lifetime of the donor dye when no acceptor is nearby, and R is the scalar distance separating the donor and acceptor dipoles. All of the quantities in equation 2-4 are either measurable or (in principle) computable; two are given additional attention here.

The orientation factor κ^2 ranges from 0 to 4, and depends on the relative orientation between the transition dipole moments of the donor and acceptor (Lakowicz, 2006). In most experiments, both dye molecules are assumed to be in rapid rotational diffusion, with their dipole moments effectively sampling all orientations uniformly; in this case, κ^2 = 2/3. It is possible to set limits on κ^2 by measuring anisotropy values for the donor and acceptor and computer simulations can also be employed in this endeavor (Iqbal et al., 2008a, 2008b; Ouellet et al., 2011). In much of the literature, κ^2 = 2/3 is assumed to be true; deviation from this value is generally not given much attention.

The spectral overlap J is a significant term to consider, because like Q_D it depends on the photo-physical properties of the specific donor and acceptor molecules being used. J is defined by the shared area between the normalized donor emission spectra and the acceptor excitation spectra (Figure 2-3):

$$J = \int_0^\infty F_D(\lambda)\varepsilon_A(\lambda)\lambda^4 d\lambda \qquad \textbf{2-5}$$

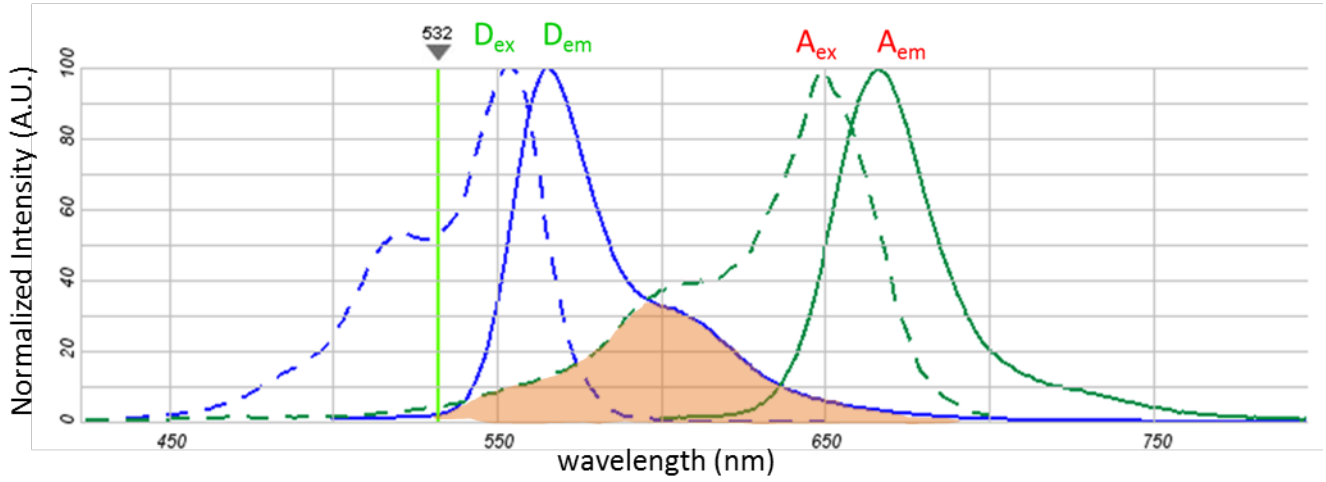

Figure 2-3: Illustration of spectral overlap parameter *J*.

The excitation spectra (dotted lines) and emission spectra (solid lines) for prototypical donor fluorophore (Cy3, blue lines) and acceptor fluorophore (Cy5). Also indicated is a typical laser-excitation wavelength for Cy3 (532 nm). The spectral overlap J is indicated by the shaded region defined by the area under both the donor emission and acceptor excitation spectra. Note that although J is shown here with reference to fluorescence spectra of the donor/acceptor, FRET is not the result of the exchange of any real photons.

Where $F_D(\lambda)$ is the normalized fluorescence emission of the donor over the wavelength range $(\lambda + \Delta\lambda)$, and $\varepsilon_A(\lambda)$ is the normalized molar absorption of the acceptor over the range $(\lambda + \Delta\lambda)$. Donor and acceptor dyes should be chosen so that their spectral overlap is maximized (Haugland et al., 1969), and other photo-physical properties of the dyes should be considered as well. Both should have high quantum yields and not be prone to photo-blinking. Finally, dyes should be chosen such that their Förster radius (discussed below) is relevant to the length scales being investigated.

Equation 2-4 can be usefully rewritten as:

$$k_{FRET} = \frac{1}{\tau_D}\left(\frac{R_0}{R}\right)^6 \qquad \textbf{2-6}$$

Where:

$$R_0^6 = \frac{9000(\ln 10)\kappa^2 Q_D J}{128\pi^5 n^4 N_A \tau_D} \qquad \textbf{2-7}$$

And:

$$\boldsymbol{\tau_D^{-1} = k_{IC} + k_{ISC} + k_Q + k_F} \qquad \textbf{2-8}$$

Equation 2-6 and equation 2-8 when combined with equation 2-2 yields:

$$E_{FRET} = \frac{1}{1+\left(\frac{R}{R_0}\right)^6} \qquad \textbf{2-9}$$

This expression for E_{FRET} emphasizes the distance-dependent nature of FRET; because of the exponent, small changes in R between the donor and acceptor can result in a large change in measured E_{FRET}. It is this distance dependence that renders FRET so useful as a molecular-scale ruler. By measuring the E_{FRET} for a given dye-pair experimentally (equation 2-3), one can then use equation 2-9 to determine the distance R separating the two molecules. R_0 is called the Förster radius for a defined donor-acceptor pair, and denotes the separation distance at which 50% FRET transfer takes place. The Förster radius is another important parameter to consider when selecting fluorophore pairs for an experiment, and depends on the exact dye pair that is used.

The relationship between R and E_{FRET} is shown in (Figure 2-2). From the plot it is clear that FRET is most useful for measuring distances that are similar to R_0. At much smaller R, E_{FRET} saturates to 100%; when R is much larger than R_0, the effect of FRET is too small to be measured accurately. Typical R_0 values for commonly used dye pairs (*e.g.*, cyanine dyes Cy3/Cy5; (Mujumdar et al., 1996)) are around 50 Å; the measurable R range for such a dye pair is thus around 20-80 Å. Because this length scale is relevant in many biological processes (Selvin, 2000), FRET studies have proved profoundly useful in measuring protein dynamics and interactions at the molecular level. The FRET technique is well-suited for studying structural

dynamics and distributions in proteins and DNA (Figure 2-4) (Heyduk, 2002; Joo et al., 2006; Myong et al., 2006; Schuler and Eaton, 2008; Rothenberg and Ha, 2010); With high enough time resolution it is possible to directly observe conformational trajectories of individual molecules, allowing the direct measurement of kinetic parameters (Figure 2-5) (McKinney et al., 2003).

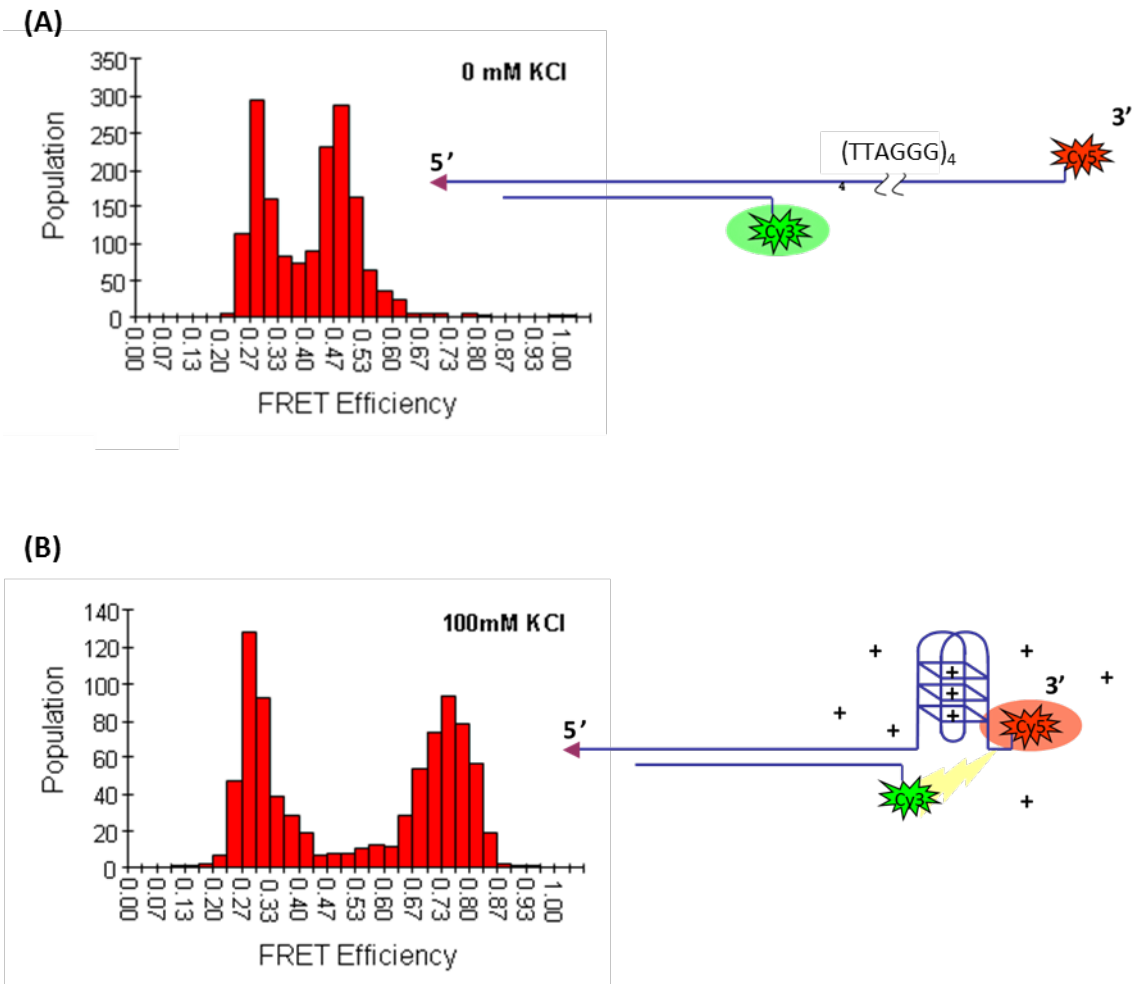

Figure 2-4: smFRET studies of G-Quadruplex DNA.

(A) Fluorescently labeled G-quadruplex (G4) DNA consists of a long ssDNA featuring TTAGGG repeats. In the absence of cations the ssDNA is extended, resulting in a large separation between the fluorescent dyes and consequently low FRET (note E_{FRET} peak in histogram at ~0.5). **(B)** In the presence of cations (here, 100 mM KCl) the G4 DNA folds up into a compact structure, bringing the fluorescent dyes close enough together and resulting in increased FRET (E_{FRET} peak now appears at ~0.75). Note that the peak at E_{FRET} ~0.27 is the so-called 'zero-peak' and is not the result of FRET transfer (see section 2.2.1.1 for additional discussion concerning the zero-peak).

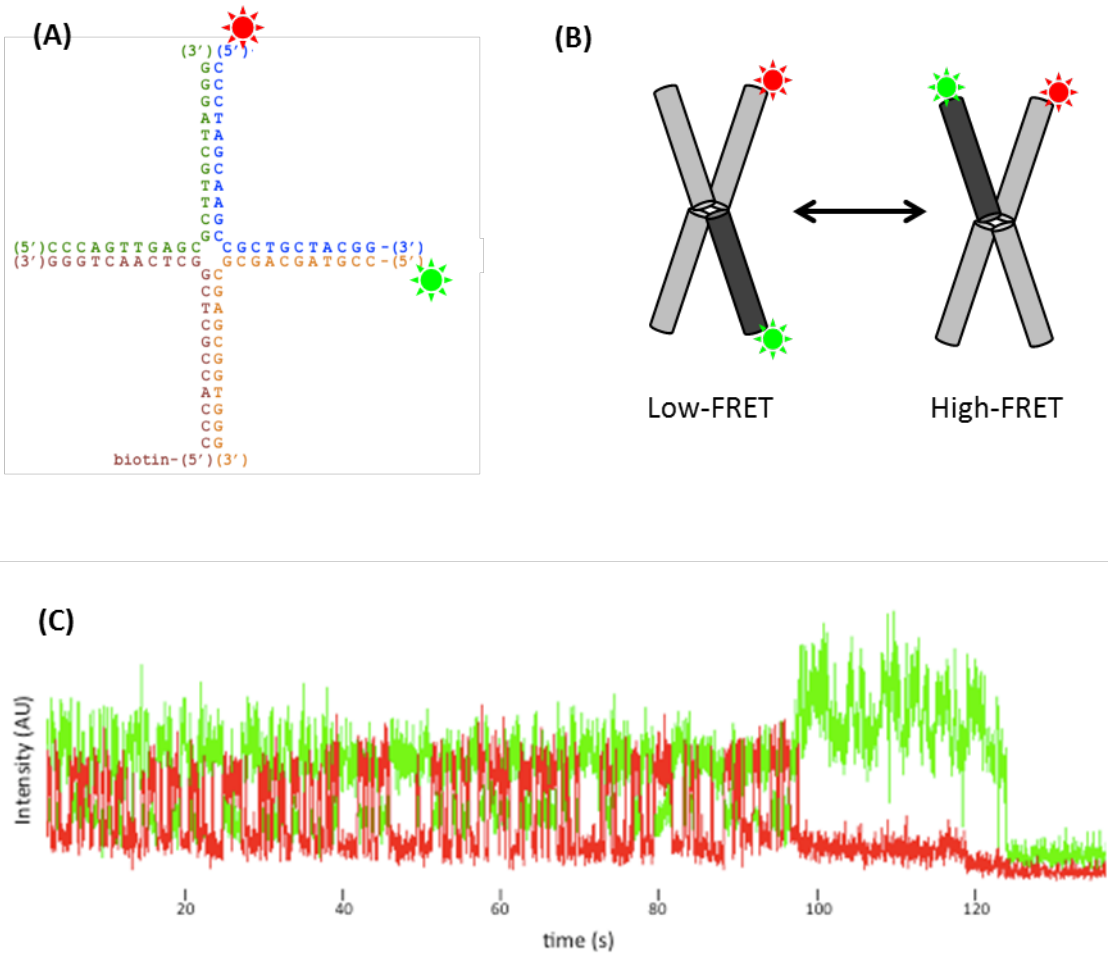

Figure 2-5: smFRET studies of HJ isoform transition rates.

(A) Fluorescently labeled HJ structure, with fluorescent dyes on separate arms. **(B)** In the presence of Mg^{++} ions, the HJ adopts one of two structural isoforms, resulting in either high or low FRET. The rate of inter-conversion between the two isoforms depends on the concentration of Mg^{++}. **(C)** A typical fluorescence signal from an experiment with the HJ of **(A)** showing anti-correlated donor and acceptor signals (green = donor signal, red = acceptor signal) due to the process illustrated in **(B).** Dwell time analysis can be performed on such trajectories to measure interconversion rates for different experimental conditions.

2.2 CONSTRUCTION OF A SINGLE MOLECULE FRET MICROSCOPE

(Parts of this section appear (Fagerburg and Leuba, 2011))

The principle challenge involved in measuring smFRET is the same as that of measuring single-molecule fluorescence- namely, achieving a sufficiently high enough signal to noise ratio (SNR) to be able to discern the fluorescence signal from a single molecular dye-pair (Moerner and Fromm, 2003). This challenge is usefully attacked from three directions: 1) use of photo-physically robust fluorophores, 2) minimization of background signal, and 3) employing high-sensitivity detectors. The first of these aspects is perhaps the easiest to address, and may be considered for each separate experiment, whereas the latter two represent important decisions that must be settled before construction of an instrument can begin. Practically speaking, smFRET microscopes for biological use are typically based on either a wide-field microscopy system using total internal reflection methods to reduce background or else a confocal geometry for both excitation and observation (Ha, 2001). Each of these options has its specific advantages and disadvantages, and also determines the type of detector that must be used.

Instruments based on a confocal geometry rely on extremely small (ideally, diffraction limited) confocal excitation/observation volume to cut down on background fluorescence signal (Figure 2-6) (Zheng et al., 2007). This is typically in the femto-liter (10^{-15} L) range, and only molecules within this volume will contribute to the measured fluorescence signal. At small enough concentrations, detection of signal from individual molecules is possible, either as they freely drift through the confocal volume in solution (yielding data for milli-second time scales), or for longer periods of time if they are attached to the surface of a flow-cell (up to

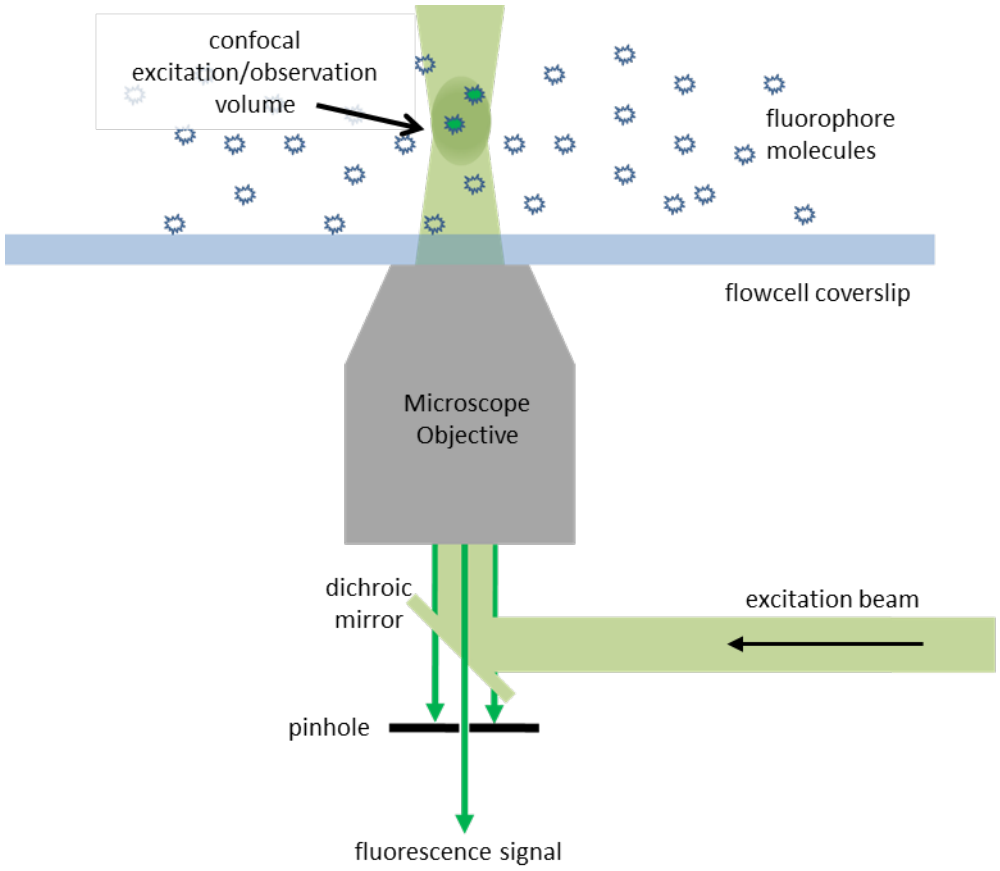

Figure 2-6: Basic confocal microscope geometry.

A confocal microscope shares the same excitation optics layout as a standard epifluorescence microscope. An incoming excitation laser beam is directed through a microscope objective by a dichroic mirror; this dichroic allows fluorescence signal to be collected from the same objective. The advantage of a confocal microscope depends on a small pinhole (~10 um) that is precisely positioned at the back focal point of the microscope objective. This pinhole blocks all light rays that do not originate from the front focal point of the microscope objective (in reality, these 'points' are actually diffraction limited volumes of ~fL size), effectively eliminating the background signal produced by molecules outside of this defined (confocal) volume.

minutes-long time scales). It is the nature of confocal microscopes to report signal only from the confocal volume, whose minimum size (under ideal conditions) is diffraction limited. This means that a confocal microscope requires only a point-source detector such as an avalanche photo-diode (APD), but it also means that in order to acquire an image, the confocal volume must be physically scanned (typically using a piezoelectric stage) over the field of view. APDs are fast and extremely sensitive detectors, and the virtue of a confocal-based smFRET microscope lies in its ability to achieve high time resolution (Moerner and Fromm, 2003). However, when recording data from surface-bound molecules, unless the microscope is driven by an automated stage it is quite difficult to manually collect a large number of single molecule traces (Sabanayagam et al., 2004).

In contrast, a wide-field smFRET microscope is based on a standard inverted optical microscope geometry, and can collect data from many hundreds of molecules in parallel, albeit at slower time resolution (Selvin and Ha, 2007; Harris et al., 2008). In order to achieve single-molecule sensitivity, a CCD camera with enhanced sensitivity must be used, and additional considerations for selective fluorescence excitation must be made (Ha, 2001; Moerner and Fromm, 2003). Typically, an electron-multiplying CCD (EMCCD) is used as the detector. The amount of time it takes to read a full frame of data from the CCD determines the maximum possible time resolution for data acquisition; current technology sets this around the 10 ms time range (100 Hz data acquisition rate)(Moerner and Fromm, 2003). In order to eliminate as much fluorescence background as possible, it is necessary to implement some form of total internal reflection fluorescence (TIRF) technique (Axelrod et al., 1984; Moerner and Fromm, 2003). TIRF requires that an incident light source be reflected off of a surface at an angle greater than the critical angle determined by the optical properties of the surface and the surrounding medium

(Axelrod et al., 1984). This results in the light being totally (internally) reflected by the surface, while producing a thin region of electromagnetic field on the opposite side of the surface (Figure 2-7). Only fluorophores that are within this region will be excited; in a typical smFRET experiment molecules are attached to the surface so that they can be observed for long time periods. Typically, TIRF illumination is implemented using excitation lasers that are either directed through the microscope's objective (and thus forming an evanescent field on the interior surface of a flow-cell coverslip), or coupled to a flow-cell via a prism (resulting in an evanescent field formed on surface farthest away from the microscope objective) (Figure 2-7). Both are relatively straightforward to set up; the objective-based system is perhaps more reliable in the sense that the evanescent field is always the same shape and at the same position, while the prism-based system generally yields slightly higher SNR and is more amenable to experiments involving flow (Ha, 2001).

We chose to construct a prism-based TIRF wide-field smFRET microscope primarily for the advantages it offers in collecting large numbers of molecular data traces in parallel, while under flow. These features allow for experiments in which proteins and reagents are injected and their effects immediately after (or indeed, during) injection are measured on an entire population at the same time. Such experiments are not possible in a confocal microscope, as individual molecules can only be observed one-at-a-time.

It is my sincere hope that in addition to providing the technical details of the hardware and calibration protocols used in this work, the following sections will also be useful for future operators of the smFRET instrument here described.

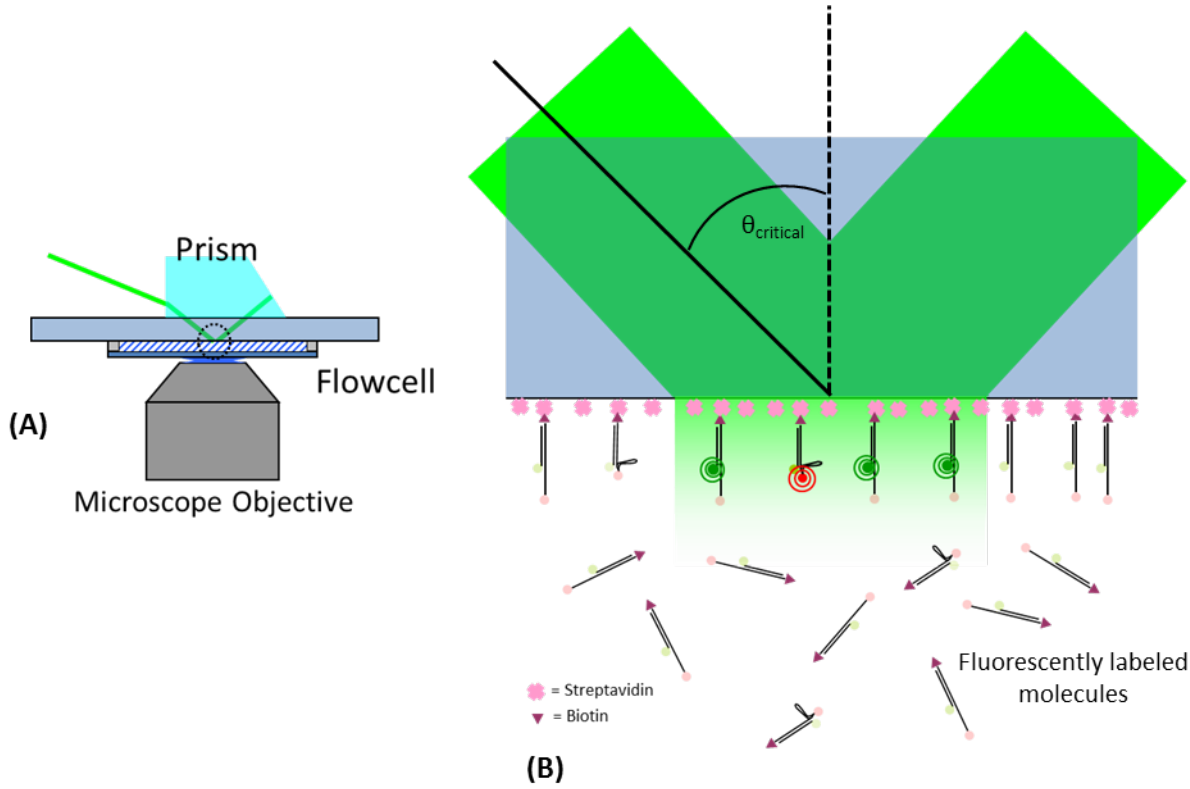

Figure 2-7: Schematic of evanescent field in a prism-based TIRF microscope.

(A) In a prism-based TIRF microscope, the incident excitation laser beam is coupled to the flowcell by a fused silica prism so that it encounters the flow-cell surface at an angle greater or equal to that of the critical angle ($\theta_{critical}$) of the flow-cell/buffer system. **(B)** This results in total internal reflection of the beam at the flow-cell surface, establishing an evanescent field on the interior surface of the flow-cell. The evanescent field penetrates a few hundred nanometers into the flow-cell, and will only fluorescently excite molecules within this region. Attaching labeled molecules to the flow-cell via biotin-streptavidin chemistries ensures that immobilized molecules can be monitored for long durations.

2.2.1 Description of Instrument

The microscope used in this work is an improvement on an earlier design used in the lab, and was built on a floating optical table using a mixture of commercial components and custom hardware fabricated in a machine shop (Figure 2-8). It is a prism-based total internal reflection fluorescence (TIRF) microscope employing a stripped-down commercial base (Olympus IX71). Prism-based TIRF rather than objective-based is employed because the former allows for injection of samples into the flow cell while imaging. In a prism-based TIRF system, the molecules under study reside near the comparatively thick and rigid microscope slide; in an objective-based system, the molecules being observed are near the much thinner coverslip, which can deform under the small pressures of sample injection leading to defocusing and consequent loss of signal (Selvin and Ha, 2007).

The excitation optics consist of two lasers; a 532 nm solid state laser (CrystaLaser) is used to excite donor molecules, and a 637 nm solid state laser is used to excite acceptor molecules (Melles Griot) (see section 2.2.1.1 for more details). The output power of both laser beams are attenuated using metal-film neutral density filters. Acceptor laser output is additionally modulated using an opto-mechanical shutter (Uniblitz); the donor laser's output is modulated directly with TTL logic signals. The 637 nm laser path includes two first-surface mirrors on gimbaled mounts, allowing for fine adjustment of the laser path, which is essential for proper ALEX function. The two beam paths are combined with a dichroic mirror (Chroma Technology), directed to the TIRF microscope stage via first-surface mirrors, and further directed to a Pellin-Broca prism through a convex focusing lens (f~35 mm). The prism is coupled to the flow-cell slide via optical grade oil; it refracts the incident laser light and (if the

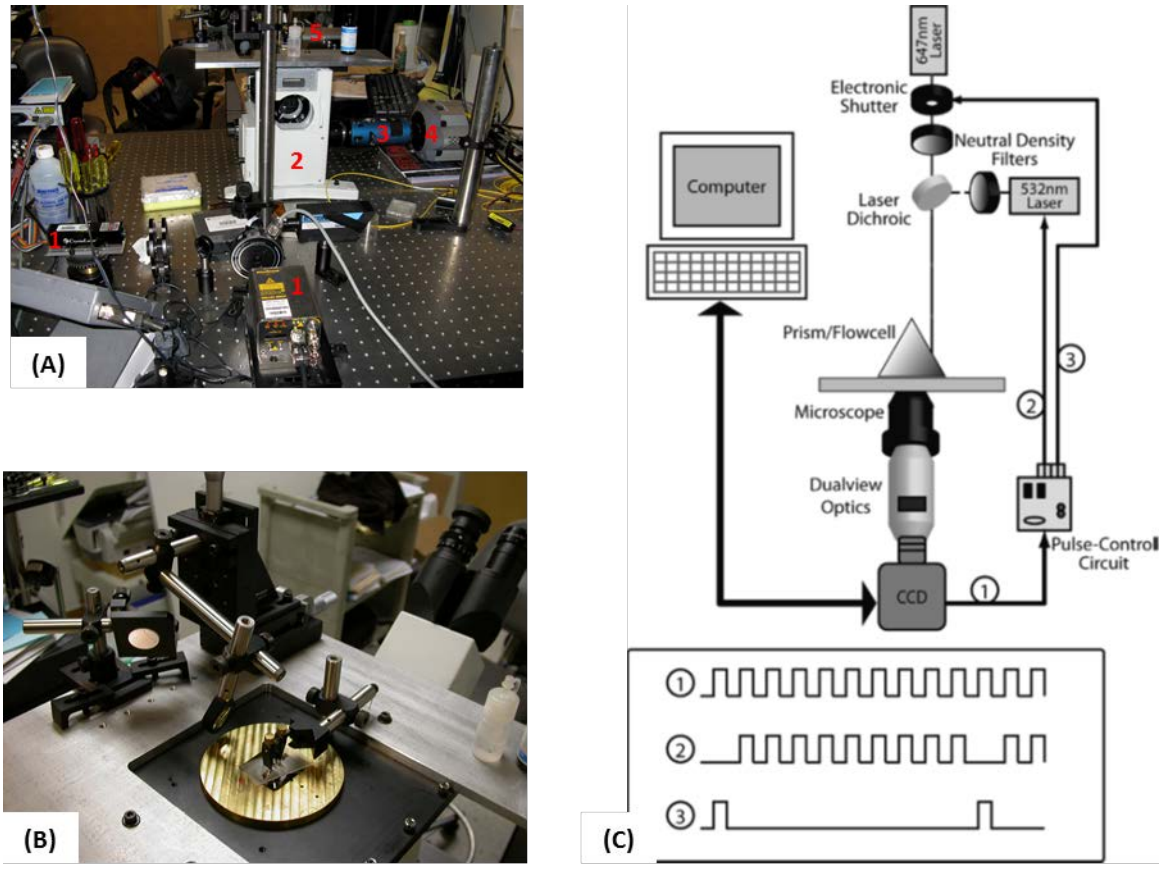

Figure 2-8: Homebuilt wide-field TIRF smFRET microscope.

(A) Rear view of microscope showing optical paths. Labeled components are: (1) solid-state excitation lasers, (2) commercial microscope base, (3) dual-view emission optics, (4) EMCCD, and (5) microscope stage with prism mount. **(B)** Close up of prism mount and excitation laser focusing lens. A flow-cell is under the prism, ready for imaging by microscope. **(C)** Schematic showing simplified optical layout of TIRF smFRET microscope. Inset shows example ALEX pulse control signals on labeled lines, as generated by pulse control circuit. Shown is a pulse train for directly exciting acceptor molecules every 10th image.

system is configured correctly) ensures that it is incident on the flow-cell slide at an angle greater than the critical angle, resulting in total internal reflection of the laser beam at the slide surface and establishing an evanescent field just inside the flow-cell (Figure 2-7) (Axelrod et al., 1984). The laser focusing lens is mounted on an armature whose three principle axes are controlled by micrometers (Figure 2-8B). By adjusting these micrometers the position of the reflected laser spot on the flow cell slide (and thus the position of the evanescent field within the flow-cell) can be fine-tuned with a high degree of control.

Fluorescence emission is collected through a 60x 1.2NA water-immersion objective (Olympus) and first passes through a 550LP (Chroma Technology) filter to remove any scattered donor-excitation laser light. The fluorescence emission is next split into two separate paths via a DualView unit (Optical Insights, Inc.) that contains a 610 nm dichroic mirror and additional optics for each path. Wavelengths shorter than 610 nm are sent down the donor signal path, where they are additionally filtered by a 580/40 nm bandpass filter (Chroma Technology); wavelengths longer than 610nm are sent down the acceptor signal path, where they are filtered by a 660LP filter (Chroma technology). Filtered donor and acceptor path fluorescence signals are finally imaged onto separate halves of a thermo-electrically cooled EMCCD (Andor iXon). Using the optics described here, the system images a field of view that measures 90 μm by 90 μm; while the dual view is being used, this yields images that effectively cover 90 μm by 45μm, spectrally resolved into both donor and acceptor wavelength ranges (560 nm – 600 nm and > 660 nm, respectively). Because the Andor iXon EMCCD chip contains 512 by 512 pixel elements, each on-screen pixel represents ~175 nm per side.

The performance of the microscope described here was originally characterized by imaging G4 DNA samples (Figure 2-4). These experiments allowed us to verify that the

instrument could discern single molecule fluorescence signals at sensitivity suitable for the measurement of smFRET and also enabled the measurement noise levels on such signals. Subsequent experiments with rapidly flipping HJs (Figure 2-5) further allowed us to characterize the microscope's performance when data was collected at maximum time resolution.

2.2.1.1 ALEX System

Of special note in the smFRET system described here is the fact that it employs two excitation lasers- one directly excites donor-dye molecules, while the other is used for directly exciting acceptor molecules. Used together, they can alternately directly excite donor molecules in one frame, and acceptor molecules in the next frame in a scheme called ALEX (Alternating Laser Excitation) (Kapanidis et al., 2004). This confers the advantage of regularly interrogating active acceptor molecules, allowing one to identify signals originating from true composite pairs of donor/acceptor molecules. This, in turn, enables the suppression of the so-called 'zero-peak' which often appears in smFRET histograms as a large population of apparently low-FRET signals, and is due to the inclusion of fluorescence data from molecules that contain only an active donor dye (Kapanidis et al., 2004). Eliminating such a zero-peak enhances the lower-end range of FRET measurements that can be made and also makes it easier to identify blinking events, which are potentially long-lived states during which an acceptor dye molecule emits no photons (and which are easily mistakenly identified as low-FRET transitions).

These advantages become possible because of the additional information that direct acceptor excitation yields. With such a scheme one can measure both the fluorescence emissions of donor and acceptor dyes under donor excitation ($I_{D,ex}^{D,em}$ and $I_{D,ex}^{A,em}$) as well as under acceptor excitation ($I_{A,ex}^{D,em}$ and $I_{A,ex}^{A,em}$). Note that $I_{D,ex}^{A,em}$ is typically non-zero because of FRET, whereas $I_{A,ex}^{D,em}$

should be negligible because there is no 'reverse-FRET' mechanism. In addition to calculating FRET (which involves just $I_{D,ex}^{D,em}$ and $I_{D,ex}^{A,em}$), it becomes possible to define a new quantity, defined as the stoichiometry parameter, S:

$$s = \frac{I_{D,ex}^{D,em} + I_{D,ex}^{A,em}}{I_{D,ex}^{D,em} + I_{D,ex}^{A,em} + I_{A,ex}^{D,em} + I_{A,ex}^{A,em}} \approx \frac{I_{D,ex}^{D,em} + I_{D,ex}^{A,em}}{I_{D,ex}^{D,em} + I_{D,ex}^{A,em} + I_{A,ex}^{A,em}} \quad \textbf{2-10}$$

This value is very near one when $I_{A,ex}^{A,em}$ is zero (i.e. donor only case) and very near zero when $I_{D,ex}^{D,em}$ is zero (acceptor only case). If $I_{A,ex}^{A,em}$ is nearly equal to $I_{D,ex}^{D,em}$ (under properly configured system, equal number of donors to acceptors) then S ~ 0.5.

The utility of the S value becomes manifest when smFRET-ALEX data is plotted as a two-dimensional scatter-plot, with S values along one dimension and FRET values along the other (Figure 2-9). Such plots make it immediately clear to the analyst whether or not the molecule under consideration is a bona fide FRET pair or not, by revealing where its fluorescence signals cluster.

In order to record ALEX data, it is necessary to alternately excite the sample with two different lasers (one for direct donor excitation and the other for direct acceptor excitation), while ensuring that the laser excitation periods are synchronized with the collection of image data. In the instrument described here, this was achieved by using the digital 'fire' output line from the Andor iXon EMCCD; this line outputs a TTL-high logic signal while the camera is acquiring a frame of image data. The resulting pulse train is sent to a pulse-control circuit that produces the control signals for the donor and acceptor excitation lasers, firing only the donor

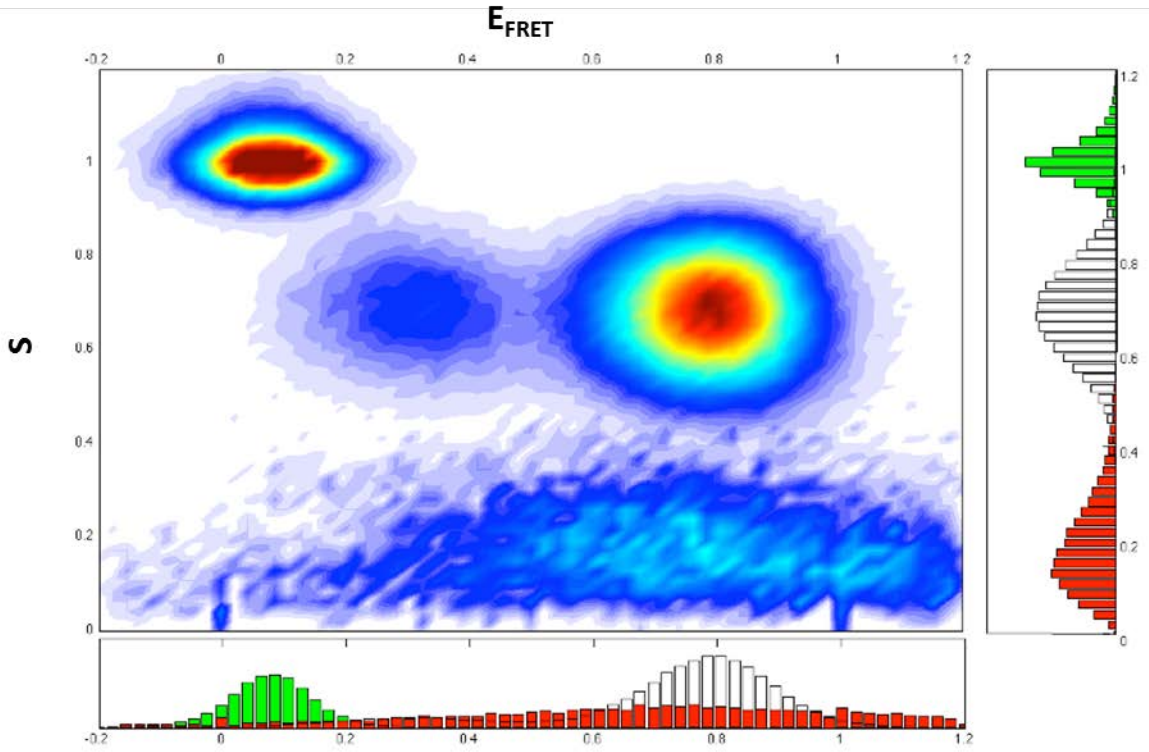

Figure 2-9: Scatter-plot of S versus EFRET for example smFRET pairs.

The information gained from the ALEX technique allows for the calculation of both EFRET and S at each time point. When these quantities are used to generate a scatterplot with EFRET along the x-axis and S along the y-axis the resulting patterns enable graphical identification of signals originating from donor/acceptor pairs. Here the EFRET and S values for a collection of molecules are plotted together to illustrate the three regions of interest. The region of S > ~0.8 contains molecules with an active donor, but no active acceptor. Conversely, the region S < ~0.4 contains molecules with only an active acceptor, but no donor. In this plot, signals centered around S ~ 0.7 represent an ideal range containing molecules with one active donor and one active acceptor. The value of S that this ideal range clusters around depends on the relative laser powers used to excite the donors and acceptors directly. Ideally, laser power is adjusted so that

directly excited lone donor emission is equal to directly excited acceptor emission; in this case the ideal range should cluster around S ~0.5.

laser for (N-1) frames, and then firing only the acceptor laser on the Nth frame (Figure 2-10); this sequence is repeated until all data has been collected. A jumper in the circuit allows the user to set the value of N from 2 (every other frame) to 15. Additionally, the pulse-control circuit contains two astable 555-circuits that are used to shape the duration of the laser control pulses.

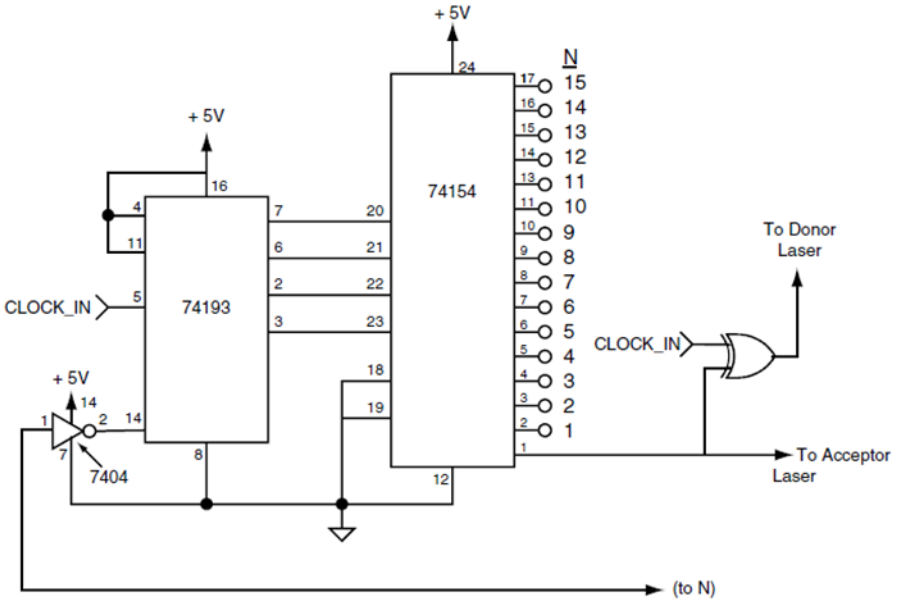

Figure 2-10: Schematic of ALEX pulse-control circuit.

The ‘CLOCK_IN’ pulse train originates from the EMCCD ‘Fire’ port, which transitions from logic-low to logic-high every time an image exposure begins and ends. The line marked ‘(to N)’ is connected to one of the pins of the 74154 chip, and selects how many frames of donor-excited images will be taken before an acceptor frame is triggered. The duty cycles of the pulses on the laser control output lines are shaped by further circuitry before being used to drive the excitation lasers. Sample pulse trains appear in Figure 2-8.

2.2.2 Data Collection, Calibration and Characterization

Single molecule experiments generally demand exacting preparation of surfaces and reagents in order to minimize experimental artifacts that can lead to lower SNR (Rasnik et al., 2005; Heyes et al., 2007). Additionally, microscope and optics settings must be tuned to ensure that the instrument is operating optimally. The regular alignment and calibration of optical systems is a necessary step to ensure that data quality is as high as possible.

We have adopted a standard geometry for experimental flow-cells that allows for two separate experiments to be performed while maintaining adequate clearance for prism contact on the microscope stage (Figure 2-11). The foundation of the flowcell (defining the surface on which the evanescent field will form, and also where the observed molecules will be bound) consists of a fused silica slide (Finkenbeiner) into which four 1.25 mm diameter holes have been drilled (Figure 2-11). Regular glass slides cannot be used, because they contain many microscopic imperfections that scatter reflected laser light, severely decreasing SNR. In order to minimize protein interactions with the slide surface, we coat all flow-cell surfaces with polyethylene glycol (PEG) before assembly (Fagerburg and Leuba, 2011). Fluorescently labeled molecules are attached to the PEG surface via biotin-streptavidin chemistry (Hermanson, 2008; Koopmans et al., 2008). Just prior to imaging, the flow-cell is injected with an oxygen scavenger buffer that also contains reagents to discourage photo-blinking of the donor and acceptor dyes (Rasnik et al., 2006; Kong et al., 2007).

Preparing the microscope for data collection requires two major sets of considerations; CCD settings should be optimized, and laser optics should be adjusted for maximum SNR. Like all CCDs, EMCCDs exhibit a small amount of thermally-induced background noise called dark current (Moerner and Fromm, 2003). This noise is significant enough to obscure single molecule

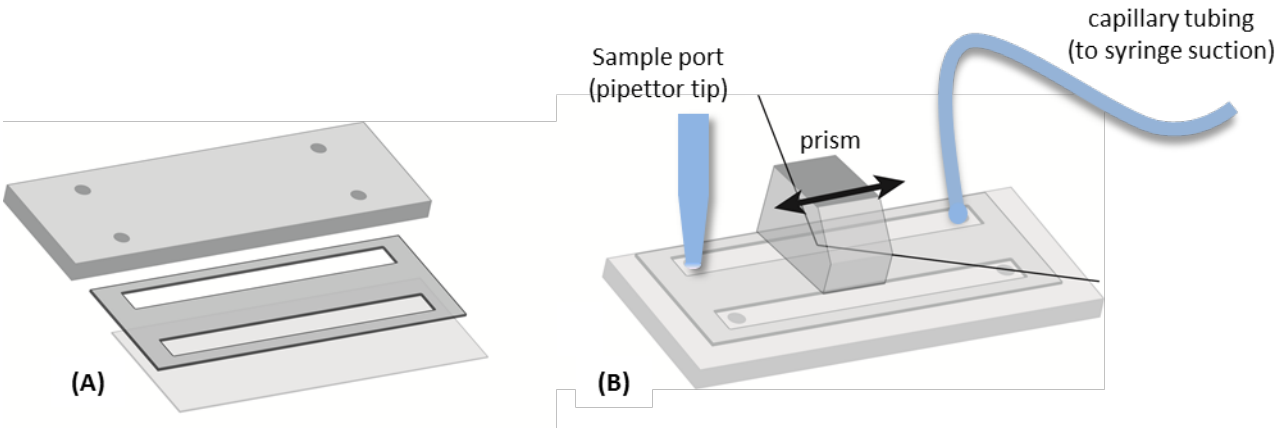

Figure 2-11: Schematic of an smFRET experimental flow-cell.

(A) Flow-cells are composed of three layers: a fused silica slide with 1.25 mm drilled holes forms the base, on top of which is fused a thin layer of Parafilm with sample chamber cutouts, followed by a standard coverslip. **(B)** The flow cell geometry is designed so that an attached sample chamber (consisting of a 1 mL pipettor tip) and capillary tubing (to allow for sample injection) will not obstruct the TIRF prism placement.

signals and should be minimized as much as possible by cooling the CCD chip. For all experiments described here, the EMCCD chip was kept at a temperature of -90 C using a thermo-electric cooler whose performance was further assisted by pumping an anti-freeze solution over it. Optimal settings were determined for the camera and used consistently for all experiments (see Appendix A for EMCCD settings). Important considerations for the laser systems include ensuring that optimal power levels are used, and also that the region over which the evanescent field is established is uniform.

Establishing the evanescent field region requires directing the laser through the prism so that it encounters the flow-cell slide surface at angle greater than the critical angle (Figure 2-7, Figure 2-12). Looking down on the top of the prism/microscope stage will reveal a series of three laser spots, resulting from scattered laser light as (Figure 2-12B) 1) the incident laser beam crosses the oil layer between the prism and slide, 2) internally reflects at the slide surface, and 3) reflected beam again crosses the oil layer. The central spot of this series must be positioned over the center of the microscope objective; this is most easily achieved by adjusting the position of the laser focusing lens using the micrometer adjustment screws (Figure 2-12). The evanescent field region will be observable under the microscope via scattering due to imperfections on the slide surface within the flow cell. It should appear uniform in brightness and not contain interference fringes. If necessary, the axial position of the laser focusing lens can be adjusted to alter the shape of the evanescent field region. Laser power should be adjusted so that signal intensities are as high as possible, without saturating the EMCCD detector. For 100 ms exposures, ~7 mW of donor excitation power has proved sufficient.

If all optics of the microscope have been adjusted correctly then the evanescent field should excite molecules over the entire field of view; individual molecules will appear as distinct

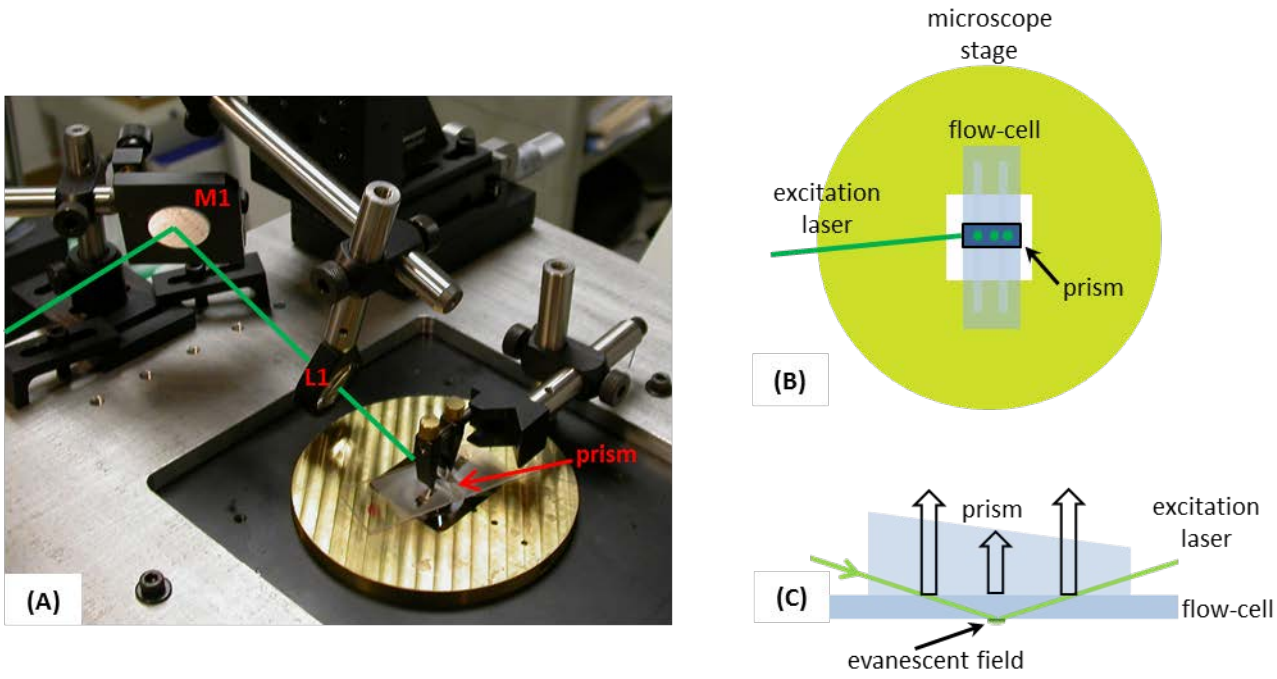

Figure 2-12: Establishing the evanescent field for smFRET excitation.

(A) Close up of the microscope stage, showing the optical path of the incident excitation laser beam. Mirror M1 and lens L1 must be adjusted so that the beam enters the prism and encounters the flow-cell at greater than the critical angle defined by the flow-cell slide/buffer interface. Fine adjustment of L1 is required to position the evanescent field above the microscope objective for imaging. **(B)** Looking down on the prism from above, three spots produced by scattered laser light are visible (spots not drawn to scale). **(C)** These spots are due to scattering from (1) the incident laser beam as it crosses the prism-oil-flow-cell interface, (2) the evanescent field produced by total internal reflection of the beam, and (3) the reflected laser beam as it again crosses the prism-oil-flow-cell interface. The position of L1 must be fine-tuned to set the middle spot (evanescent field) over the microscope objective.

spots several pixels in diameter, with a SNR between 10-20 (Figure 2-13). Before recording data, it is important to check that the signal intensities are not saturating the EMCCD's range, which indicates either incorrect EMCCD settings, or an excitation laser power that is too high (Figure 2-14). Note that we typically observe a small additional background signal (in addition to the background signal produced by dark current) when either of the excitation lasers is on, which is presumably due to insufficient rejection of scattered laser light. If the microscope has been properly tuned, this background should be at least an order of magnitude lower than the fluorescence signals of interest, and is dispatched via a thresholding step in the data analysis stage (see section 2.2.3).

In order to improve peak finding during the data analysis stage, we implement a software-based adaptive mapping procedure that corrects for differences in distortion between the donor and acceptor signal paths. This mapping procedure requires that calibration data be collected using a sample consisting of Neutravidin-coated, 40 nm fluorescent spheres (TransFluoSpheres, Molecular Probes). These spheres yield fluorescence signals at both donor and acceptor wavelengths simultaneously. A 1 to 10,000 dilution of fluorescent spheres generally produces optimal coverage of the field of view; alternatively, images from multiple regions can be superimposed to achieve uniform coverage. These calibration images are fed as input to the IDL script 'roughfretmap.pro,' which requires the user to manually identify three signals on the donor side of the image and their corresponding signals on the acceptor side. This script generates a set of parameters for a rough, affine mapping of the donor onto the acceptor region. These parameters, as well as the calibration images are then used as input by 'tif_nxgn1_cm.pro,' to generate a polynomial warping function to more accurately map the donor to the acceptor region.

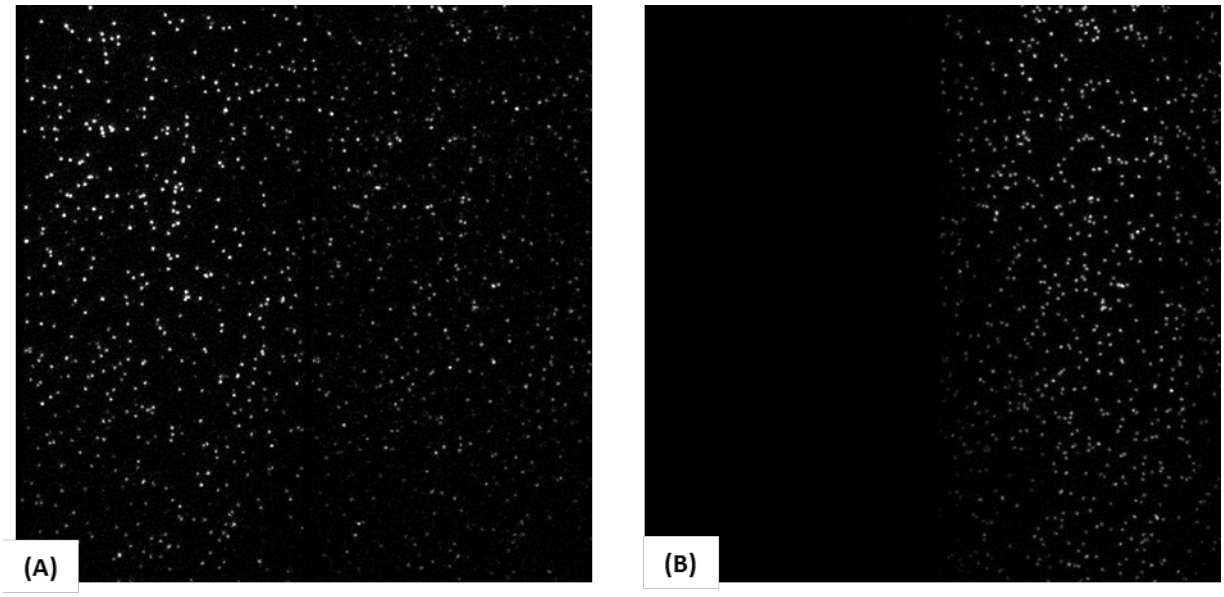

Figure 2-13: Sample smFRET data images.

(A) Image acquired with donor excitation. Proper laser and EMCCD settings result in a uniform evanescent field and robust images. Image frames actually contain two copies of the same field of view (FOV): the left half shows the FOV imaged through donor emission optics, and the right half shows the FOV imaged through acceptor emission optics. Careful preparation of flow-cell surfaces and correct sample concentrations (typically 50 pM – 200 pM) ensure that signals are neither too crowded nor too sparse. Ideally, signal density should be such that the peak finding software identifies 200 – 350 signals per frame. **(B)** The same experiment under direct acceptor excitation. If the output power of both the donor and acceptor excitation lasers have been optimally matched then directly excited acceptor signals should be approximately as bright as directly excited donor signals. This function is used during the data analysis stage (described in section 2.2.3) to more accurately locate signal pairs.

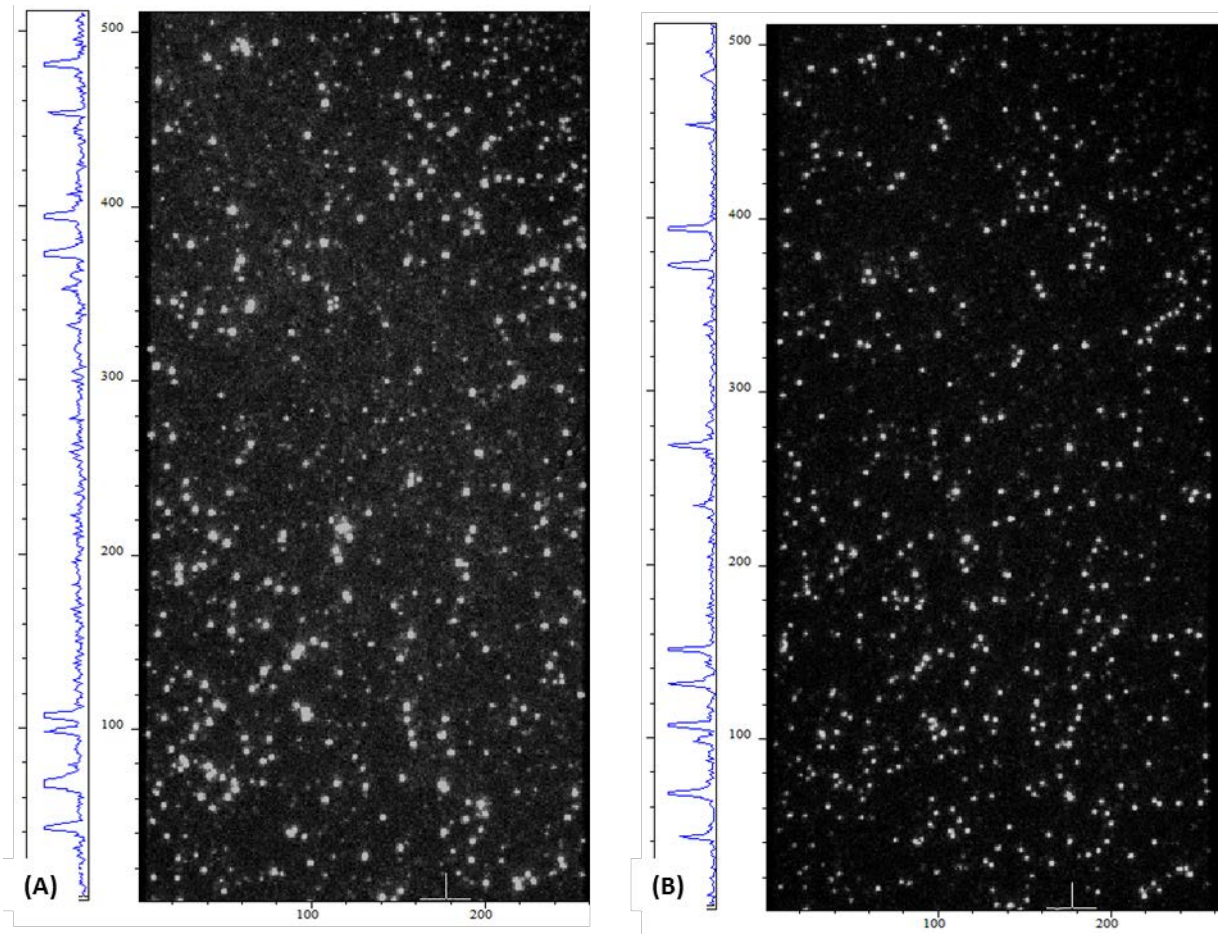

Figure 2-14: Saturation of EMCCD yields poor data quality.

(A) This data was taken with a poor combination of EMCCD settings and excitation laser power. The intensity plot to the left of the image shows signal intensity for a single row of pixels in the image, and signal peaks exhibit flat plateaus that are diagnostic of EMCCD saturation. These saturated signals will result in incorrect EFRET calculations. **(B)** Data from the same experiment, but with laser power lowered so that saturation does not occur. Signal peaks (from the same row of pixels as in **(A)**) are sharply defined.

In order to use ALEX effectively, the donor and acceptor lasers must be adjusted so that the evanescent field regions they produce coincide with each other. This is done by first aligning the beams so that they are co-axial when they emerge from the laser-combining dichroic (Figure 2-8). This will typically bring the two evanescent field regions relatively close to each other; further adjustment is achieved by 'walking' the acceptor field position by adjusting the tilt of the two mirrors in its path. Donor and acceptor laser power must also be adjusted so that the donor and acceptor fluorescence signals are of comparable magnitude; in general, we have found that the acceptor laser power should be about 20-30% less than that of the donor in order to achieve this parity. It may also be necessary at this stage to adjust the pulse-shaping circuit described in section 2.2.1.1 in order to ensure that acceptor molecules are not directly excited at the same time as the donors. At high time resolutions there is sometimes a slight overlap in fluorescence signals due to residual acceptor excitation; this can be remedied by decreasing the duration of the acceptor laser control pulse. The difference in the relative fluorescence intensities of directly excited donors and directly excited acceptors will affect the calculated S values during data analysis. Ensuring that these intensities are comparable will yield signal clusters that are distributed in the central region of an S versus EFRET plot. This in turn will make identification of bona fide FRET pairs easier.

2.2.3 Data Analysis

Using the microscope described in sections 2.2.1-2, we collect 14-bit tiff image stacks using Andor's proprietary imaging and CCD-control software package (Andor Solis). The size of the resulting image stack files depend on the imaging time resolution and the length of time that image data is collected. Image stack files are typically spooled directly to disk and must be

processed by a 90° rotation and horizontal flipping of the frame data. This is accomplished with the Matlab (MathWorks) script ‘tiffdir.m’. These transformed image stacks serve as the raw data for smFRET analysis and are further processed according to the procedure outlined in Figure 2-15.

Individual fluorophore fluorescence signals are first recovered from raw data image stacks using two IDL (ITTVis, now Exelis) scripts, both modified from original code kindly provided by the laboratory of Dr. Taekjip Ha. The IDL script ‘p_ffp_both_all.pro’ averages the first ten frames of a given image stack and uses this frame to search for candidate signal peaks. First the left half of this averaged frame (corresponding to the microscope field of view as imaged through donor-fluorophore optics, described in section 2.2.1) is mapped onto the right half (acceptor-signals) using polynomial transformation parameters determined by the mapping calibration described in section 2.2.2. The resulting search frame is half the horizontal size of a frame acquired from the CCD, and represents the sum of the donor and acceptor signals for all fluorophore pairs. Thus, regardless of whether a fluorophore pair is in a low-FRET state (*i.e.*, mostly donor-signal), high-FRET state (i.e. mostly acceptor-signal), or intermediate-FRET state (*i.e.*, roughly equal donor and acceptor signal), it will appear in the search frame with equal intensity. The search frame is then thresholded at a user-defined level; all pixels that are less than the threshold are set to a value of zero. The value of this threshold should be chosen so that it is well-above the typical CCD background level of a smFRET experiment (~200-300 counts, in our system), but well below the range of bona fide fluorophore fluorescence signals. Typically, a threshold value of 1000 meets these criteria. Next, ‘p_ffp_both_all.pro’ searches for candidate signals in the thresholded search frame by identifying the pixel coordinates of isolated patches of maximum local intensity. Each patch is assessed on the basis of size and how well it is described

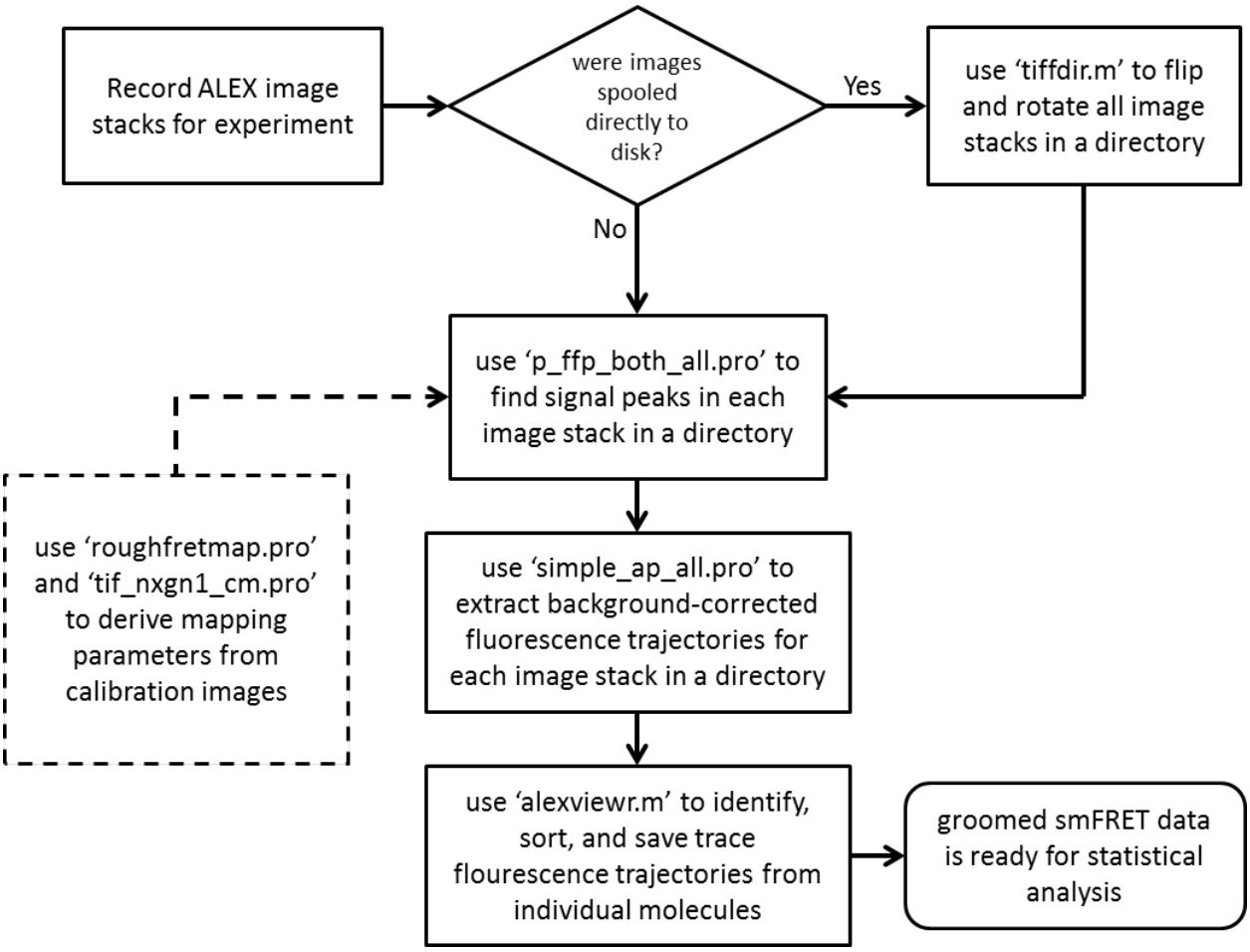

Figure 2-15: Flowchart of smFRET data analysis process.

Program names with a .m extension are matlab scripts; program names with '.pro' extensions are IDL scripts [all code is attached to ETD]. The mapping step (dashed box) does not need to be carried out every time data is taken.

by a Gaussian intensity distribution. True single-pair molecular signal sources should image as optical point-sources, with a nearly Gaussian intensity profile whose diameter is determined (approximately) by the diffraction limit (~300nm in the case of our optics and excitation wavelength). Signal patches that are significantly larger than this, or that fail to exhibit a Gaussian intensity distribution are likely either aggregations of dye molecules or other artifacts, and are excluded from further analysis. At the end of its execution, 'p_ffp_both_all.pro' outputs an indexed list of candidate signal coordinates; each set of donor signal coordinates is paired with the coordinates (transformed according to the mapping parameters described in section 2.2.2) of its corresponding acceptor signal.

This list of donor/acceptor signal coordinates becomes the input for the second IDL script, 'simple_ap_all.pro,' which is responsible for extracting the fluorescence intensity trajectories for each donor/acceptor pair. This is accomplished by simply stepping through each image in the image stack and integrating the pixel values within a 5x5 box centered on the signal coordinates previously identified by 'p_ffp_both_all.pro.' Additionally, the local fluorescence background is removed from each signal at this stage (Fagerburg and Leuba, 2011). The result of this stage is a binary file containing the donor and acceptor fluorescence intensity values for each signal identified in the images, over the course of the entire image stack.

The final stages of data analysis consist of identifying and selecting bona fide smFRET signal traces from single fluorophore pairs, followed by statistical analysis appropriate to the experiment being performed. All of this is done in Matlab using custom written scripts. The selection of traces is facilitated using the script 'alexviewr.m' (source code for this program is reproduced in Appendix B). This script reads in all of the signal intensity data output by 'simple_ap_all.pro' and displays a user-friendly interface for viewing/selecting trace data for

individual molecules one-at-a-time (Figure 2-16). It splits the signal data into two sets of donor/acceptor fluorescence signal trajectories- one corresponding to the frames recorded under donor-laser excitation, and the other corresponding to frames recorded under acceptor-laser excitation. In addition to displaying these separate trajectories, the script

also displays the calculated FRET trajectory (using $E_{FRET} = \frac{I_A}{I_D + I_A}$) for the given molecule, and renders a scatter-plot of S versus FRET. This latter feature makes it easy to identify signals that originate from a single molecular dye pair. As described in section 2.2.1.1, these signals occupy a defined region of the S versus FRET scatter-plot centered around S ~ 0.5; if quality of the data is high, the script can be configured to automatically reject molecules whose S values are outside of a proscribed range. Typically, however, the user will view traces from all of the molecules individually, saving those that exhibit the characteristics of single-pair signals (i.e. good S range, single-step photo-bleaching, and anti-correlated donor/acceptor dynamics). The 'alexviewr.m' script returns a matrix of fluorescence intensity trajectories for each of the molecules that the user has elected to save. These values can be subsequently used to calculate FRET and/or S values, which are then typically used to generate population histograms. The trajectory output data from 'alexviewr.m' is also amenable for use with vbFRET, a Matlab tool that analyzes FRET trajectories using a hidden Markov model to identify molecular states (McKinney et al., 2006; Bronson et al., 2009).

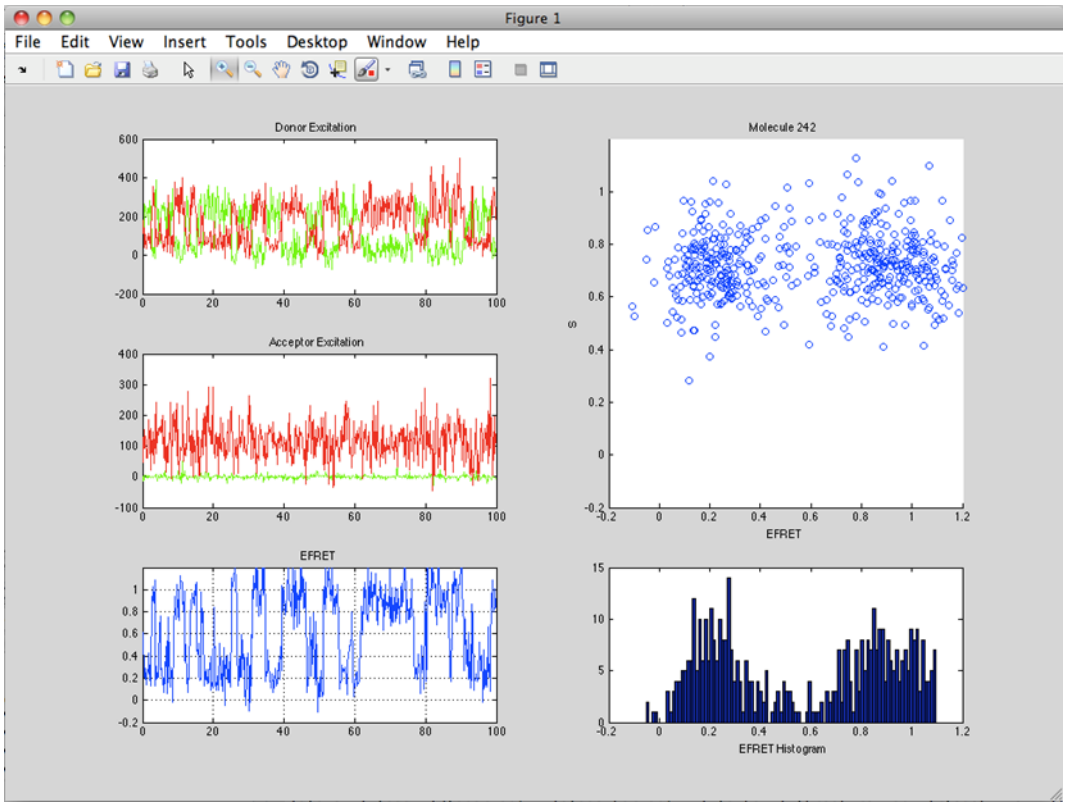

Figure 2-16: Graphical user interface for smFRET trace selection software ('alexviewr.m'). This software displays fluorescence signal trajectories for individual molecules one at a time, and allows the user to save or reject each trace. It also allows the selection of a user-defined portion of a trace, as well as specifying a particular molecule to view. Fluorescence signal trajectories from either donor or acceptor excitation are shown in separate panels. The calculated E_{FRET} trajectory is displayed, as well as an S versus E_{FRET} scatterplot and a histogram of E_{FRET} values for the current molecule.

3.0 SMFRET STUDIES OF RECA FILAMENTS AND PCRA

3.1 INTRODUCTION

Helicases play essential roles in DNA replication, repair, recombination, and transcription (Singleton et al., 2007; Lohman et al., 2008). Whereas the major replicative helicase in bacteria, DnaB, actively converts double-stranded DNA (dsDNA) at the replication fork into single-stranded DNA (ssDNA) for use as a template by the DNA polymerase, other helicases such as PcrA and UvrD facilitate replication by removing various protein barriers from the DNA (Maples and Kushner, 1982; Petit et al., 1998; Benkovic et al., 2001; Petit and Ehrlich, 2002; Florés et al., 2005; Veaute et al., 2005; Bidnenko et al., 2006; Anand et al., 2007; Lestini and Michel, 2007; Fonville et al., 2010). One such barrier is the RecA nucleoprotein filament, which is formed during recombination or when RecA binds to ssDNA gaps to facilitate DNA repair. If these filaments persist on the DNA, they can impede an advancing replisome (Petit and Ehrlich, 2002; Veaute et al., 2005; Lestini and Michel, 2007; Fonville et al., 2010). Thus, unregulated RecA nucleoprotein filaments can be detrimental to a cell and mechanisms must exist to regulate RecA function.

One such mechanism involves disruption of RecA filaments by DNA helicases. For example, the DNA helicase PcrA present in Gram-positive bacteria such as *S. aureus* and *G. stearothermophilus* disrupts RecA filaments by displacing them from the DNA (Anand et al., 2007; Park et al., 2010). The homologous UvrD helicase from the Gram-negative bacterium E. coli also inhibits RecA-mediated DNA strand exchange and disrupts RecA filaments (Veaute et al., 2005; Centore and Sandler, 2007). This regulation of RecA function likely supports bacterial growth and survival since suppressors of a *pcrA* knock-out have been isolated in the recFOR genes that are involved in RecA-mediated recombination in Bacillus subtilis (Petit and Ehrlich, 2002). Moreover, conditional PcrA mutants of *B. subtilis* exhibit a hyper-recombinogenic

phenotype, and E. coli UvrD mutants are rescued by PcrA (Petit et al., 1998; Petit and Ehrlich, 2002). It is known that the ATPase and helicase activities of *S. aureus* PcrA and *Mycobacterium tuberculosis* UvrD are not essential for inhibiting RecA functions (Anand et al., 2007; Singh et al., 2010; Williams et al., 2011). Nevertheless, a recent report suggests that RecA filament disruption results from translocation of PcrA on ssDNA (Park et al., 2010).

The RecA recombinase promotes ATP-dependent joint-molecule formation and the exchange of DNA strands between homologous DNA molecules (Cox, 2007a). RecA binds to ssDNA in the presence of ATP to form helical nucleoprotein filaments that serve as the scaffolding upon which homologous recombination occurs (DasGupta et al., 1981; West et al., 1981; Cox, 2007b). ATP binding, hydrolysis and product release play critical roles in RecA filament stability and function (Kowalczykowski and Eggleston, 1994). Binding of ATP to a RecA-DNA complex leads to the formation of the high-affinity ssDNA-binding state of RecA required for DNA strand exchange and other DNA-repair related functions (Menetski et al., 1990). ATP hydrolysis by RecA induces the low-affinity RecA-ADP ssDNA-binding state required for its dissociation during subsequent stages of recombination. Since the nucleotide-bound state of RecA determines its affinity for ssDNA, we hypothesized that the ATPase activity of RecA may play a major role in the disruption of nucleoprotein filaments by regulatory proteins such as PcrA.

Here, we have used PcrA from *G. stearothermophilus* and single-molecule fluorescence approaches to study the mechanism of disruption of RecA nucleoprotein filaments. We demonstrate that ATP hydrolysis by RecA is essential for PcrA-mediated displacement of the recombinase from ssDNA. Our results show that the conversion of RecA from its high-affinity

DNA binding state (ATP-bound) to the low-affinity DNA binding state (ADP-bound) is required for the disruption of the RecA filament by a translocating PcrA.

3.2 MATERIALS AND METHODS

3.2.1 Proteins

The *G. stearothermophilus* PcrA clone was obtained from Dale Wigley, and sub-cloned into a pET-14b plasmid with an N-terminal His_6 tag. It was purified as described earlier after confirming the DNA sequence (Chang et al., 2002). *E. coli* RecA protein was a kind gift from Pierro Bianco. The RecA K72R overexpression clone was a kind gift from Michael Cox. Overexpression and purification of RecA and the RecA K72R mutant was carried out as reported earlier for wild-type RecA (Bianco and Weinstock, 1996). Protein purity was assessed using Coomassie-stained gels and concentration was measured using UV spectroscopy (on a Nanodrop instrument).

PcrA functionality was verified using a helicase unwinding assay. Reactions containing 20 nM PcrA and ~4 nM of tailed duplex DNA substrates (with either 5' or 3' ssDNA tails) were incubated 37 C for the indicated amounts of time (Figure 3-1). PcrA was incubated with DNA substrates for 5 min after which the unwinding assay was initiated by adding 3 mM ATP and 12 nM of unlabeled 18 base common oligonucleotide. Substrates were prepared and annealed similarly to previously described work (Anand and Khan, 2004), however IR dyes (IDT) were employed rather than radioactive labeling of substrates. The products of the reaction were

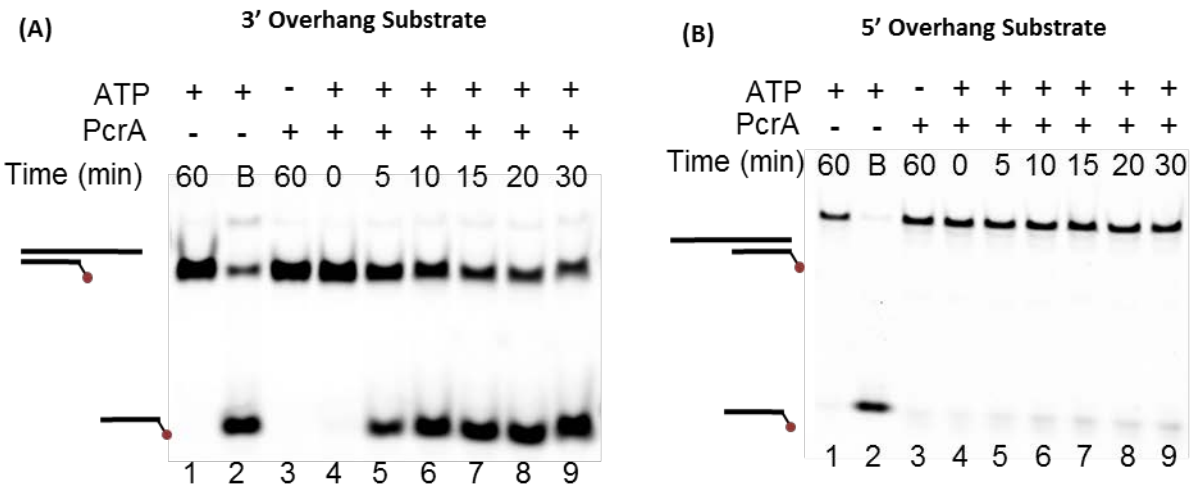

Figure 3-1: PcrA directional unwinding assay gels.

(A) PcrA 3' to 5' unwinding activity is robust. **(B)** PcrA 5' to 3' unwinding activity is effectively non-existent, reflecting the directional nature of the translocase. Lane 2 in both gels contains substrate that was boiled at 95C for 5 minutes before loading.

resolved by electrophoresis on 10% native PAGE as previously described (Anand and Khan, 2004). Gels were then imaged using the Li-Cor Biosystems Odyssey scanner that detects IR-dye.

The ATPase activity for both wild-type RecA and K72R were compared using a NADH spectrophotometric assay (Figure 3-2) (Campbell and Davis, 1999b). 1 μM of each protein was incubated either in the absence or presence of ssDNA (a dT(40) substrate), and the change in NADH concentration was monitored using a Cary Eclipse Fluorescence Spectrophotometer.

RecA and K72R were further assayed for functionality using a strand-exchange reaction (Figure 3-2). The strand exchange assay was performed as described previously (Anand et al., 2007) except that the dsDNA substrate was radioactively end-labeled using T4 polynucleotide kinase (NEB) and Υ^{32P}-ATP (GE Life Sciences).

3.2.2 DNA Constructs

All oligonucleotides were synthesized by Integrated DNA Technologies. Fluorescent dyes were covalently attached to either the 5' or 3' ends of specific sequences. Sequences of all oligonucleotides used in this work appear in (Table 3-1). The principal construct used in smFRET studies, PcrA-Spool, was formed by annealing the park(dT40)Cy5 and park(dT40)Cy3 oligonucleotides at a 1:1.1 ratio in a small volume (10 ul) of T50 buffer (10 mM Tris-HCl pH 8, 50 mM NaCl). This reaction was heated at 94 C for 2 minutes then allowed to cool slowly on the benchtop overnight.

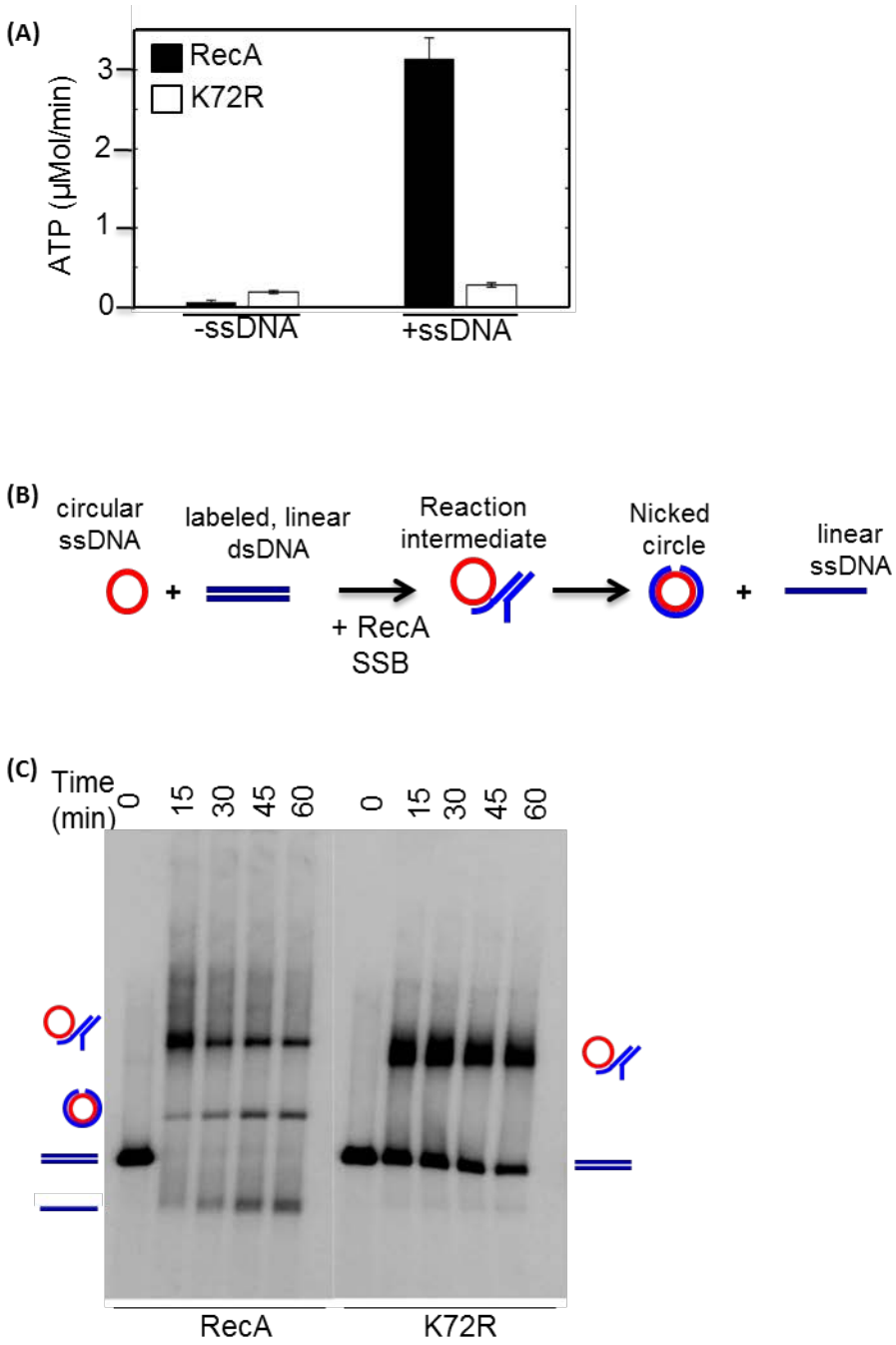

Figure 3-2: Comparison of wild-type RecA with ATPase mutant K72R.

(A) K72R exhibits greatly reduced ssDNA-dependent ATPase activity compared with wild-type RecA. **(B)** Schematic representation of RecA-mediated DNA strand exchange reaction. RecA forms an active filament on circular ssDNA that facilitates strand exchange from a linear,

homologous dsDNA substrate. Both strands of the dsDNA substrate are radioactively labeled, which allows tracking of the reaction products. **(C)** Comparison of DNA strand exchange activity of wild-type RecA and K72R mutant. Wild-type RecA is able to drive the strand exchange to completion, as evidenced by the increasing amount of ssDNA produced over time. K72R is able to initiate the strand exchange reaction by forming a joint molecule, but is unable to drive the reaction to completion.

Table 3-1: Oligonucleotide sequences used in this work.

Unwinding assay labeled common oligonucleotide
5'-/IR-Dye/-GCC TCG CTG CCG TCG CCA-3'
Unwinding assay 3' overhang oligonucleotide
5'-TGG CGA CGG CAG CGA GGC TTT TTT TTT TTT TTT TTT TT-3'
Unwinding assay 5' overhang oligonucleotide
5'-TTT TTT TTT TTT TTT TTT TTT GGC GAC GGC AGC GAG GC-3'
park(dT40)Cy5
5'-/biotin/-TGG CGA CGG CAG CGA GGC -/CY5/-3'
park(dT40)Cy3
5'-/CY3/-TTT TTT TTT TTT TTT TTT TTT TTT TTT TTT TTT TTT TTT TTT TGC CTC GCT GCC GTC GCC A-3'

3.2.3 smFRET Experiments

All smFRET experiments were carried out in flow-cells described in section 2.2.2, and data was collected using the prism-based total internal reflection microscope described in section 2.2.1. The buffer conditions used were as previously described for studying RecA displacement by PcrA (Park et al., 2010) and consist of PcrA Buffer: (20 mM Tris-HCl pH 8; 10 mM KCl; 5 mM $MgCl_2$). All experiments were performed by first injecting 50-200 pM of PcrA-Spool substrate into prepared flow-cell and allowing this to incubate for two minutes. Excess oligonucleotides were removed by injecting several flow-cell volumes of PcrA buffer before subsequent injection of proteins. Additionally, imaging buffer composed of an enzymatic oxygen scavenging system and a triplet-state quencher was present, consisting of 0.04 mg/ml bovine catalase (Roche Analytics), 1 ug/ml Glucose Oxidase (Type VII, from *A. niger*; Sigma), 0.4% glucose (Sigma), and 2mM Trolox (Acros Organics). All experimental data was collected at room temperature using 100ms time resolution with ALEX.

Fluorescence signals for individual molecules were background corrected and FRET calculated for each frame as described in section 2.2.3. Normalized histograms were constructed from these data without any smoothing. We used consistent bin widths (0.02 E_{FRET} units/65 bins total) and range (E_{FRET} = -0.2 to 1.2) for all histograms; the number of points used to generate a histogram was typically >100,000. RecA disruption bar graph data was generated by summing the histogram data over all bins less than E_{FRET} = 0.43. The percentage of disruption was determined using % disruption = (r-p)/r, where r is the sum of histogram data from an experiment including RecA, but prior to the addition of PcrA, and p is the same sum after the addition of PcrA. The percentage of repetitive looping bar graph was generated by summing histogram data over all bins greater than E_{FRET} = 0.61 and calculating (p-r). These experiments

were repeated three times for each concentration of PcrA. Error bars in the graphs indicate the standard deviations for these triplicate measurements.

3.3 RESULTS

3.3.1 smFRET of RecA Filaments

The PcrA-Spool oligonucleotide construct consists of a short (18 nt) dsDNA duplex with a long (40 nts) 5' poly-dT tail (Figure 3-3). The terminal end of the 5' dT tail is labeled with a cyanine-3 (Cy3) dye molecule, while at the ssDNA/dsDNA duplex junction the opposite strand is labeled with a cyanine-5 (Cy5) dye molecule; together these form a matched donor(Cy3)-acceptor(Cy5) FRET pair. A biotin moiety at the other end of the duplex junction (and on the same strand as the Cy5 label) enables surface-tethering of the PcrA-Spool construct to the surface of the experimental flow-cell. Imaged in PcrA buffer with 1 mM ATP the construct exhibits a FRET population histogram with a mean at E_{FRET}~0.4.

The 5' ssDNA tail functions as a substrate for the nucleation and growth of RecA filaments; with a binding footprint of 3 nts, it is expected that up to 13 RecA monomers can polymerize on this region. Because RecA filament formation has been shown to extend the contour length of the DNA to which it binds (Stasiak and Di Capua, 1982), formation of such a filament should lead to a dramatic decrease in FRET. There is no reason why the nascent RecA filament could not extend into the dsDNA region of the PcrA-Spool construct, however since this region lies outside of the fluorescently labeled ssDNA such a dsDNA-RecA filament would not be expected to affect the measured E_{FRET}.

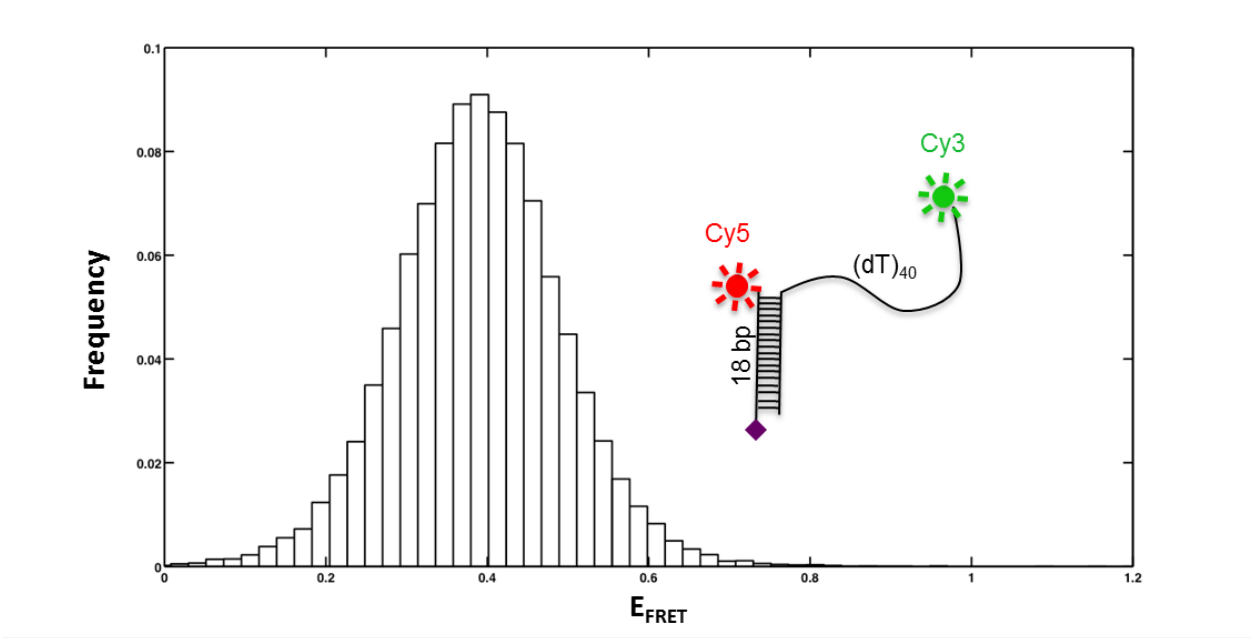

Figure 3-3: EFRET population histogram of PcrA-Spool substrate.

PcrA-Spool is the principal substrate for the smFRET experiments reported here; it consists of a short dsDNA region and a long, ssDNA dT tail labeled with a Cy3 dye. The strand opposite the dT tail is labeled with a biotin moiety (for surface immobilization) and a Cy5 dye, forming a FRET pair with Cy3. In standard buffer with 1mM ATP, the population E_{FRET} histogram for PcrA-Spool features a single peak at $E_{FRET} \sim 0.4$.

3.3.1.1 RecA and ATP Yield a Dynamic Filament Population

Incubation of RecA protein and 1mM (saturating) ATP with the PcrA-Spool construct leads to a substantial change in the shape of the FRET population histogram (Figure 3-4). This histogram is well fit by a dual-Gaussian distribution, with both peaks exhibiting similar widths (~0.07 E_{FRET} units). One peak features a mean of E_{FRET}=0.38 and likely results from naked PcrA-Spool molecules exhibiting unperturbed FRET. The second peak exhibits a much lower mean of EFRET=0.21, and is the result of RecA filament assembly on the PcrA-Spool substrate (Park et al., 2010). The assembly of a RecA nucleoprotein filament in the presence of ATP stretches the ssDNA by a factor of ~1.5 (Stasiak and Di Capua, 1982). This increase in extension between the Cy3 and Cy5 dye molecules leads to a reduction of FRET, producing the low-FRET peak in the histogram. The height of this peak depends on the concentration of RecA used; changing the concentration of RecA produces a correlated change in the amplitude low-FRET peak in the histogram. At high concentrations of RecA a higher proportion of molecules foster RecA filament formation, however an additional high-FRET population appears as well (Figure 3-5). This population is believed to result from nonspecific RecA interactions due to excess protein and was considered undesirable.

The coexistence of two peaks- one representing RecA filaments and the other representing naked DNA reflects the dynamic assembly and disassembly of RecA on DNA in the presence of ATP as shown previously (Figure 3-4B) (Shan and Cox, 1996; Yu et al., 2001; Park et al., 2010). At 1 uM RecA, the filament population peak is about the same height and width as the naked DNA population peak, suggesting dynamic equilibrium conditions where an approximately equal number of molecules are bound up in a nucleoprotein state as those that are not; we decided to use this physiologically relevant RecA concentration as the standard for our

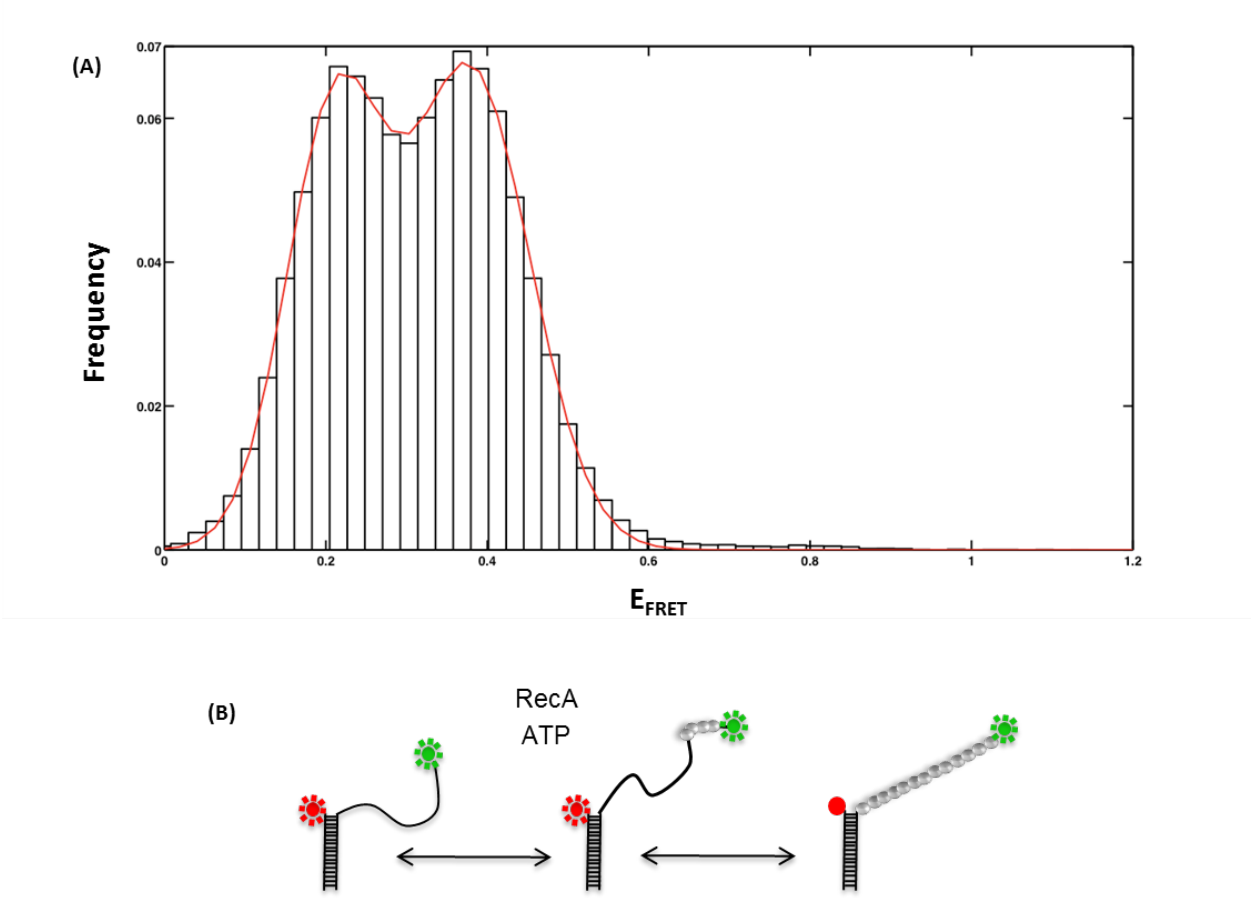

Figure 3-4: RecA and ATP form dynamic filament populations on PcrA-Spool substrate.

(A) E_{FRET} population histogram from an experiment with 1 uM RecA and 1 mM ATP. This histogram is well fit by two Gaussian distributions, one with a mean E_{FRET} =0.38 (i.e. naked DNA) and one with a mean E_{FRET}=0.21 (extended RecA filament formed on PcrA-Spool). **(B)** Model illustrating the dynamic RecA filament assembly and disassembly process responsible for producing the histogram in **(A)**.

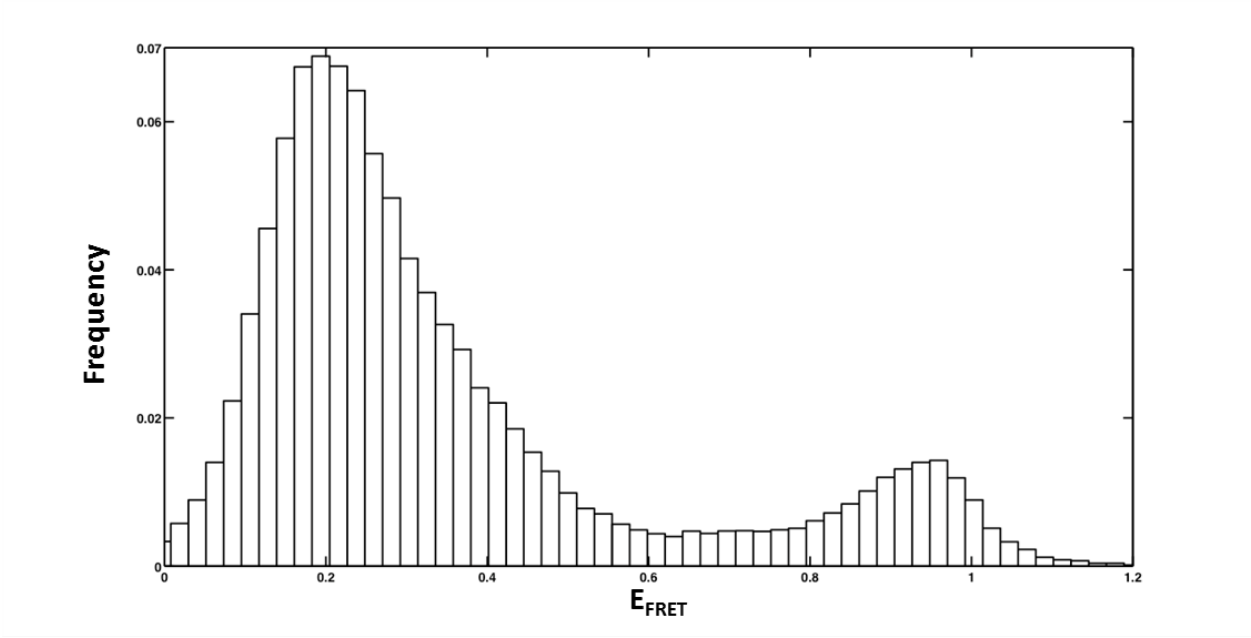

Figure 3-5: EFRET population histogram of PcrA-Spool, 6 uM-RecA, and 1 mM-ATP.

At high concentrations of RecA, a greater proportion of molecules foster RecA filaments, as evidenced by the greater peak height at low E_{FRET}. However, a high-E_{FRET} population also appears, suggesting that excess RecA in buffer is promoting additional interactions that complicate filament population analysis.

experiments. It is expected that the range of observed E_{FRET} values between 0.2 and 0.4 are due to filaments of varying lengths, as individual RecA monomers cycle on and off of the growing and shrinking filaments. We were not typically able to observe FRET changes indicative of individual monomer addition or dissociation.

3.3.1.2 Negligibly-Hydrolyzed ATP Analogs Lock RecA into More Stable Filaments

RecA filaments formed in the presence of the negligibly-hydrolyzed ATP-analog ATPγS have been shown to be stable for many hours (Weinstock et al., 1981; Watanabe et al., 1994). When 1 uM RecA and 1 mM ATPγS are incubated with PcrA-Spool, the resulting FRET population histogram exhibits a single, well-defined peak at E_{FRET}=0.2, indicating that all molecules have formed stable, extended nucleoprotein filaments (Figure 3-6). Interestingly, this peak is unchanged even if the flow-cell is rinsed with buffer and 1 mM ATP is subsequently injected, demonstrating that the RecA-ATPγS filament does not exchange bound nucleotide with free nucleotide in the buffer.

Similar results are obtained if ADP*AlF_4 is substituted for ATPγS (Figure 3-6). This ATP-analog mimics the geometrically strained bond in the γ-phosphate of the bound ATP molecule at the moment just before hydrolysis takes place (Chen et al., 2008).

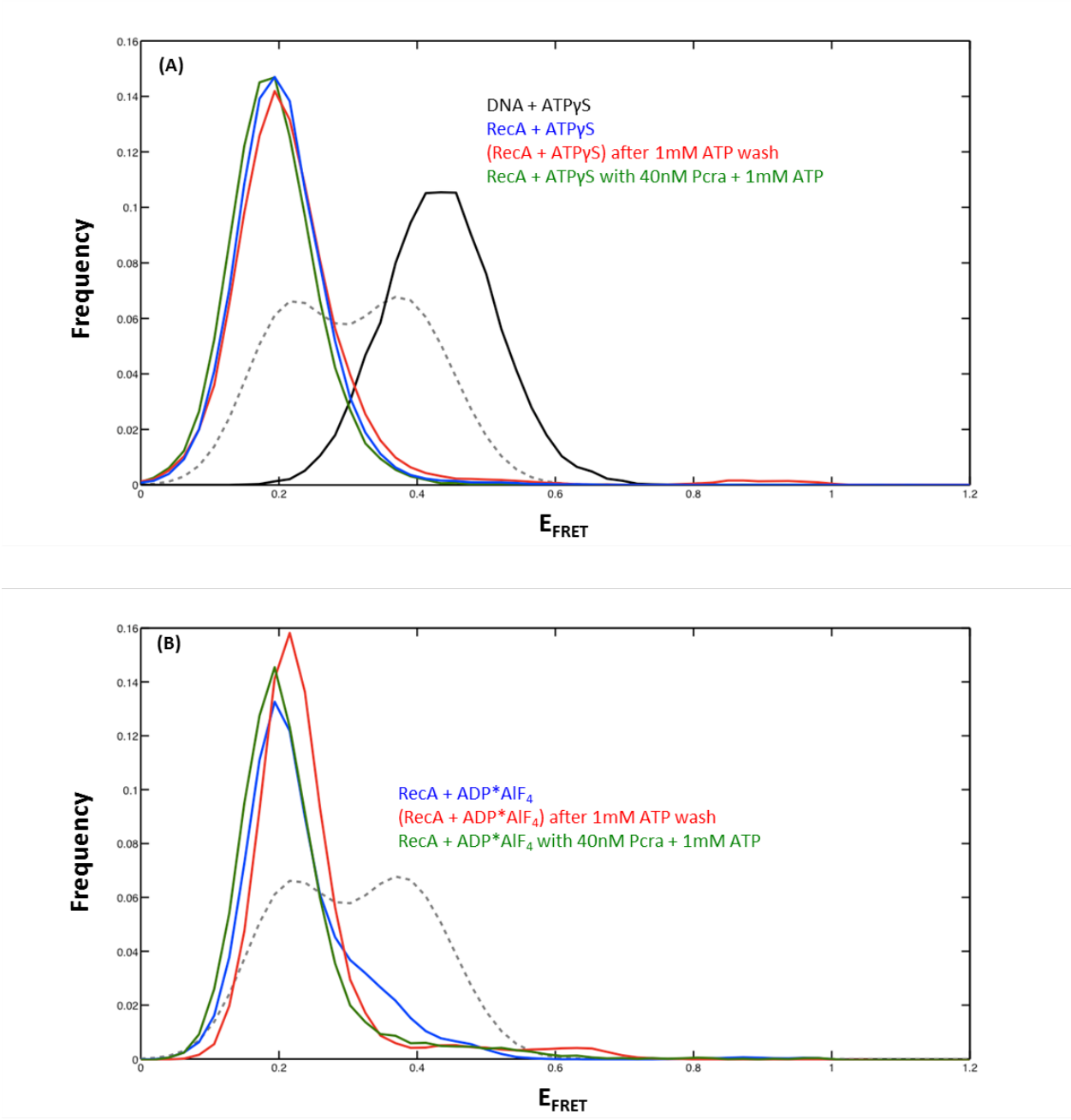

Figure 3-6: RecA and negligibly-hydrolyzed ATP analogs form stable filaments.

(A) Overlaid E_{FRET} population histograms from experiments with 1 uM RecA, 1 mM ATPγS. RecA and ATPγS form stable filaments that do not exchange nucleotide with solution and are not displaced by PcrA. Histogram of wild-type RecA and ATP from (Figure 3-4) is shown in

gray for comparison. **(B)** Overlaid E_{FRET} population histograms from experiments with 1 uM RecA, 5 mM ADP*AlF_4. RecA and ADP*AlF_4 produce similarly robust filaments that resist nucleotide exchange as well as displacement by PcrA. . Histogram of wild-type RecA and ATP from (Figure 3-4) is shown in gray for comparison.

3.3.1.3 A RecA ATPase Mutant Yields Stable Filaments with ATP

The RecA mutant K72R forms filaments *in vitro,* but shows a substantial decrease in ATPase activity compared to wild type protein (Figure 3-2) (Rehrauer and Kowalczykowski, 1993; Britt et al., 2011). When 1 uM of K72R is incubated with PcrA-Spool and 1 mM ATP the resulting FRET population exhibits a single, well-defined peak at E_{FRET}=0.2, indicating the formation of a stable filament (Figure 3-7). K72R also assembles stable filaments with ATPγS or dATP substituting for ATP. In all cases, the resulting FRET population histograms are identical (Figure 3-7). FRET histograms of K72R and 1mM ATP are indistinguishable from similar histograms produced from experiments with wild type RecA and ATPγS or ADP*AlF_4 (Figure 3-6), highlighting the role that RecA ATPase activity plays in destabilizing filament structure. Abolishing this activity, either by incubating RecA with negligibly-hydrolysable ATP analogs or by employing RecA mutants that lack ATPase activity leads to stable, long-lived filaments.

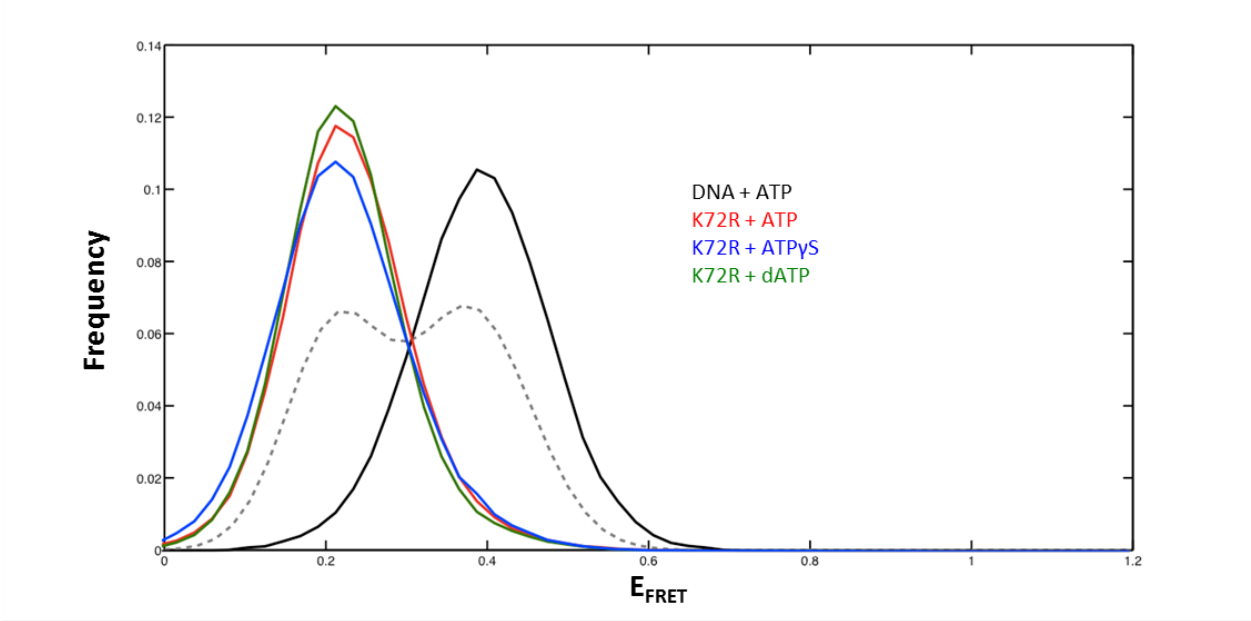

Figure 3-7: RecA ATPase mutant K72R forms stable filaments with a variety of nucleotide cofactors.

Overlaid E_{FRET} population histograms from experiments with 1 uM K72R and various nucleotide cofactors. K72R forms stable filaments on PcrA-Spool, even with ATP. . Histogram of wild-type RecA and ATP from (Figure 3-4) is shown in gray for comparison.

3.3.2 smFRET of PcrA and RecA Filaments

Having demonstrated the ability of our system to distinguish naked DNA from RecA filaments, we set out to investigate the interaction of the PcrA translocase with such filaments at the single-molecule level. In particular, we were interested in the requirements and characteristics of PcrA-driven disruption of RecA filaments. If translocation of PcrA on ssDNA were sufficient to disrupt RecA filaments, RecA displacement should be insensitive to its nucleotide-bound state. To test this hypothesis, we compared the disruption efficiencies of RecA filaments assembled in the presence of ATP with those assembled in the presence of ATPγS and ADP*AlF_4. We also assessed the ability of PcrA to remove the RecA ATPase mutant K72R from ssDNA.

3.3.2.1 PcrA Exhibits ATP-Dependent Looping on a ss/dsDNA Junction

PcrA has been shown to repetitively process the PcrA-Spool substrate; it remains stationary at the ssDNA/dsDNA junction and continuously reels in the ssDNA dT tail (Figure 3-8A). We call this continuous reeling process ‘repetitive looping' as described earlier (Park et al., 2010). At the single-molecule level, this repetitive looping activity of PcrA produces a saw-tooth pattern of dye emission intensities and corresponding E_{FRET} as it reels in the ssDNA tail in the 3’ to 5’ direction (Figure 3-8B). DNA translocation by PcrA bound at the ss/dsDNA junction brings the Cy3 donor dye at the 5’ end of the ssDNA tail into close proximity with the Cy5 acceptor dye at the junction, producing an increase in E_{FRET}. Upon completion of one round of PcrA translocation on the ssDNA tail, the release of the ssDNA allows it to return to its starting position and restores the E_{FRET} signal to the initial value of ~0.5. The frequency of this repetitive

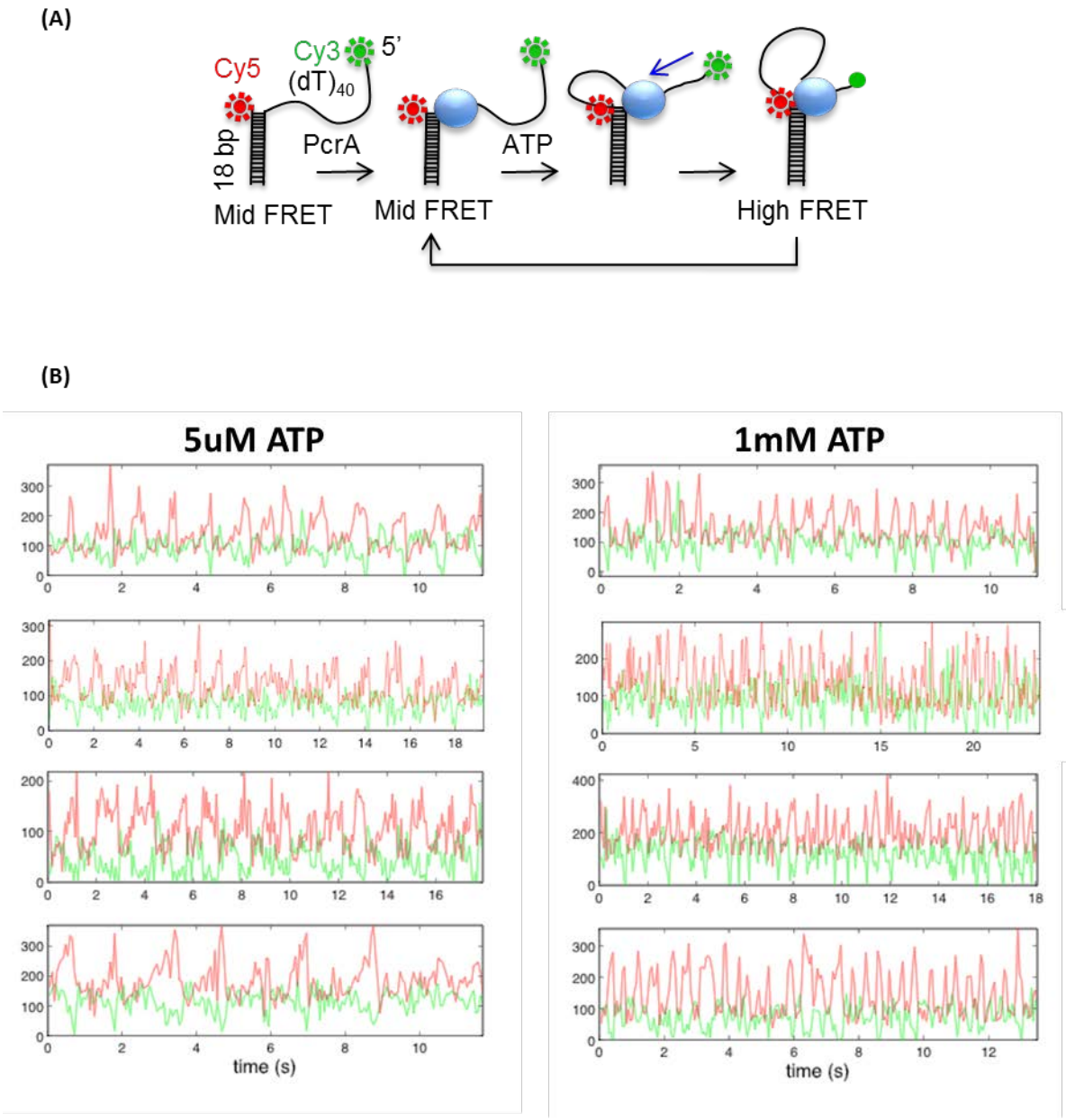

Figure 3-8: PcrA translocase repetitively processes PcrA-Spool substrate in an ATP-dependent manner.

(A) Model of the repetitive looping behavior of PcrA translocase. The PcrA molecule remains bound to the ssDNA/dsDNA junction and 'reels in' the ssDNA tail via its 3' -> 5' translocase activity. At the end of one cycle, the ssDNA tail is released and the process is repeated. **(B)** The rate at which PcrA reels in the ssDNA tail depends on the amount of ATP present. Fluorescence

intensity time traces (green = Cy3, red = Cy5) reveal that looping is slower at 5 uM ATP compared with 1 mM ATP.

looping is dependent on the concentration of ATP, with higher concentrations yielding faster looping behavior (Figure 3-8).

When assembled into a histogram, these smFRET traces yield two populations of molecules with peak E_{FRET} values of ~0.5 and ~0.8 (Figure 3-9). These populations reflect the cycling of the complex between low- and high-FRET states due to PcrA remaining bound at the ss/ds junction of the substrate and repetitively reeling in the ssDNA tail via its translocase activity. It should be noted that the binding of PcrA to the PcrA-Spool substrate introduces a slight shift from E_{FRET}~0.4 (unbound PcrA-Spool substrate) to slightly higher E_{FRET}~0.5 (Figure 3-9); we believe the reason for this due to the isometric stabilization of the Cy5 dye due to the protein induced fluorescence enhancement (PIFE) effect (Myong et al., 2006). The PIFE effect leads to a small fluorescence enhancement of some fluorophores (including both Cy3 and Cy5) when a protein is nearby. It is likely that PIFE also affects the Cy3 signal in our substrate (due to proximal binding of RecA in a fully assembled filament), but this will result only in slightly lowering the observed E_{FRET} for RecA filaments and is not expected to complicate our analysis any further.

3.3.2.2 PcrA Displaces RecA Filaments in a Concentration-Dependent Manner

The addition of PcrA to preformed RecA-ATP filaments reduces the population of low-FRET molecules (FRET$\leq$ 0.2); two populations of molecules with peak FRET values of 0.5 and 0.8 appear under these conditions, which reflect the displacement of RecA by PcrA and the subsequent repetitive looping of ssDNA by the translocase (Figure 3-10). The efficacy of this displacement activity was found to increase with increasing PcrA concentration (Figure 3-11). A two-way ANOVA with triplicate measurements was performed on the data, revealing a significant difference between WT and K72R RecA on both percent RecA filament disruption

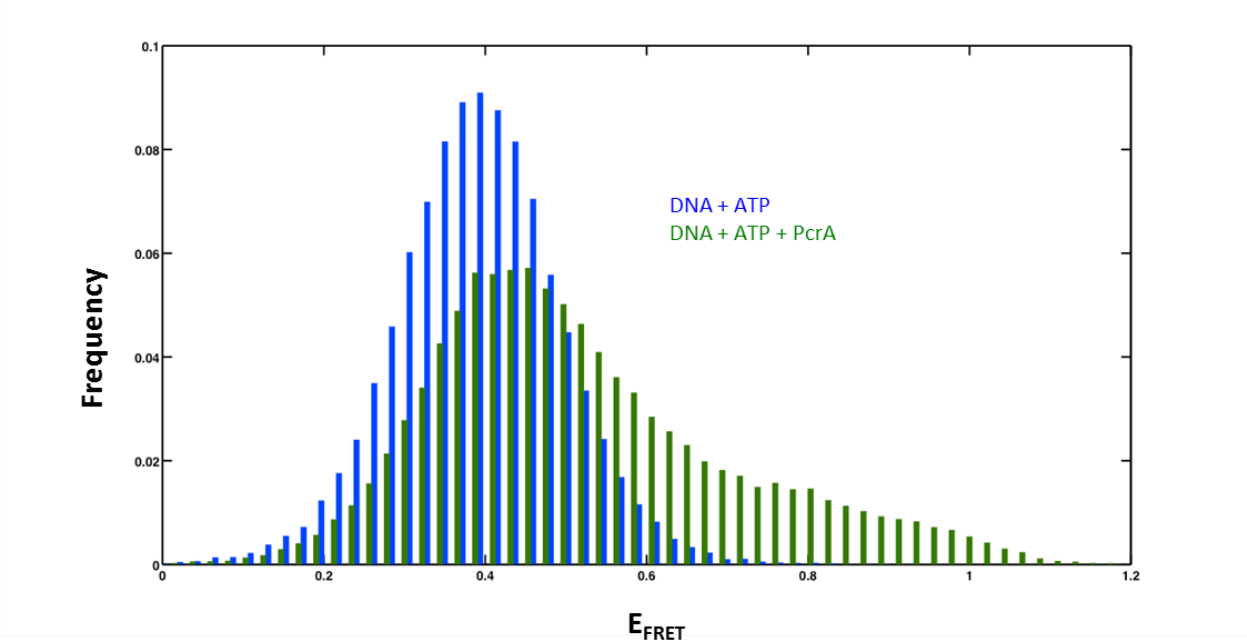

Figure 3-9: EFRET histogram of PcrA looping behavior on PcrA-Spool substrate.

When looping traces like those in (Figure 3-8B, 1 mM ATP) are used to generate an E_{FRET} histogram, the resulting distribution features a peak that is slightly shifted from E_{FRET}~0.4 (naked PcrA-Spool substrate) to higher E_{FRET}. Additionally, the presence of an extended population out to high-E_{FRET} reflects the looping of the PcrA-Spool ssDNA tail by PcrA.

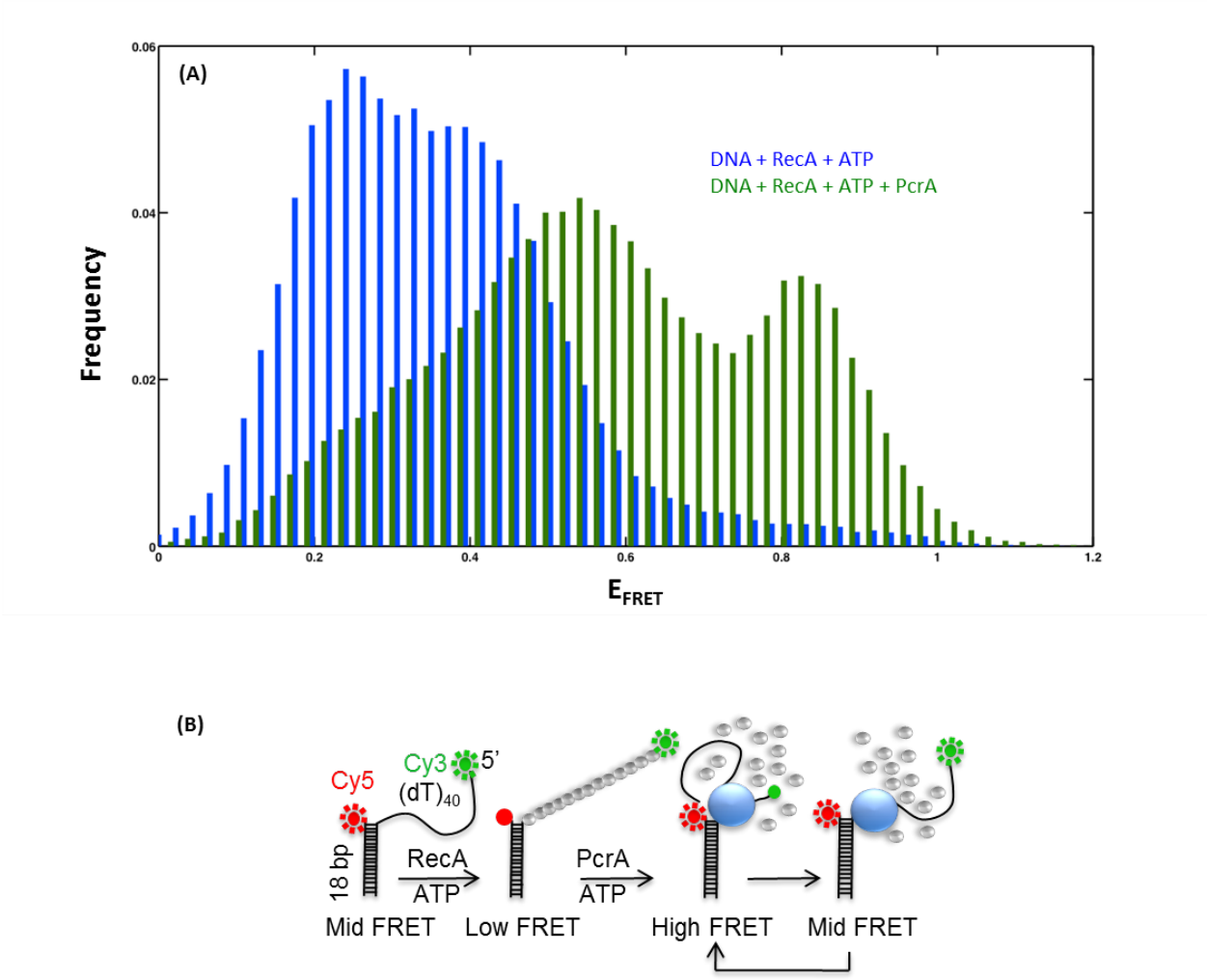

Figure 3-10: PcrA disrupts RecA filaments in vitro.

(A) E_{FRET} population histograms from an experiment with 1 uM RecA, 1 mM ATP, and 20 nM PcrA. Addition of 20 nM PcrA leads to a large decrease in peak height for the low-E_{FRET} population (RecA filaments), and a concomitant increase in high-E_{FRET} population due mostly to repetitive looping of PcrA-Spool. **(B)** Proposed model showing PcrA-driven disruption of RecA filaments aided by the translocase activity of PcrA.

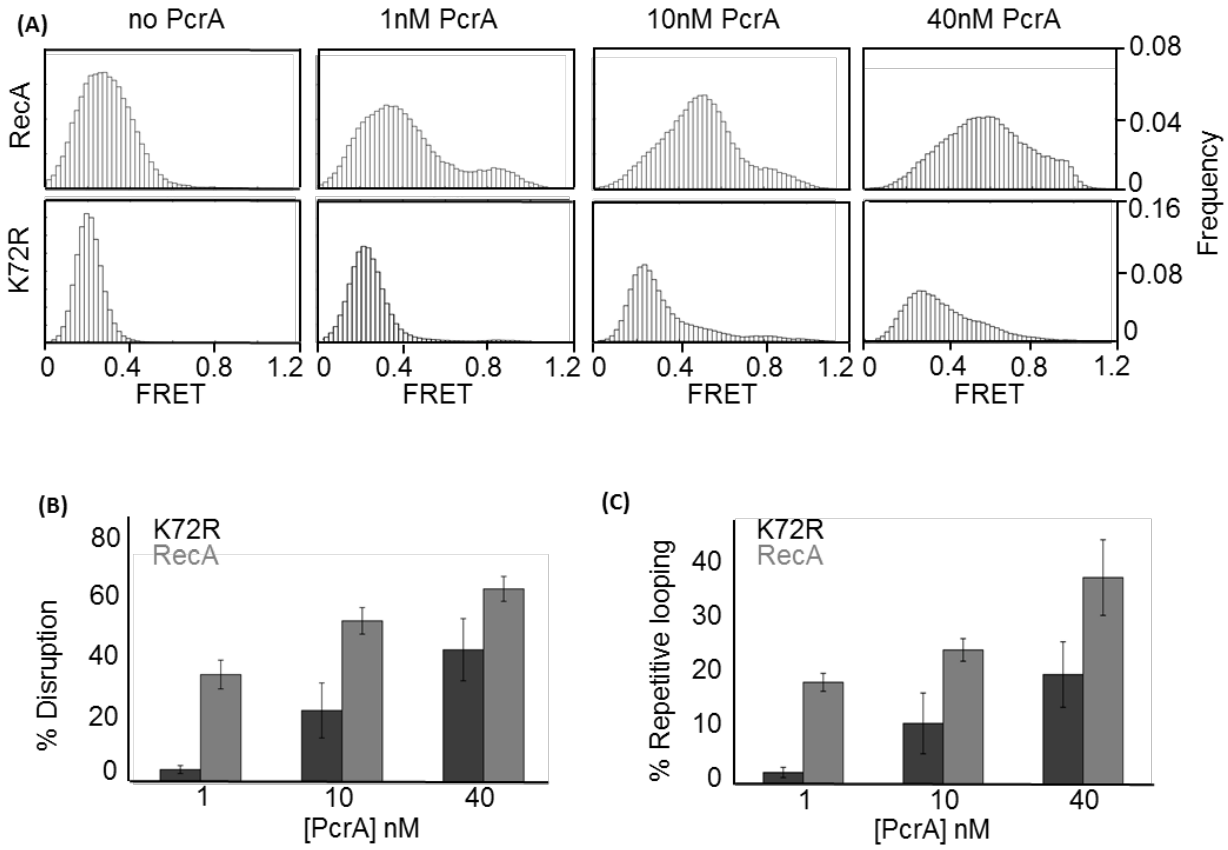

Figure 3-11: Comparative disruption of RecA or K72R filaments by different concentrations of PcrA.

(A) E_{FRET} histograms showing the effect of increasing PcrA concentrations on an initial population of either RecA filaments (top row) or K72R filaments (bottom row). When incubated with RecA filaments, PcrA causes a significant decrease in the filament population, and a corresponding increase in the E_{FRET} population due to repetitive looping. In contrast, K72R filament populations are decreased to a lesser extent, and exhibit a comparatively smaller high-E_{FRET} population. PcrA concentrations above 40nM were not tested because of the risk of dimerization. **(B)** Quantification of experiments represented in **(A)**, showing the greater extent of PcrA's filament disruption activity on RecA compared to K72R filaments. **(C)** Quantification of

experiments represented in **(A)**, showing the amount of high-E_{FRET} population exhibited in RecA or K72R experiments. This population is due to PcrA's looping behavior and is reduced in the K72R experiments. Details concerning the construction of these bar graphs can be found in section 3.2.3.

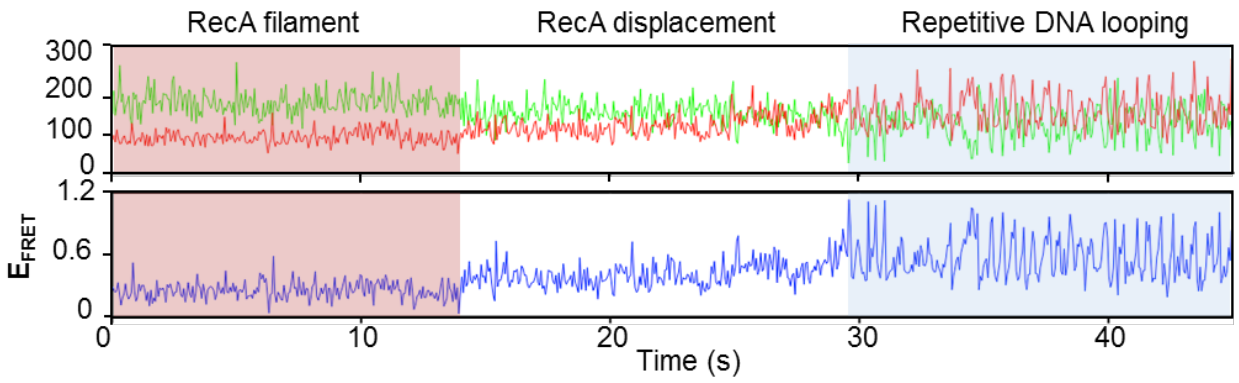

Figure 3-12: smFRET trace of PcrA disrupting a single RecA filament.

An exemplary time-trajectory showing a single RecA filament disruption event; individual fluorescence intensities (green = Cy3, red = Cy5) are shown on top, and the calculated E_{FRET} values are shown below in blue. The reporter molecule (PcrA-Spool) begins in a low-FRET state representative of an assembled RecA filament (red-shaded region). Over a 15 s period the system moves through mid-range E_{FRET} as RecA molecules are displaced from the DNA by PcrA, after this the trace shows PcrA looping of the ssDNA tail of PcrA-Spool (blue-shaded region), indicating that all RecA has been removed.

[F(1,12)=79.4, p=1.2e-6] and percent spooling by PcrA [F(1,12)=59.3, p=5.6e-6]. The concentration of PcrA had a significant effect on both percent RecA filament disruption [F(2,12)=41.3, p=4.2-6] and spooling by PcrA [F(2,12)=27.2, p=3.5e-5]. Furthermore, there was no interaction between type of RecA on the PcrA concentration-dependent response of either RecA filament disruption [F(2,12)=1.2, p=0.34] or spooling by PcrA [F(2,12)=0.40, p=0.67]. PcrA concentrations were kept below 40 nM, because the enzyme is believed to dimerize above this range (Niedziela-Majka et al., 2007; Yang et al., 2008).

In exemplary time traces, disruption of RecA filaments was observed as a gradual increase in the fluorescence intensity of the acceptor dye with a corresponding decrease in donor dye intensity followed by the saw-tooth pattern of dye intensities and FRET signal, consistent with the repetitive looping activity of PcrA (Figure 3-12). When RecA was injected into a flow-cell containing pre-incubated, actively looping PcrA-substrate complexes, only minor pauses were observed in the single-molecule trace data; histograms both pre- and post-injection of PcrA are identical (Figure 3-13). These results demonstrate that under conditions in which PcrA and RecA can both hydrolyze ATP, the helicase readily disrupts the nucleoprotein filaments formed by the recombinase. Since the translocase activity of PcrA continues unabated after a fully formed RecA filament is disrupted, these results also suggest that wild-type RecA is not able to reassemble stable filaments in the presence of the translocating helicase.

3.3.2.3 PcrA Displaces RecA Filaments Made with ADP

Addition of RecA to the DNA substrate in the presence of 5 mM ADP reduced the peak FRET in more than one-half of the molecules from 0.4 to 0.2, indicating filament assembly (Figure 3-14A) (5 mM ADP was used instead of 1 mM, so that results could be more easily compared to ADP*AlF_4 experiments described below, where the higher concentration is needed to ensure

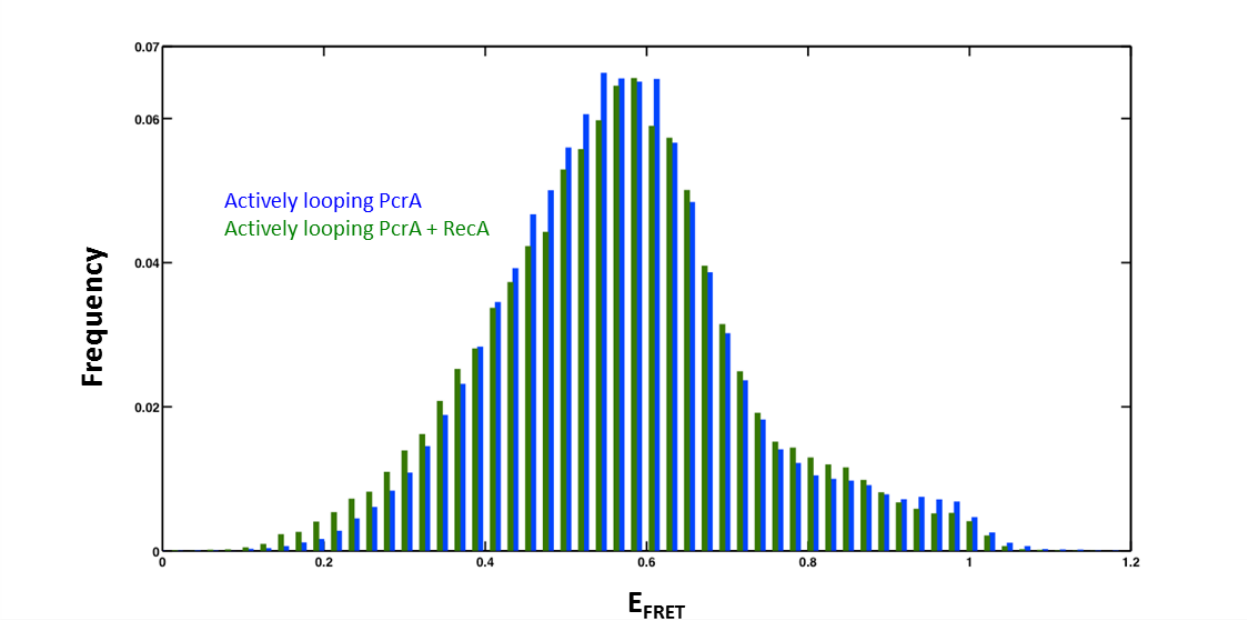

Figure 3-13: Addition of RecA has no effect on actively looping PcrA complexes.

Overlaid histograms from an experiment where 1 nM PcrA and 1 mM ATP were pre-incubated with PcrA-Spool, producing actively looping complexes (blue). Even after the addition of 1uM RecA, looping continued unabated, and there is no change in the original histogram (green).

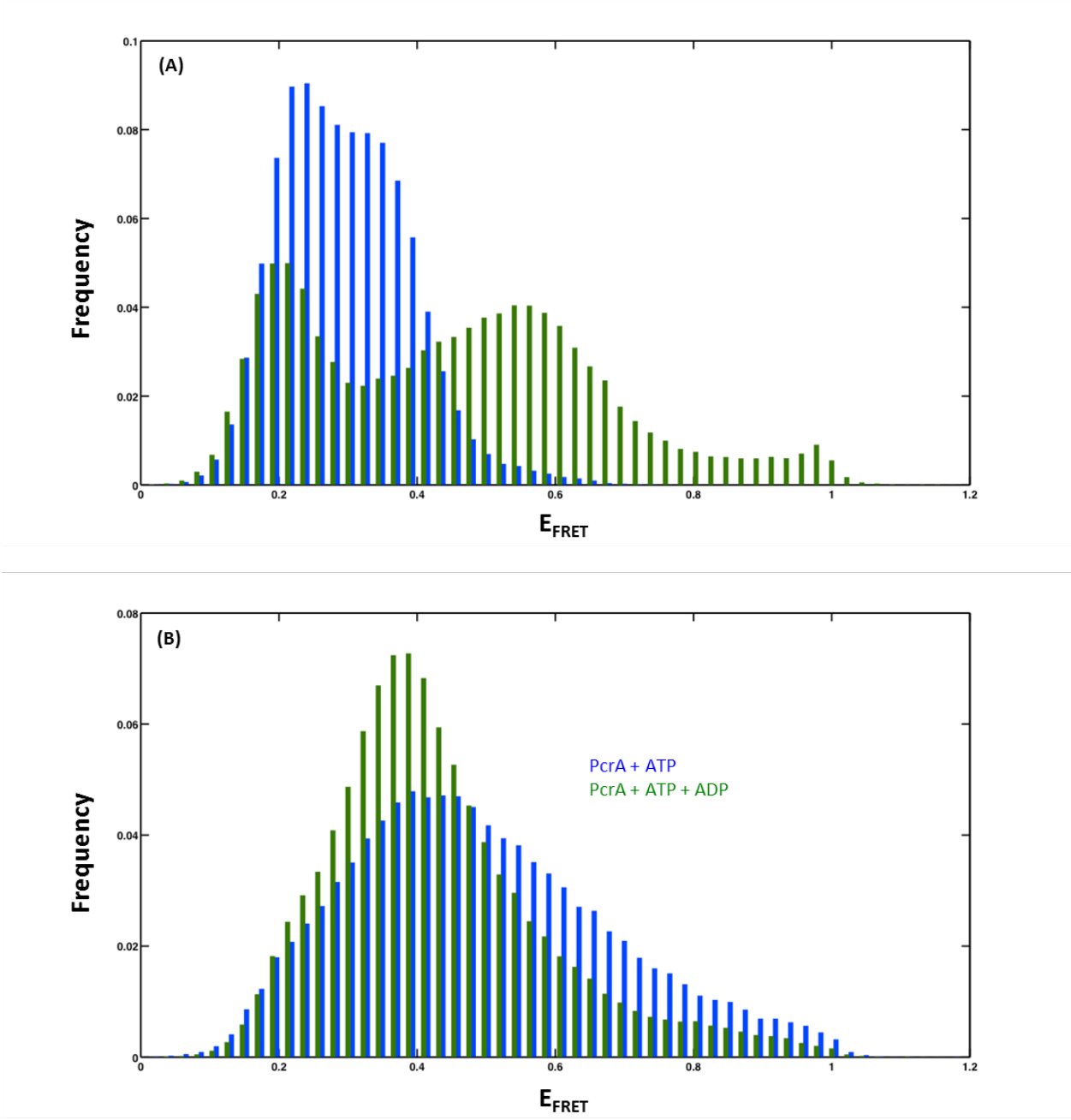

Figure 3-14: PcrA disrupts RecA-ADP filaments, but residual ADP reduces PcrA's spooling efficiency.

(A) E_{FRET} population histograms from an experiment with 1 uM RecA and 5 mM ADP (blue). Addition of 10 nM PcrA and 1 mM ATP leads to a decrease in peak height for the low-E_{FRET} population (RecA filaments), albeit to lower efficiency than for filaments comprised of RecA

and ATP. **(B)** The spooling efficiency of PcrA is reduced in the presence of excess ADP, likely contributing to the lower filament disruption efficiency observed in **(A)**.

ADP*AlF_4 generation). Upon addition of PcrA and ATP, there was a 30% reduction in the population of molecules with a peak E_{FRET} of 0.2. The concomitant increase in high-FRET population reflects repetitive looping by PcrA in the presence of RecA and ADP. These results demonstrate that PcrA disrupts low-affinity RecA-ADP filaments, albeit less efficiently than RecA-ATP filaments. This lower efficiency is likely due, at least in part, to the inhibition of the translocase activity of PcrA by the excess of ADP used to form RecA-ADP filaments, because both the translocase activity of PcrA as well as the displacement of RecA-ATP filaments decreased in the presence of excess ADP (Figure 3-14B). Because RecA has a higher affinity for ATP compared to ADP, it was not possible for us to flush out the PcrA-poisoning ADP without compromising the RecA-ADP filaments.

3.3.2.4 PcrA Cannot Displace RecA Filaments Made with Negligibly-Hydrolysable ATP Analogs

In contrast with RecA-ATP filaments, RecA filaments formed with either ATPγS or ADP*AlF_4 are not removed by PcrA translocation. We first assembled either RecA-ATPγS or ADP*AlF_4 filaments on the ssDNA substrate. These filaments yielded a single FRET peak of E_{FRET}=0.2 in the population histogram as described in section 3.3.1.2. Next, the flow-cell containing the stabilized RecA filaments was washed with a buffer containing ATP to remove any free nucleotide analog that could inhibit PcrA, followed by the addition of PcrA in the same ATP-containing buffer. In both cases, the distribution of FRET values remained unchanged, demonstrating that PcrA was unable to disrupt RecA-ATPγS or RecA-ADP*AlF_4 filaments (Figure 3-6).

We confirmed that residual ATPγS was not responsible for the failure of PcrA to disrupt these filaments by performing a control reaction in which the DNA substrate was treated with ATPγS in the absence of RecA, washed with a buffer containing ATP to remove ATPγS, and subsequently incubated with PcrA and ATP (Figure 3-15). The results showed that the substrate molecules exhibited both low- and high-FRET peaks of 0.5 and 0.8, respectively, consistent with the repetitive looping of ssDNA by PcrA.

3.3.2.5 PcrA Displaces Filaments Made from a RecA ATPase Mutant with Lower Efficiency

To determine whether PcrA can disrupt stable K72R-ATP filaments, we tested the disassembly of these filaments using different concentrations of PcrA (Figure 3-11). At the lowest concentration of PcrA tested (1 nM), there was little disruption of K72R filaments (4±1%) compared to wild-type RecA (35±5%). Differences in disruption of K72R and wild-type

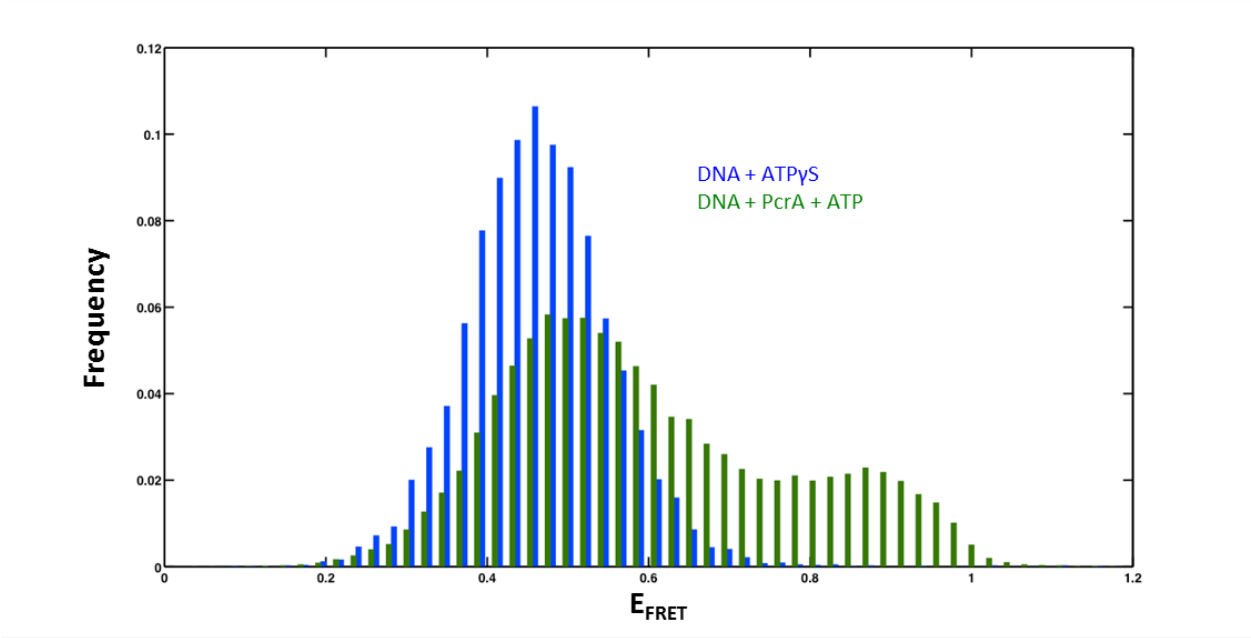

Figure 3-15: Residual ATPγS does not impede looping by PcrA.

Overlaid histograms from an experiment starting with DNA and 1 mM ATPγS (blue). Flushing the flow-cell with 1 nM PcrA and 1 mM ATP leads to robust looping behavior by PcrA, demonstrating that any residual ATPγS remaining in the flow-cell does not impede PcrA.

RecA filaments by PcrA were evident even at the highest concentration of PcrA tested (40 nM PcrA; 43±10% vs. 62±4%, respectively, for K72R vs. wild-type). Concentrations of PcrA higher than 40 nM were not tested in the displacement assays as previous studies have reported dimerization of PcrA above this concentration, which converts it to a processive helicase (Niedziela-Majka et al., 2007; Yang et al., 2008). These results showing that PcrA disrupts K72R filaments at a lower efficiency than those of wild-type RecA suggest that the formation of low-affinity RecA-ADP complex is essential for filament disruption by the helicase.

In addition to the differences in the displacement efficiencies, we noticed a striking difference in the percentage of substrates that exhibited an E_{FRET} value ≥ 0.61 following the addition of PcrA. Depending on the PcrA concentration, there was a two- to ten-fold decrease in the high-FRET population in the presence of K72R compared to wild-type RecA (Fig. 3e). Since the high-FRET population predominantly reflects the looping activity of PcrA, our observations suggest that K72R has an inhibitory effect on the translocase activity of the helicase.

3.3.2.6 RecA ATPase-Mutant K72R Compromises PcrA's Looping Activity

We tested the potential inhibitory effect of the K72R mutant on the translocase activity of PcrA by injecting K72R into PcrA looping reactions. On ssDNA, PcrA translocates in a 3' to 5' direction, whereas RecA polymerizes in a 5' to 3' direction (Register and Griffith, 1985; Dillingham et al., 2000). In a "head-on collision" between the translocase and a polymerizing filament, the 3' to 5' ATP-dependent translocation of PcrA would be expected to be blocked by the 5' to 3' polymerization of K72R, which generates stable nucleoprotein filaments. To test this, we injected K72R mutant into a flow-cell containing pre-incubated substrate, ATP and actively looping PcrA. The saw-toothed E_{FRET} trajectories (diagnostic of PcrA looping) were halted in many cases after the injection of K72R (Figure 3-16).

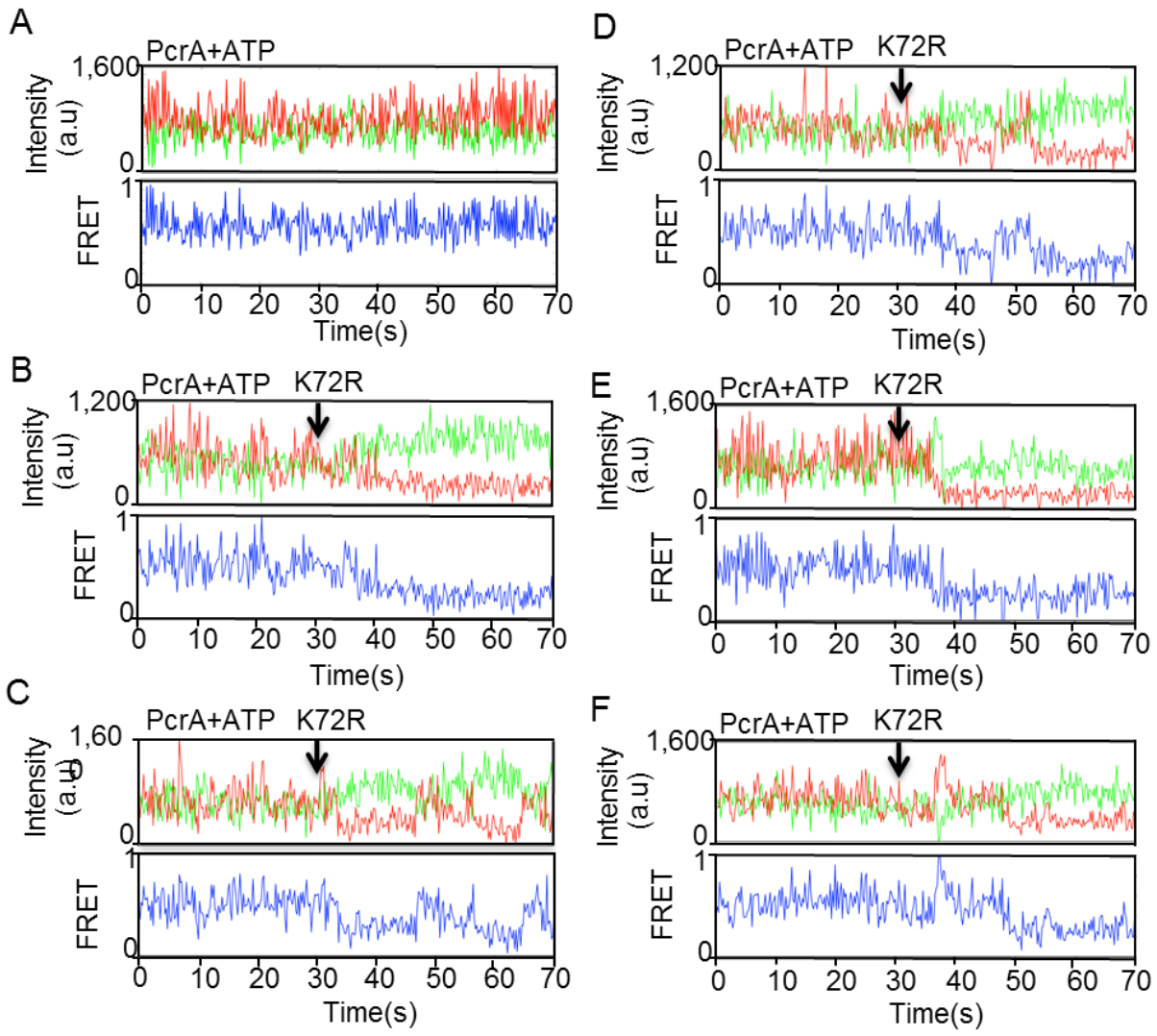

Figure 3-16: RecA K72R impedes translocation of PcrA on ssDNA.

Fluorescence intensities of Cy3 (green) and Cy5 (red) during repetitive looping of ssDNA by 10 nM PcrA on the smFRET substrate before and after the addition of 1 μM K72R at t=30 s (black arrow) . Corresponding E_{FRET} values (blue) are also shown. Only data until t=70 s are shown. **(A)** Control reaction showing unabated repetitive looping of ssDNA by PcrA. **(B)-(F)** Inhibition of repetitive looping activity of PcrA by K72R filament formation.

This is in direct contrast with similar experiments performed with wild-type RecA, where injection of the recombinase had no effect on PcrA's translocase activity (Figure 3-13) Following the addition of K72R, acceptor dye intensity dropped, with a corresponding decrease in FRET indicating the assembly of K72R filaments (Figure 3-16). The absence of saw-tooth pattern in E_{FRET} or fluorescence signal intensities after the injection of K72R indicated that PcrA translocation was arrested by the filament formation. The E_{FRET} histogram of observations post K72R injection showed an 82% reduction in the population of molecules that exhibited peak E_{FRET} values ≥ 0.8 (Figure 3-17). The appearance of a new peak at 0.2 FRET under these conditions confirms the assembly of stable K72R filaments.

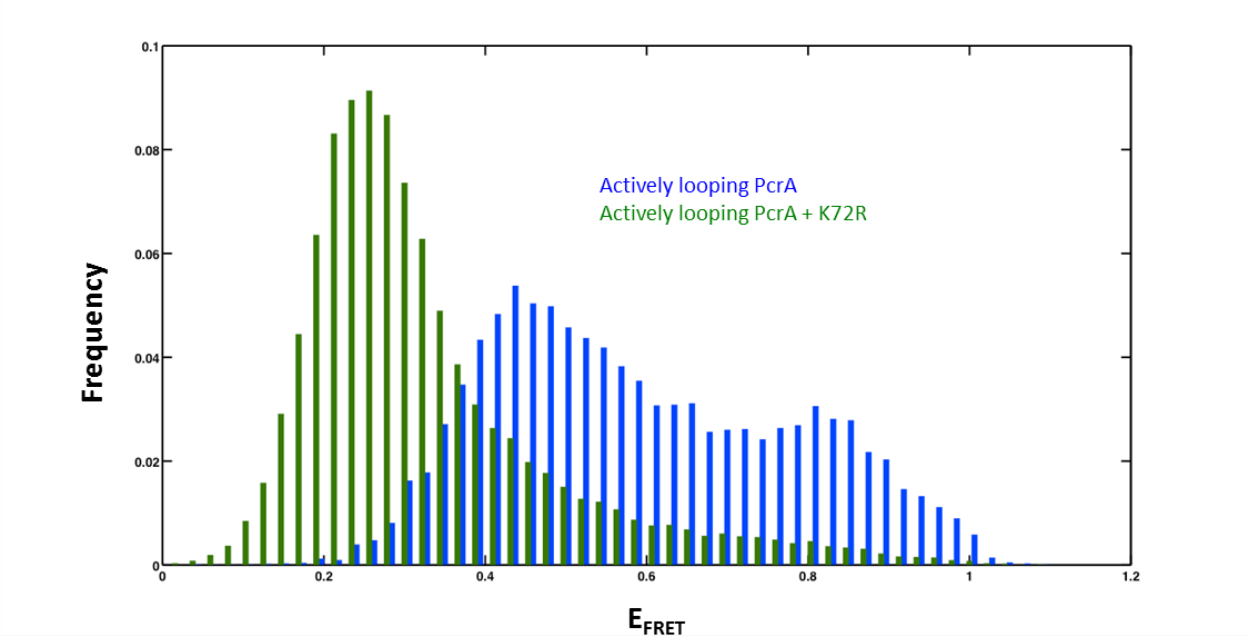

Figure 3-17: Addition of K72R arrests actively looping PcrA complexes.

Overlaid histograms from an experiment where 1 nM PcrA and 1 mM ATP were pre-incubated with PcrA-Spool, producing actively looping complexes (blue). Upon addition of 1 uM K72R, looping was observed to be halted for many molecules. The histogram post-injection shows that many molecules have assembled a K72R filament and resist processing by PcrA (green).

3.4 CONCLUSIONS

The results presented here demonstrate that both the stability of RecA nucleoprotein filaments, as well as their ability to be removed by the PcrA translocase depends on the state of ATP hydrolysis within RecA. This is consistent with a model of at least two ssDNA binding states of RecA- a high affinity state where the recombinase has not yet hydrolyzed a bound ATP molecule, and a lower affinity state wherein ATP has been hydrolyzed to ADP and interacts more weakly with the ssDNA (Menetski and Kowalczykowski, 1985). Our data suggests that PcrA is only able to remove this lower-affinity RecA, highlighting the role that the recombinase's ATPase activity plays in filament disruption and thus its importance in the general regulation of HR.

Taken together, our results suggest that the ATPase activity of the recombinase is required by DNA helicases in order to disrupt nucleoprotein filaments for the regulation of recombination. It is possible that PcrA stimulates the ATPase activity of RecA as shown for Srs2 and Rad51 (Antony et al., 2009). Alternatively, PcrA could utilize the basal rate of ATP hydrolysis by RecA to disrupt RecA filaments. Future studies will be directed towards understanding the role of protein-protein interactions and the intersubunit cooperativity of the RecA filaments in RecA filament disruption by PcrA and related helicases.

4.0 GENERAL DISCUSSION

4.1 RECA ATPASE ACTIVITY IS REQUIRED FOR PCRA-DRIVEN DISRUPTION OF FILAMENTS

The work presented here demonstrates that the ATPase activity of RecA is essential for its displacement from ssDNA by PcrA, thereby identifying a novel component in the regulation of this recombinase by an essential helicase. Using a smFRET microscope built in-house, we were able to leverage the advantages of single-molecule techniques to gain insights into an important biological system. Our studies show that the translocase activity of PcrA alone is insufficient to displace RecA from ssDNA. Additionally, results from single-molecule experiments involving a head on-collision between RecA and PcrA on a ssDNA "track" show that the ATPase activity of RecA, which generates the low-affinity ADP-bound form of the protein on ssDNA, is essential for PcrA to remove this barrier, underscoring the significance of this enzymatic activity of RecA in its regulation by PcrA. In the absence of its ATPase activity, the RecA filament presents an insurmountable barrier to the translocase. We propose a new model for RecA displacement by PcrA that involves the hydrolysis of ATP to generate the low-affinity ssDNA binding state of RecA (Figure 4-1).

The functions of the ATPase activity of RecA have been a topic of much debate (Cox, 1994; Cox et al., 2005). It is dispensable for the SOS response, and also DNA strand exchange, except at stages such as branch migration and the bypass of heterologous inserts, which both require RecA dissociation (Cox and Lehman, 1981; Kahn et al., 1981; Kim et al., 1992). Studies have shown that ATPase mutants of RecA such as K72R and E38K/K72R exhibit reduced levels of in vivo recombination and DNA repair following UV treatment (Centore and Sandler, 2007; Britt et al., 2011). Taken together, these results suggest that the *in vivo* defects observed with

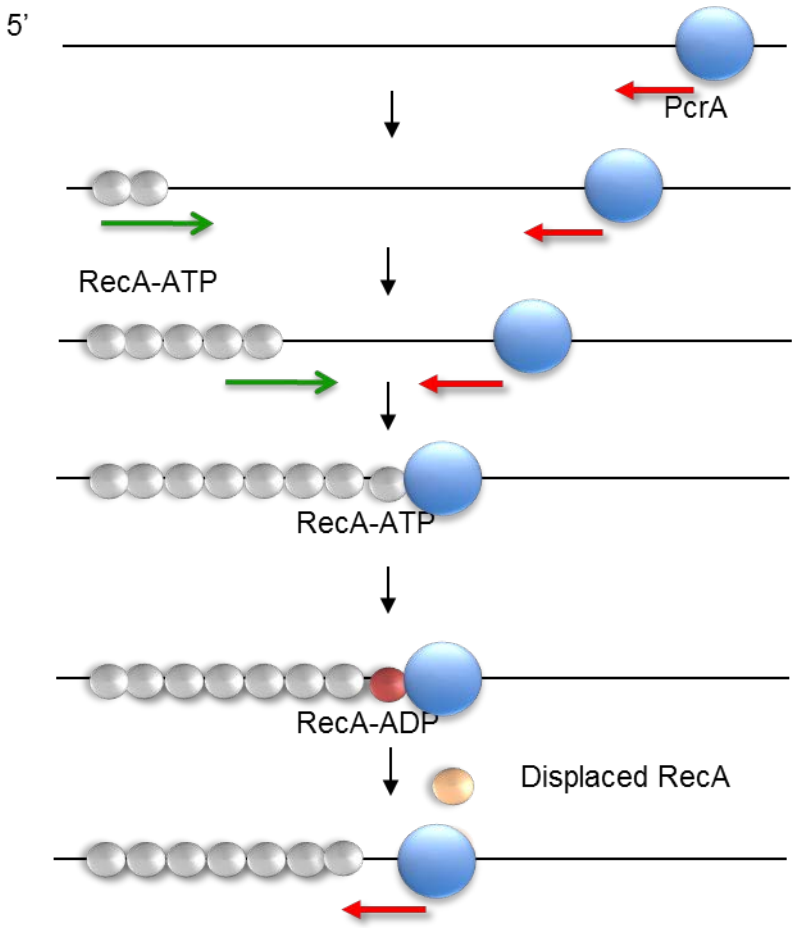

Figure 4-1: Model of PcrA-driven RecA removal dependent on RecA ATPase activity.

In our revised model of PcrA-driven RecA filament disruption, individual monomers of RecA are removed by PcrA only if they are in a low-affinity DNA binding state. Transition to this state is dependent on RecA's hydrolysis of bound ATP; until this ATP cofactor is hydrolyzed, RecA remains in a high-affinity DNA binding state and cannot be displaced.

these ATPase mutants of RecA might also originate from the inability of DNA helicases/translocases to disrupt stable mutant RecA filaments.

While PcrA and related helicases appear to displace only specific proteins, others such as RecBCD and Dda can displace a range of proteins such as core histones and streptavidin (Eggleston et al., 1995; Petit et al., 1998; Petit and Ehrlich, 2002; Veaute et al., 2005; Krejci et al., 2003; Veaute et al., 2003; Florés et al., 2005; Bidnenko et al., 2006; Lestini and Michel, 2007; Yeruva and Raney, 2010; Finkelstein et al., 2010; Fonville et al., 2010). These differences may be due to a broad range of mechanisms used to displace proteins bound to the DNA. In the case of RecBCD, it is clear that mechano-chemical forces generated as a result of helicase translocation are sufficient for displacing non-specific proteins bound to the DNA (Finkelstein et al., 2010). This is also the case for the disruption of biotin-streptavidin interactions by Dda (Byrd and Raney, 2004). However not all protein displacements by helicases can occur solely due to their translocation on the DNA, as translocation by itself cannot provide specificity during protein displacement (Anand et al., 2007; Antony et al., 2009; Singh et al., 2010; Ward et al., 2010; Williams and Michael, 2010).

Nucleoprotein filaments formed by recombinases such as RecA and Rad51 represent a novel impediment for a translocating helicase. In the absence of ATP hydrolysis, a filament represents a formidable barrier consisting of hundreds to thousands of protein monomers bound tightly to the DNA. Upon ATP hydrolysis, the change from high- to low-affinity DNA binding state of a recombinase protein could allow the helicase to sequentially displace monomers from these filaments. Our findings suggest reconsideration of a recent study reporting that PcrA dismantles RecA filaments by uniformly “reeling in” the ssDNA, implying that the translocase activity of PcrA alone is sufficient to mechanically disrupt RecA filaments (Park et al., 2010).

In contrast, our results suggest that PcrA and related helicases have evolved other, more subtle mechanisms in addition to translocation to efficiently displace protein filaments from the DNA, and that such displacement might require the active participation of both protein partners. Additional evidence for this view comes from observations made on the Srs2 helicase, which has been shown to stimulate the ATPase activity of Rad51 during the displacement of preformed Rad51 filaments from the DNA (Antony et al., 2009). In the absence of ATP hydrolysis, Rad51 filaments present an insurmountable barrier for the translocating Srs2 similar to the situation with RecA filaments and PcrA. Such findings are consistent with the results presented herein and suggest that the ATPase activity of the recombinase is required by at least some DNA helicases and translocases for filament disruption, and that this may be a conserved theme in both prokaryotes and eukaryotes.

4.1.1 A Revised Model for Displacement of RecA Filaments by PcrA

Contrary to prior models of RecA filament disruption by translocases (Park et al., 2010), we find that there is a necessary role for the ATPase activity of RecA. We thus propose a revised filament-disruption model in which ATP hydrolysis by the recombinase sets the tempo for filament removal by a DNA translocase (Figure 4-1). Under this model, PcrA's translocase activity is effectively blocked by RecA until it completes a cycle of ATP hydrolysis, resulting in a low-affinity binding state for the recombinase. At this point, PcrA is able to displace RecA and traverse 3 nucleotides, bringing it into contact with the next RecA monomer in the filament, where the cycle can start again.

Although there is little information about the specific protein contacts made by PcrA and RecA, it stands to reason that the translocase can interact directly with only the 3' terminal RecA

monomer in a nascent filament. This terminal monomer should be comparatively vulnerable to displacement both because of its direct interaction with the translocase, and also because it is involved in a RecA-RecA interaction with only one partner. It is presumed that RecA-RecA interactions throughout the filament are largely responsible for the filament's stability, as ATP hydrolysis takes place throughout (Cox et al., 2005).

Intriguingly, there is evidence in the literature that disruption of RecA filaments by UvrD depends on species-species parity between the two proteins (Singh et al., 2010). This suggests that specific surface residues at the PcrA-RecA contact interface are conserved within specific organisms, and further raises the possibility that some sort of allosteric interaction may be involved in PcrA-RecA regulation.

4.2 FUTURE EXPERIMENTS

Although we have here established that the ATPase activity of RecA is required for filament disruption by PcrA, many questions remain unanswered regarding the mechanisms behind this requirement. Future work will focus on further characterizing the PcrA-RecA interaction and gaining more insight into the extent of PcrA's influence on RecA's ATPase activity.

One of the larger questions left unanswered concerns the generality of the ATPase requirement for filament disruption. Stated another way, will helicases and translocases other than PcrA exhibit a similar pattern of RecA filament disruption, namely requiring the recombinase to turnover ATP in order to be removed? UvrD has been shown to displace RecA from DNA (Veaute et al., 2005), and is expected to perform similarly to PcrA; any deviation would suggest that our ATPase-dependent model does not describe complete process. It would

be worthwhile to investigate other helicases and translocases as well, however these must exhibit a 3' -> 5' activity in order to be amenable to our assay. An alternative route would involve extending our study to look at RecA filament disruption on dsDNA, in which case a larger set of candidate helicases and/or translocases could be studied.

In a similar vein, it would be interesting to further investigate the disruption of RecA filaments comprised of recombinase from different sources. Previous research has suggested that species parity has a measurable impact on the efficiency of RecA filament removal by UvrD (Singh et al., 2010). Our experimental system allows us to look for such an effect directly in the PcrA-RecA relationship. Any evidence for such an effect would suggest the possibility of an allosteric component to the PcrA-RecA interaction, which would lend further support to the theory that PcrA's translocase activity is not the sole factor in RecA filament disruption.

Perhaps the most intriguing thread to pursue is whether PcrA, like its ortholog Srs2, is capable of stimulating the ATPase activity of the recombinase (Antony et al., 2009). Previous studies have shown that the ATPase activity of *S. aureus* PcrA is not required in its disruption of RecA filaments (Anand et al., 2007), but how it achieves this remains unknown. The possibility that PcrA causes the destabilization of RecA filaments by stimulating their ATPase activity is an attractive possible answer to this question. The most straightforward way to test this hypothesis hinges on the successful purification of a *G. stearothermophilus* PcrA mutant that is deficient in its ATPase activity. Such a mutant could be employed in our smFRET assays and its filament disrupting activity directly compared to that of wild-type PcrA. Given the sensitive nature of the smFRET technique even small differences in disruption rates are measureable, in principle.

Biochemically, it would be illuminating to supplement our single molecule data with bulk measurements. These would be especially valuable with regards to measuring the ATPase

activity of the PcrA-RecA filament system. Such experiments will help to answer the question of whether or not PcrA has any effect on the ATPase rate of RecA. Although we attempted to make such measurements using a NADH-coupled spectrophotometric assay, the background ATPase rate of PcrA was too great to allow for any useful measurements. The use of a *G. stearothermophilus* PcrA ATPase mutant will eliminate this complication. Alternatively, it may be possible to employ a stopped-flow bulk ATPase activity to obtain equivalent information.

A further avenue of work that has the potential for more general application involves adding a third excitation laser to the smFRET TIRF microscope described in chapter 2. The wavelength of the laser should be chosen to supplement the two already available (532 nm and 637 nm); practically speaking this would suggest a blue laser, in the range of ~405 nm-488 nm. Such an addition would require an extensive reworking of the microscope emission-collection optics, as an additional channel would need to be added and the DualView unit (Figure 2-8) would need to be replaced with optics that split the image into three separate regions instead of two. Additional optics electronics would also be needed to incorporate and control the new excitation beam, although these additions shouldn't pose any great difficulties. The principle advantage afforded by such a system is that it allows for the detection of a third fluorophore, which enables monitoring whether or not a labeled protein is present (Blosser et al., 2009). This ability can be used to great effect in dissecting both the stoichiometries of bound proteins, as well as in measuring kinetics. In the case of the work described here, a third fluorophore could be employed to report on the arrival (and departure) of a PcrA monomer to an assembled RecA filament. Such experiments would reveal how long a time PcrA was resident at a filament before disruption occurs. It should be noted that with sufficient planning, the three-laser system

described above could be also used for three-color FRET experiments, wherein two separate distances can be monitored in the same measurement (Hohng et al., 2004).

In closing, it should also be noted that the PcrA-looping assay described here could be used to study other facets of the helicase. These include its ability to removal other barriers on DNA, such as SSB protein or G-quadruplexes. One intriguing application of such studies would be to determine an upper-limit to the amount of force that PcrA can generate by assaying its ability to navigate a variety of barriers, ranking these according to the amount of predicted free energy their removal would require.

APPENDIX A

ANDOR IXON EMCCD SETTINGS FOR SMFRET EXPERIMENTS

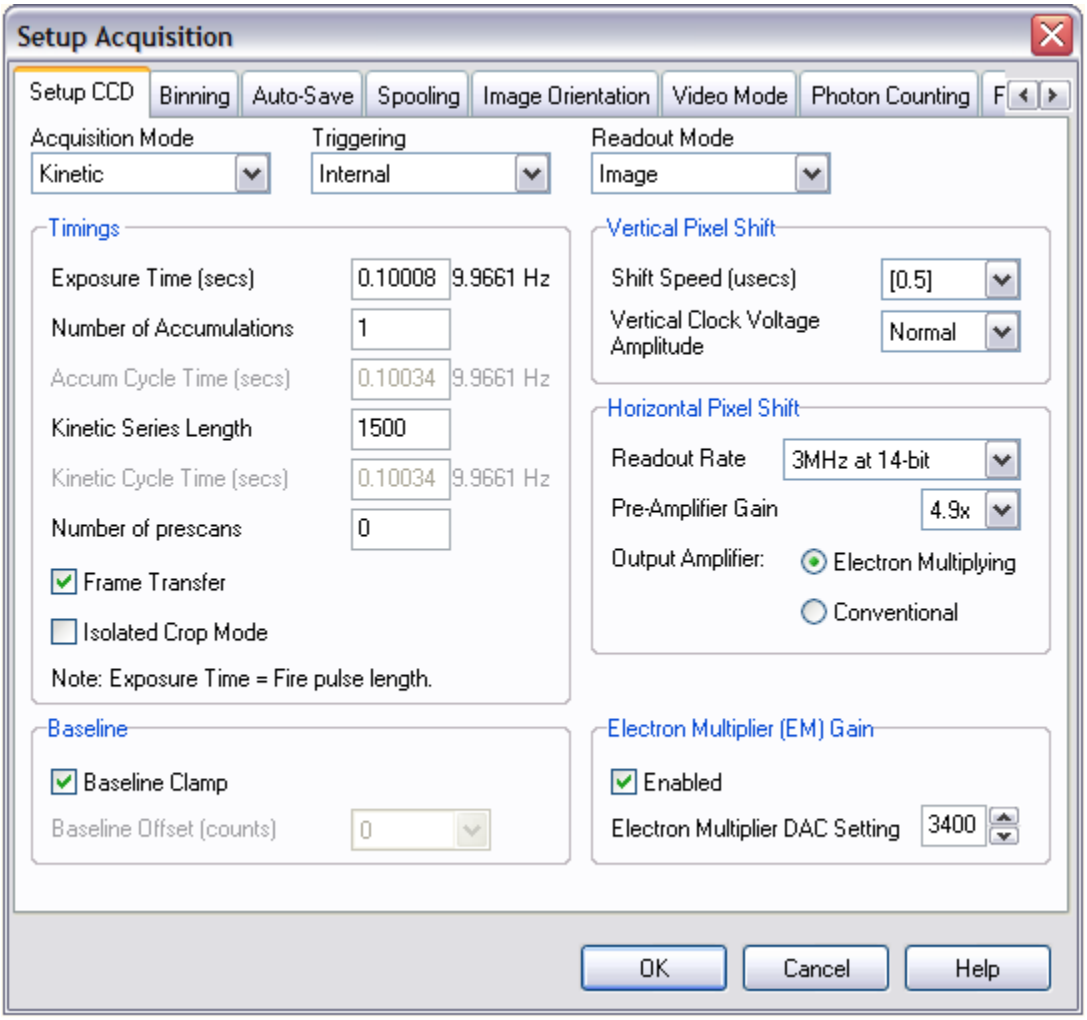

Appendix A- Standard EMCCD settings used for recording smFRET image data.

APPENDIX B

ALEXVIEWR.M SOURCE CODE

```
function [data labels don_only acc_only ] = alexviewr (fname)
%% usage: [data labels]=tracepickr ('fname')
% where fname is root file name
%
% 'data' is a 1xN cell array (N is number of molecule traces saved)
% that contains N Tnx4 arrays of trace data
% (columns are Dem_Dex, Aem_Dex, Dem_Aex, Aem_Aex)
%
%  'labels'  is  a  1xN  cell  array  containing  the  names  (filename  +
molecule#)
% of the sources of the traces in data
%
%   'don_only' is reserved for traces from signals that contain only a
donor
%  dye (as identified by user)

%  'acc_only' is reserved for traces from signals that contain only an
%  acceptor dye (as identified by user)
%
% -these can be fed directly into vbFRET (as a .mat file)

workdir= ('I:\Matt\junk\Analysis\');  %where the .traces file exists
cd(workdir);
timeunit=0.2; %define CCD frame increment in seconds


%close all; % close all figure windows

%% Definitions

fid=fopen([fname '.traces'],'r');
len=fread(fid,1,'int32');

time = 2*timeunit*(1:len);

Ntraces=fread(fid,1,'int16');
```

```
      disp(['Number of time traces: ' num2str(Ntraces/2) ', Number of frames
is ' num2str(len)])
      raw=fread(fid,Ntraces*len,'int16');
      fclose(fid);

      %% prepare data structures for organizing trace data

        index=(1:Ntraces*len);
        Data=zeros(Ntraces,len);

        Dem_Dex=zeros(len/4,Ntraces/2);        % vector for data points under
donor-excitation laser
        Aem_Dex=zeros(len/4,Ntraces/2);

        Dem_Aex=zeros(len/4,Ntraces/2);        % vector for data points under
acceptor-excitation laser
        Aem_Aex=zeros(len/4,Ntraces/2);

        data = {};
        labels = {};
        don_only = {};
        acc_only = {};

        Data(index)=raw(index);
        Data = Data';                  % Nth column of Data contains Dem time-
intensity of Nth molecule
                                       % N+1th column of Data contains
Aem
                                       %    time-intensity    for    Nth
molecule

        %% read donor and acceptor traces into appropriate vectors

        % index vectors to pull out appropriate intensity values

        % for indexing rows (time-series) of Data
        iDex = 1:2:len;
        iAex = 2:2:len;

        % for indexing columns of Data
        iDem=1:2:(Ntraces);
        iAem=2:2:(Ntraces);

        i=1:Ntraces/2; % molecule # index
        j=1:len/2;     % time index

         % trace data is put into a matrix wherein each column n represents
         % the intensity data from the nth molecule
         Dem_Dex(j,i) = Data(iDex,iDem); % + beta*donor(i,:)
         Aem_Dex(j,i) = Data(iDex,iAem);  %-beta*donor(i,:);

         Dem_Aex(j,i) = Data(iAex,iDem);
         Aem_Aex(j, i) = Data(iAex,iAem);

         saved = 0; % number of traces saved
         don_saved = 0; % number of donor-only traces saved
         acc_saved = 0; % number of acceptor-only traces saved
```

```
        % for testing purposes
        for i=1:Ntraces/2

            Dem_Dex_plot = Dem_Dex(:,i);
            Aem_Dex_plot = Aem_Dex(:,i);

            Dem_Aex_plot = Dem_Aex(:,i);
            Aem_Aex_plot = Aem_Aex(:,i);

           trace_length = size(Dem_Dex_plot,1);
           time = timeunit*(0:trace_length-1);

           start_mark = 1;
           end_mark = trace_length;

             ready_to_continue = 0;


             % depending on which frame the red laser data starts on
             flip = 1;  % for now, just changing this value (in program) for
each trace
             if (flip == 0)
                 temp   =   Dem_Aex_plot;   Dem_Aex_plot   =   Dem_Dex_plot;
Dem_Dex_plot = temp;
                 temp   =   Aem_Aex_plot;   Aem_Aex_plot   =   Aem_Dex_plot;
Aem_Dex_plot = temp;
             end

             while ready_to_continue ~= 1



                 FRET = Aem_Dex_plot./(Aem_Dex_plot+Dem_Dex_plot);
                 S   =   (Dem_Dex_plot   +   Aem_Dex_plot)./(Dem_Dex_plot   +
Aem_Dex_plot + Dem_Aex_plot + Aem_Aex_plot );

                 figure(1);
                 subplot(3,2,1);
plot(time,Dem_Dex_plot,'g',time,Aem_Dex_plot,'r');
                 title('Donor Excitation');
                 subplot(3,2,3);
plot(time,Dem_Aex_plot,'g',time,Aem_Aex_plot,'r');
                 title('Acceptor Excitation');

                 subplot(3,2,5); plot(time,FRET);
                   temp=axis;
                   temp(3)=-.2;
                   temp(4)=1.2;
                   axis(temp);
                   grid on; zoom on;
                   title('EFRET');

                 subplot(3,2,[2 4]);
                 bounds=find(-0.5 < S & S < 1.5);
                 S=S(bounds);FRET=FRET(bounds);
                 bounds=find(-0.5 < FRET & FRET < 1.5);
```

```
                S=S(bounds); FRET=FRET(bounds);
      %           z=hist2d(FRET,S,20);
      %           surf(z);
                scatter(FRET,S);
                  temp=axis;
                  temp(1)=-.2;
                  temp(2)=1.2;
                  temp(3)=-.2;
                  temp(4)=1.2;
                  axis(temp);
                  title(['Molecule ' num2str(i)]);
                  xlabel('EFRET');ylabel('S');

                subplot(3,2,6);
                bounds=find(-0.1 < FRET & FRET < 1.1);
                hist(FRET(bounds),100);
                  temp=axis;
                  temp(1)=-.2;
                  temp(2)=1.2;
                  axis(temp);
                xlabel('EFRET Histogram');

                ans=input('(s)ave,  (p)ass,  (d)onor-only,  (a)cceptor-only,
(g)o to, (x)tract region, (r)eset view, (f)lip, or (e)nd?','s');

                switch lower(ans)

                    case 'g'  % go to molecule n
                        nml = input('which molecule?');
                        i=nml;

                       Dem_Dex_plot = Dem_Dex(:,i);
                       Aem_Dex_plot = Aem_Dex(:,i);

                       Dem_Aex_plot = Dem_Aex(:,i);
                       Aem_Aex_plot = Aem_Aex(:,i);

                        if (flip == 0)
                            temp    =    Dem_Aex_plot;    Dem_Aex_plot    =
Dem_Dex_plot; Dem_Dex_plot = temp;
                            temp    =    Aem_Aex_plot;    Aem_Aex_plot    =
Aem_Dex_plot; Aem_Dex_plot = temp;
                        end

                        trace_length = size(Dem_Dex_plot,1);
                      time = timeunit*(0:trace_length-1);

                    case 'e' % Skeletor option, rouse Battle Cat
                        return;

                    case 'r'
                       Dem_Dex_plot = Dem_Dex(:,i);
                       Aem_Dex_plot = Aem_Dex(:,i);

                       Dem_Aex_plot = Dem_Aex(:,i);
                       Aem_Aex_plot = Aem_Aex(:,i);
                        if (flip == 0)
```

```
                                temp    =    Dem_Aex_plot;    Dem_Aex_plot    =
Dem_Dex_plot; Dem_Dex_plot = temp;
                                temp    =    Aem_Aex_plot;    Aem_Aex_plot    =
Aem_Dex_plot; Aem_Dex_plot = temp;
                            end

                          trace_length = size(Dem_Dex_plot,1);
                          time = timeunit*(0:trace_length-1);

                        case 's'
                            saved = saved + 1;
                            data{saved}     =     [Dem_Dex_plot     Aem_Dex_plot
Dem_Aex_plot Aem_Aex_plot];
                            labels{saved} = [fname '_mol'  num2str(i)];
                            ready_to_continue = 1;

                        case 'd'
                            don_saved = don_saved + 1;
                            don_only{don_saved}   =   [Dem_Dex_plot   Aem_Dex_plot
Dem_Aex_plot Aem_Aex_plot];
                            ready_to_continue = 1;

                        case 'a'
                            acc_saved = acc_saved + 1;
                            acc_only{acc_saved}   =   [Dem_Dex_plot   Aem_Dex_plot
Dem_Aex_plot Aem_Aex_plot];
                            ready_to_continue = 1;

                        case 'p'
                            ready_to_continue = 1;

                        case 'f'
                            %flip = mod(flip+1, 2);

                        case 'x'
                            figure(1);
                            subplot(3,2,1);
                            [X, Y] = ginput(2);

                            new_start = abs(floor(X(1)/timeunit));
                            if new_start < 1
                                new_start = 1;
                            end

                            new_end = abs(floor(X(2)/timeunit));
                            if new_end>length(Dem_Dex_plot)
                                new_end=length(Dem_Dex_plot);
                            end

                            if new_start > new_end
                                drrrg = new_start;
                                new_start = new_end;
                                new_end = drrrg;
                            end

                            Dem_Dex_plot = Dem_Dex_plot(new_start:new_end);
                            Aem_Dex_plot = Aem_Dex_plot(new_start:new_end);
```

```
                    Dem_Aex_plot = Dem_Aex_plot(new_start:new_end);
                    Aem_Aex_plot = Aem_Aex_plot(new_start:new_end);

                    trace_length = size(Dem_Dex_plot,1);
                    time = timeunit*(0:trace_length-1);

                end

            end

        end
    end
```

BIBLIOGRAPHY

Anand, S.P., and Khan, S.A. (2004). Structure-specific DNA binding and bipolar helicase activities of PcrA. Nucleic Acids Res. *32*, 3190–3197.

Anand, S.P., Chattopadhyay, A., and Khan, S.A. (2005). The PcrA3 mutant binds DNA and interacts with the RepC initiator protein of plasmid pT181 but is defective in its DNA helicase and unwinding activities. Plasmid *54*, 104–113.

Anand, S.P., Mitra, P., Naqvi, A., and Khan, S.A. (2004). Bacillus anthracis and Bacillus cereus PcrA helicases can support DNA unwinding and in vitro rolling-circle replication of plasmid pT181 of Staphylococcus aureus. J. Bacteriol. *186*, 2195–2199.

Anand, S.P., Zheng, H., Bianco, P.R., Leuba, S.H., and Khan, S.A. (2007). DNA helicase activity of PcrA is not required for the displacement of RecA protein from DNA or inhibition of RecA-mediated strand exchange. J. Bacteriol. *189*, 4502–4509.

Antony, E., Tomko, E.J., Xiao, Q., Krejci, L., Lohman, T.M., and Ellenberger, T. (2009). Srs2 disassembles Rad51 filaments by a protein-protein interaction triggering ATP turnover and dissociation of Rad51 from DNA. Mol. Cell *35*, 105–115.

Arenson, T.A., Tsodikov, O.V., and Cox, M.M. (1999). Quantitative analysis of the kinetics of end-dependent disassembly of RecA filaments from ssDNA. J. Mol. Biol. *288*, 391–401.

Axelrod, D., Burghardt, T.P., and Thompson, N.L. (1984). Total internal reflection fluorescence. Annu. Rev. Biophys. Bioeng. *13*, 247–268.

Ayora, S., Carrasco, B., Cárdenas, P.P., César, C.E., Cañas, C., Yadav, T., Marchisone, C., and Alonso, J.C. (2011). Double-strand break repair in bacteria: a view from Bacillus subtilis. FEMS Microbiol. Rev. *35*, 1055–1081.

Bachrati, C.Z., and Hickson, I.D. (2008). RecQ helicases: guardian angels of the DNA replication fork. Chromosoma *117*, 219–233.

Beernink, H.T., and Morrical, S.W. (1999). RMPs: recombination/replication mediator proteins. Trends Biochem. Sci. *24*, 385–389.

Benkovic, S.J., Valentine, A.M., and Salinas, F. (2001). Replisome-mediated DNA replication. Annu. Rev. Biochem. *70*, 181–208.

Bianco, P.R., and Weinstock, G.M. (1996). Interaction of the RecA protein of Escherichia coli with single-stranded oligodeoxyribonucleotides. Nucleic Acids Res. *24*, 4933–4939.

Bidnenko, V., Lestini, R., and Michel, B. (2006). The Escherichia coli UvrD helicase is essential for Tus removal during recombination-dependent replication restart from Ter sites. Mol. Microbiol. *62*, 382–396.

Bird, L.E., Subramanya, H.S., and Wigley, D.B. (1998). Helicases: a unifying structural theme? Curr. Opin. Struct. Biol. *8*, 14–18.

Blosser, T.R., Yang, J.G., Stone, M.D., Narlikar, G.J., and Zhuang, X. (2009). Dynamics of nucleosome remodelling by individual ACF complexes. Nature *462*, 1022–1027.

Bork, J.M., Cox, M.M., and Inman, R.B. (2001). The RecOR proteins modulate RecA protein function at 5' ends of single-stranded DNA. EMBO J. *20*, 7313–7322.

Brendza, K.M., Cheng, W., Fischer, C.J., Chesnik, M.A., Niedziela-Majka, A., and Lohman, T.M. (2005). Autoinhibition of Escherichia coli Rep monomer helicase activity by its 2B subdomain. Proc. Natl. Acad. Sci. U.S.A. *102*, 10076–10081.

Britt, R.L., Chitteni-Pattu, S., Page, A.N., and Cox, M.M. (2011). RecA K72R filament formation defects reveal an oligomeric RecA species involved in filament extension. J. Biol. Chem. *286*, 7830–7840.

Bronson, J.E., Fei, J., Hofman, J.M., Gonzalez, R.L., Jr, and Wiggins, C.H. (2009). Learning rates and states from biophysical time series: a Bayesian approach to model selection and single-molecule FRET data. Biophys. J. *97*, 3196–3205.

Byrd, A.K., and Raney, K.D. (2004). Protein displacement by an assembly of helicase molecules aligned along single-stranded DNA. Nat. Struct. Mol. Biol. *11*, 531–538.

Campbell, M.J., and Davis, R.W. (1999a). On the in vivo function of the RecA ATPase. J. Mol. Biol. *286*, 437–445.

Campbell, M.J., and Davis, R.W. (1999b). Toxic mutations in the recA gene of E. coli prevent proper chromosome segregation. J. Mol. Biol. *286*, 417–435.

Centore, R.C., and Sandler, S.J. (2007). UvrD limits the number and intensities of RecA-green fluorescent protein structures in Escherichia coli K-12. J. Bacteriol. *189*, 2915–2920.

Chang, T.-L., Naqvi, A., Anand, S.P., Kramer, M.G., Munshi, R., and Khan, S.A. (2002). Biochemical characterization of the Staphylococcus aureus PcrA helicase and its role in plasmid rolling circle replication. J. Biol. Chem. *277*, 45880–45886.

Chaudhuri, R.R., Allen, A.G., Owen, P.J., Shalom, G., Stone, K., Harrison, M., Burgis, T.A., Lockyer, M., Garcia-Lara, J., Foster, S.J., et al. (2009). Comprehensive identification of essential Staphylococcus aureus genes using Transposon-Mediated Differential Hybridisation (TMDH). BMC Genomics *10*, 291.

Chen, Z., Yang, H., and Pavletich, N.P. (2008). Mechanism of homologous recombination from the RecA-ssDNA/dsDNA structures. Nature *453*, 489–484.

Clark, A.J., and Margulies, A.D. (1965). Isolation and Characterization of Recombination-Deficient Mutants of Escherichia Coli K12. Proc. Natl. Acad. Sci. U.S.A. *53*, 451–459.

Clegg, Robert M. (1992). [18] Fluorescence resonance energy transfer and nucleic acids. In DNA Structures Part A: Synthesis and Physical Analysis of DNA, (Academic Press), pp. 353–388.

Cox, J.M., Tsodikov, O.V., and Cox, M.M. (2005). Organized unidirectional waves of ATP hydrolysis within a RecA filament. PLoS Biol. *3*, e52.

Cox, M.M. (1994). Why does RecA protein hydrolyse ATP? Trends Biochem. Sci. *19*, 217–222.

Cox, M.M. (2003). The bacterial RecA protein as a motor protein. Annu. Rev. Microbiol. *57*, 551–577.

Cox, M.M. (2007a). Motoring along with the bacterial RecA protein. Nat. Rev. Mol. Cell Biol. *8*, 127–138.

Cox, M.M. (2007b). Regulation of bacterial RecA protein function. Crit. Rev. Biochem. Mol. Biol. *42*, 41–63.

Cox, M.M., and Lehman, I.R. (1981). recA protein of Escherichia coli promotes branch migration, a kinetically distinct phase of DNA strand exchange. Proc. Natl. Acad. Sci. U.S.A. *78*, 3433–3437.

Dahan, M., Deniz, A.A., Ha, T., Chemla, D.S., Schultz, P.G., and Weiss, S. (1999). Ratiometric measurement and identification of single diffusing molecules. Chemical Physics *247*, 85–106.

DasGupta, C., Wu, A.M., Kahn, R., Cunningham, R.P., and Radding, C.M. (1981). Concerted strand exchange and formation of Holliday structures by E. coli RecA protein. Cell *25*, 507–516.

Deniz, A.A., Laurence, T.A., Dahan, M., Chemla, D.S., Schultz, P.G., and Weiss, S. (2001). Ratiometric single-molecule studies of freely diffusing biomolecules. Annu Rev Phys Chem *52*, 233–253.

Dillingham, M.S., Wigley, D.B., and Webb, M.R. (2000). Demonstration of unidirectional single-stranded DNA translocation by PcrA helicase: measurement of step size and translocation speed. Biochemistry *39*, 205–212.

Drees, J.C., Lusetti, S.L., Chitteni-Pattu, S., Inman, R.B., and Cox, M.M. (2004). A RecA filament capping mechanism for RecX protein. Mol. Cell *15*, 789–798.

Eggleston, A.K., O'Neill, T.E., Bradbury, E.M., and Kowalczykowski, S.C. (1995). Unwinding of nucleosomal DNA by a DNA helicase. J. Biol. Chem. *270*, 2024–2031.

Fagerburg, M.V., and Leuba, S.H. (2011). Optimal practices for surface-tethered single molecule total internal reflection fluorescence resonance energy transfer analysis. Methods Mol. Biol. *749*, 273–289.

Finkelstein, I.J., Visnapuu, M.-L., and Greene, E.C. (2010). Single-molecule imaging reveals mechanisms of protein disruption by a DNA translocase. Nature *468*, 983–987.

Florés, M.-J., Sanchez, N., and Michel, B. (2005). A fork-clearing role for UvrD. Mol. Microbiol. *57*, 1664–1675.

Fonville, N.C., Blankschien, M.D., Magner, D.B., and Rosenberg, S.M. (2010). RecQ-dependent death-by-recombination in cells lacking RecG and UvrD. DNA Repair (Amst.) *9*, 403–413.

Förster, T. (1948). Zwischenmolekulare Energiewanderung und Fluoreszenz. Annalen der Physik *437*, 55–75.

Förster, T. (1960). Transfer Mechanisms of Electronic Excitation Energy. Radiation Research Supplement *2*, 326–339.

Fyodorov, D.V., and Kadonaga, J.T. (2001). The many faces of chromatin remodeling: SWItching beyond transcription. Cell *106*, 523–525.

Galletto, R., Amitani, I., Baskin, R.J., and Kowalczykowski, S.C. (2006). Direct observation of individual RecA filaments assembling on single DNA molecules. Nature *443*, 875–878.

Gell, C., Brockwell, D., and Smith, A. (2006). Handbook of Single Molecule Fluorescence Spectroscopy (Oxford University Press, USA).

Gopaul, D.N., Guo, F., and Van Duyne, G.D. (1998). Structure of the Holliday junction intermediate in Cre-loxP site-specific recombination. EMBO J. *17*, 4175–4187.

Gorbalenya, A.E., Koonin, E.V., Donchenko, A.P., and Blinov, V.M. (1989). Two related superfamilies of putative helicases involved in replication, recombination, repair and expression of DNA and RNA genomes. Nucleic Acids Res. *17*, 4713–4730.

Gruenig, M.C., Renzette, N., Long, E., Chitteni-Pattu, S., Inman, R.B., Cox, M.M., and Sandler, S.J. (2008). RecA-mediated SOS induction requires an extended filament conformation but no ATP hydrolysis. Mol. Microbiol. *69*, 1165–1179.

Gudas, L.J., and Pardee, A.B. (1976). DNA synthesis inhibition and the induction of protein X in Escherichia coli. J. Mol. Biol. *101*, 459–477.

Harris, T.D., Buzby, P.R., Babcock, H., Beer, E., Bowers, J., Braslavsky, I., Causey, M., Colonell, J., Dimeo, J., Efcavitch, J.W., et al. (2008). Single-molecule DNA sequencing of a viral genome. Science *320*, 106–109.

Ha, T. (2001). Single-molecule fluorescence resonance energy transfer. Methods *25*, 78–86.

Ha, T., Enderle, T., Ogletree, D.F., Chemla, D.S., Selvin, P.R., and Weiss, S. (1996). Probing the interaction between two single molecules: fluorescence resonance energy transfer between a single donor and a single acceptor. Proc. Natl. Acad. Sci. U.S.A. *93*, 6264–6268.

Haugland, R.P., Yguerabide, J., and Stryer, L. (1969). Dependence of the kinetics of singlet-singlet energy transfer on spectral overlap. Proc. Natl. Acad. Sci. U.S.A. *63*, 23–30.

Hermanson, G.T. (2008). Bioconjugate Techniques, Second Edition (Academic Press).

Heyduk, T. (2002). Measuring protein conformational changes by FRET/LRET. Curr. Opin. Biotechnol. *13*, 292–296.

Heyer, W.-D. (2007). Biochemistry of eukaryotic homologous recombination. Top Curr Genet *17*, 95–133.

Heyes, C.D., Groll, J., Möller, M., and Nienhaus, G.U. (2007). Synthesis, patterning and applications of star-shaped poly(ethylene glycol) biofunctionalized surfaces. Mol Biosyst *3*, 419–430.

Hohng, S., Joo, C., and Ha, T. (2004). Single-molecule three-color FRET. Biophys. J. *87*, 1328–1337.

Holliday, R. (1964). A Mechanism for Gene Conversion in Fungi. Genetics Research *5*, 282–304.

Howard-Flanders, P., West, S.C., and Stasiak, A. (1984). Role of RecA protein spiral filaments in genetic recombination. Nature *309*, 215–219.

Iordanescu, S. (1993). Characterization of the Staphylococcus aureus chromosomal gene pcrA, identified by mutations affecting plasmid pT181 replication. Mol. Gen. Genet. *241*, 185–192.

Iqbal, A., Arslan, S., Okumus, B., Wilson, T.J., Giraud, G., Norman, D.G., Ha, T., and Lilley, D.M.J. (2008a). Orientation dependence in fluorescent energy transfer between Cy3 and Cy5 terminally attached to double-stranded nucleic acids. Proc. Natl. Acad. Sci. U.S.A. *105*, 11176–11181.

Iqbal, A., Wang, L., Thompson, K.C., Lilley, D.M.J., and Norman, D.G. (2008b). The structure of cyanine 5 terminally attached to double-stranded DNA: implications for FRET studies. Biochemistry *47*, 7857–7862.

Johnson, A., and O'Donnell, M. (2005). CELLULAR DNA REPLICASES: Components and Dynamics at the Replication Fork. Annual Review of Biochemistry *74*, 283–315.

Joo, C., McKinney, S.A., Nakamura, M., Rasnik, I., Myong, S., and Ha, T. (2006). Real-time observation of RecA filament dynamics with single monomer resolution. Cell *126*, 515–527.

Kahn, R., Cunningham, R.P., DasGupta, C., and Radding, C.M. (1981). Polarity of heteroduplex formation promoted by Escherichia coli recA protein. Proc. Natl. Acad. Sci. U.S.A. *78*, 4786–4790.

Kapanidis, A.N., Lee, N.K., Laurence, T.A., Doose, S., Margeat, E., and Weiss, S. (2004). Fluorescence-aided molecule sorting: analysis of structure and interactions by alternating-laser excitation of single molecules. Proc. Natl. Acad. Sci. U.S.A. *101*, 8936–8941.

Kim, J.I., Cox, M.M., and Inman, R.B. (1992). On the role of ATP hydrolysis in RecA protein-mediated DNA strand exchange. II. Four-strand exchanges. J. Biol. Chem. *267*, 16444–16449.

Kodadek, T., Wong, M.L., and Alberts, B.M. (1988). The mechanism of homologous DNA strand exchange catalyzed by the bacteriophage T4 uvsX and gene 32 proteins. J. Biol. Chem. *263*, 9427–9436.

Kong, X., Nir, E., Hamadani, K., and Weiss, S. (2007). Photobleaching pathways in single-molecule FRET experiments. J. Am. Chem. Soc. *129*, 4643–4654.

Koopmans, W.J.A., Schmidt, T., and van Noort, J. (2008). Nucleosome immobilization strategies for single-pair FRET microscopy. Chemphyschem *9*, 2002–2009.

Kowalczykowski, S.C., and Eggleston, A.K. (1994). Homologous pairing and DNA strand-exchange proteins. Annu. Rev. Biochem. *63*, 991–1043.

Kowalczykowski, S.C., and Krupp, R.A. (1995). DNA-strand exchange promoted by RecA protein in the absence of ATP: implications for the mechanism of energy transduction in protein-promoted nucleic acid transactions. Proc. Natl. Acad. Sci. U.S.A. *92*, 3478–3482.

Kowalczykowski, S.C., Clow, J., and Krupp, R.A. (1987). Properties of the duplex DNA-dependent ATPase activity of Escherichia coli RecA protein and its role in branch migration. Proc. Natl. Acad. Sci. U.S.A. *84*, 3127–3131.

Kowalczykowski, S.C., Dixon, D.A., Eggleston, A.K., Lauder, S.D., and Rehrauer, W.M. (1994). Biochemistry of homologous recombination in Escherichia coli. Microbiol. Rev. *58*, 401–465.

Krejci, L., Van Komen, S., Li, Y., Villemain, J., Reddy, M.S., Klein, H., Ellenberger, T., and Sung, P. (2003). DNA helicase Srs2 disrupts the Rad51 presynaptic filament. Nature *423*, 305–309.

Lakowicz, J.R. (2006). Principles of Fluorescence Spectroscopy (Springer).

Lee, C.-D., and Wang, T.-F. (2009). The N-terminal domain of Escherichia coli RecA have multiple functions in promoting homologous recombination. J. Biomed. Sci. *16*, 37.

Lestini, R., and Michel, B. (2007). UvrD controls the access of recombination proteins to blocked replication forks. EMBO J. *26*, 3804–3814.

Lindsley, J.E., and Cox, M.M. (1990). Assembly and disassembly of RecA protein filaments occur at opposite filament ends. Relationship to DNA strand exchange. J. Biol. Chem. *265*, 9043–9054.

Lohman, T.M., Tomko, E.J., and Wu, C.G. (2008). Non-hexameric DNA helicases and translocases: mechanisms and regulation. Nat. Rev. Mol. Cell Biol. *9*, 391–401.

Long, J.E., Renzette, N., and Sandler, S.J. (2009). Suppression of constitutive SOS expression by recA4162 (I298V) and recA4164 (L126V) requires UvrD and RecX in Escherichia coli K-12. Mol. Microbiol. *73*, 226–239.

Lusetti, S.L., and Cox, M.M. (2002). The Bacterial RecA Protein and the Recombinational DNA Repair of Stalled Replication Forks. Annual Review of Biochemistry *71*, 71–100.

Lusetti, S.L., Wood, E.A., Fleming, C.D., Modica, M.J., Korth, J., Abbott, L., Dwyer, D.W., Roca, A.I., Inman, R.B., and Cox, M.M. (2003). C-terminal deletions of the Escherichia coli RecA protein. Characterization of in vivo and in vitro effects. J. Biol. Chem. *278*, 16372–16380.

Malkov, V.A., and Camerini-Otero, R.D. (1995). Photocross-links between single-stranded DNA and Escherichia coli RecA protein map to loops L1 (amino acid residues 157-164) and L2 (amino acid residues 195-209). J. Biol. Chem. *270*, 30230–30233.

Maples, V.F., and Kushner, S.R. (1982). DNA repair in Escherichia coli: identification of the uvrD gene product. Proc. Natl. Acad. Sci. U.S.A. *79*, 5616–5620.

Martinez-Perez, E., and Colaiácovo, M.P. (2009). Distribution of meiotic recombination events: talking to your neighbors. Curr. Opin. Genet. Dev. *19*, 105–112.

Matson, S.W., Bean, D.W., and George, J.W. (1994). DNA helicases: enzymes with essential roles in all aspects of DNA metabolism. Bioessays *16*, 13–22.

McKinney, S.A., Déclais, A.-C., Lilley, D.M.J., and Ha, T. (2003). Structural dynamics of individual Holliday junctions. Nat. Struct. Biol. *10*, 93–97.

McKinney, S.A., Joo, C., and Ha, T. (2006). Analysis of single-molecule FRET trajectories using hidden Markov modeling. Biophys. J. *91*, 1941–1951.

Menetski, J.P., and Kowalczykowski, S.C. (1985). Interaction of recA protein with single-stranded DNA. Quantitative aspects of binding affinity modulation by nucleotide cofactors. J. Mol. Biol. *181*, 281–295.

Menetski, J.P., and Kowalczykowski, S.C. (1989). Enhancement of Escherichia coli RecA protein enzymatic function by dATP. Biochemistry *28*, 5871–5881.

Menetski, J.P., Bear, D.G., and Kowalczykowski, S.C. (1990). Stable DNA heteroduplex formation catalyzed by the Escherichia coli RecA protein in the absence of ATP hydrolysis. Proc. Natl. Acad. Sci. U.S.A. *87*, 21–25.

Mikawa, T., Masui, R., and Kuramitsu, S. (1998). RecA protein has extremely high cooperativity for substrate in its ATPase activity. J. Biochem. *123*, 450–457.

Moerner, W.E., and Fromm, D.P. (2003). Methods of single-molecule fluorescence spectroscopy and microscopy. Review of Scientific Instruments *74*, 3597.

Morimatsu, K., and Kowalczykowski, S.C. (2003). RecFOR proteins load RecA protein onto gapped DNA to accelerate DNA strand exchange: a universal step of recombinational repair. Mol. Cell *11*, 1337–1347.

Mujumdar, S.R., Mujumdar, R.B., Grant, C.M., and Waggoner, A.S. (1996). Cyanine-labeling reagents: sulfobenzindocyanine succinimidyl esters. Bioconjug. Chem. *7*, 356–362.

Myong, S., Stevens, B.C., and Ha, T. (2006). Bridging conformational dynamics and function using single-molecule spectroscopy. Structure *14*, 633–643.

Niedziela-Majka, A., Chesnik, M.A., Tomko, E.J., and Lohman, T.M. (2007). Bacillus stearothermophilus PcrA monomer is a single-stranded DNA translocase but not a processive helicase in vitro. J. Biol. Chem. *282*, 27076–27085.

Opresko, P.L., Cheng, W.-H., von Kobbe, C., Harrigan, J.A., and Bohr, V.A. (2003). Werner syndrome and the function of the Werner protein; what they can teach us about the molecular aging process. Carcinogenesis *24*, 791–802.

Ouellet, J., Schorr, S., Iqbal, A., Wilson, T.J., and Lilley, D.M.J. (2011). Orientation of cyanine fluorophores terminally attached to DNA via long, flexible tethers. Biophys. J. *101*, 1148–1154.

Palets, D., Lushnikov, A.Y., Karymov, M.A., and Lyubchenko, Y.L. (2010). Effect of single-strand break on branch migration and folding dynamics of Holliday junctions. Biophys. J. *99*, 1916–1924.

Panyutin, I.G., and Hsieh, P. (1994). The kinetics of spontaneous DNA branch migration. Proc. Natl. Acad. Sci. U.S.A. *91*, 2021–2025.

Park, J., Myong, S., Niedziela-Majka, A., Lee, K.S., Yu, J., Lohman, T.M., and Ha, T. (2010). PcrA helicase dismantles RecA filaments by reeling in DNA in uniform steps. Cell *142*, 544–555.

Petit, M.-A., and Ehrlich, D. (2002). Essential bacterial helicases that counteract the toxicity of recombination proteins. EMBO J. *21*, 3137–3147.

Petit, M.A., Dervyn, E., Rose, M., Entian, K.D., McGovern, S., Ehrlich, S.D., and Bruand, C. (1998). PcrA is an essential DNA helicase of Bacillus subtilis fulfilling functions both in repair and rolling-circle replication. Mol. Microbiol. *29*, 261–273.

Petrova, V., Chitteni-Pattu, S., Drees, J.C., Inman, R.B., and Cox, M.M. (2009). An SOS inhibitor that binds to free RecA protein: the PsiB protein. Mol. Cell *36*, 121–130.

Pham, P., Bertram, J.G., O'Donnell, M., Woodgate, R., and Goodman, M.F. (2001). A model for SOS-lesion-targeted mutations in Escherichia coli. Nature *409*, 366–370.

Pugh, B.F., Schutte, B.C., and Cox, M.M. (1989). Extent of duplex DNA underwinding induced by RecA protein binding in the presence of ATP. J. Mol. Biol. *205*, 487–492.

Racki, L.R., Yang, J.G., Naber, N., Partensky, P.D., Acevedo, A., Purcell, T.J., Cooke, R., Cheng, Y., and Narlikar, G.J. (2009). The chromatin remodeller ACF acts as a dimeric motor to space nucleosomes. Nature *462*, 1016–1021.

Ragunathan, K., Joo, C., and Ha, T. (2011). Real-time observation of strand exchange reaction with high spatiotemporal resolution. Structure *19*, 1064–1073.

Rasnik, I., McKinney, S.A., and Ha, T. (2005). Surfaces and orientations: much to FRET about? Acc. Chem. Res. *38*, 542–548.

Rasnik, I., McKinney, S.A., and Ha, T. (2006). Nonblinking and long-lasting single-molecule fluorescence imaging. Nat. Methods *3*, 891–893.

Register, J.C., 3rd, and Griffith, J. (1985). The direction of RecA protein assembly onto single strand DNA is the same as the direction of strand assimilation during strand exchange. J. Biol. Chem. *260*, 12308–12312.

Rehrauer, W.M., and Kowalczykowski, S.C. (1993). Alteration of the nucleoside triphosphate (NTP) catalytic domain within Escherichia coli recA protein attenuates NTP hydrolysis but not joint molecule formation. J. Biol. Chem. *268*, 1292–1297.

Renzette, N., Gumlaw, N., and Sandler, S.J. (2007). DinI and RecX modulate RecA-DNA structures in Escherichia coli K-12. Mol. Microbiol. *63*, 103–115.

Roca, A.I., and Cox, M.M. (1997). RecA protein: structure, function, and role in recombinational DNA repair. Prog. Nucleic Acid Res. Mol. Biol. *56*, 129–223.

Rosselli, W., and Stasiak, A. (1991). The ATPase activity of RecA is needed to push the DNA strand exchange through heterologous regions. EMBO J. *10*, 4391–4396.

Rossi, M.J., Mazina, O.M., Bugreev, D.V., and Mazin, A.V. (2011). The RecA/RAD51 protein drives migration of Holliday junctions via polymerization on DNA. Proc. Natl. Acad. Sci. U.S.A. *108*, 6432–6437.

Rothenberg, E., and Ha, T. (2010). Single-molecule FRET analysis of helicase functions. Methods Mol. Biol. *587*, 29–43.

Ruiz-Masó, J.A., Anand, S.P., Espinosa, M., Khan, S.A., and del Solar, G. (2006). Genetic and biochemical characterization of the Streptococcus pneumoniae PcrA helicase and its role in plasmid rolling circle replication. J. Bacteriol. *188*, 7416–7425.

Sabanayagam, C.R., Eid, J.S., and Meller, A. (2004). High-throughput scanning confocal microscope for single molecule analysis. Applied Physics Letters *84*, 1216–1218.

Schlacher, K., Pham, P., Cox, M.M., and Goodman, M.F. (2006). Roles of DNA polymerase V and RecA protein in SOS damage-induced mutation. Chem. Rev. *106*, 406–419.

Schuler, B., and Eaton, W.A. (2008). Protein folding studied by single-molecule FRET. Curr. Opin. Struct. Biol. *18*, 16–26.

Selvin, P.R. (2000). The renaissance of fluorescence resonance energy transfer. Nat. Struct. Biol. *7*, 730–734.

Selvin, P.R., and Ha, T. (2007). Single-Molecule Techniques: A Laboratory Manual (Cold Spring Harbor Laboratory Press).

Shan, Q., and Cox, M.M. (1996). RecA protein dynamics in the interior of RecA nucleoprotein filaments. J. Mol. Biol. *257*, 756–774.

Shinohara, A., Ogawa, H., and Ogawa, T. (1992). Rad51 protein involved in repair and recombination in S. cerevisiae is a RecA-like protein. Cell *69*, 457–470.

Shivashankar, G.V., Feingold, M., Krichevsky, O., and Libchaber, A. (1999). RecA polymerization on double-stranded DNA by using single-molecule manipulation: the role of ATP hydrolysis. Proc. Natl. Acad. Sci. U.S.A. *96*, 7916–7921.

Singh, P., Patil, K.N., Khanduja, J.S., Kumar, P.S., Williams, A., Rossi, F., Rizzi, M., Davis, E.O., and Muniyappa, K. (2010). Mycobacterium tuberculosis UvrD1 and UvrA proteins suppress DNA strand exchange promoted by cognate and noncognate RecA proteins. Biochemistry *49*, 4872–4883.

Singleton, M.R., and Wigley, D.B. (2002). Modularity and specialization in superfamily 1 and 2 helicases. J. Bacteriol. *184*, 1819–1826.

Singleton, M.R., Dillingham, M.S., and Wigley, D.B. (2007). Structure and mechanism of helicases and nucleic acid translocases. Annu. Rev. Biochem. *76*, 23–50.

Sommer, S., Boudsocq, F., Devoret, R., and Bailone, A. (1998). Specific RecA amino acid changes affect RecA-UmuD'C interaction. Mol. Microbiol. *28*, 281–291.

Soultanas, P., and Wigley, D.B. (2001). Unwinding the "Gordian knot" of helicase action. Trends Biochem. Sci. *26*, 47–54.

Soultanas, P., Dillingham, M.S., Wiley, P., Webb, M.R., and Wigley, D.B. (2000). Uncoupling DNA translocation and helicase activity in PcrA: direct evidence for an active mechanism. EMBO J. *19*, 3799–3810.

Stasiak, A., and Di Capua, E. (1982). The helicity of DNA in complexes with recA protein. Nature *299*, 185–186.

Stasiak, A., Di Capua, E., and Koller, T. (1981). Elongation of duplex DNA by recA protein. J. Mol. Biol. *151*, 557–564.

Story, R.M., and Steitz, T.A. (1992). Structure of the recA protein-ADP complex. Nature *355*, 374–376.

Story, R.M., Bishop, D.K., Kleckner, N., and Steitz, T.A. (1993). Structural relationship of bacterial RecA proteins to recombination proteins from bacteriophage T4 and yeast. Science *259*, 1892–1896.

Story, R.M., Weber, I.T., and Steitz, T.A. (1992). The structure of the E. coli recA protein monomer and polymer. Nature *355*, 318–325.

Storz, G., and Hengge-Aronis, R. (2000). Bacterial stress responses (ASM Press).

Stryer, L., and Haugland, R.P. (1967). Energy transfer: a spectroscopic ruler. Proc. Natl. Acad. Sci. U.S.A. *58*, 719–726.

Subramanya, H.S., Bird, L.E., Brannigan, J.A., and Wigley, D.B. (1996). Crystal structure of a DExx box DNA helicase. Nature *384*, 379–383.

Tateishi, S., Horii, T., Ogawa, T., and Ogawa, H. (1992). C-terminal truncated Escherichia coli RecA protein RecA5327 has enhanced binding affinities to single- and double-stranded DNAs. J. Mol. Biol. *223*, 115–129.

Umezu, K., Chi, N.W., and Kolodner, R.D. (1993). Biochemical interaction of the Escherichia coli RecF, RecO, and RecR proteins with RecA protein and single-stranded DNA binding protein. Proc. Natl. Acad. Sci. U.S.A. *90*, 3875–3879.

Veaute, X., Delmas, S., Selva, M., Jeusset, J., Le Cam, E., Matic, I., Fabre, F., and Petit, M.-A. (2005). UvrD helicase, unlike Rep helicase, dismantles RecA nucleoprotein filaments in Escherichia coli. EMBO J. *24*, 180–189.

Veaute, X., Jeusset, J., Soustelle, C., Kowalczykowski, S.C., Le Cam, E., and Fabre, F. (2003). The Srs2 helicase prevents recombination by disrupting Rad51 nucleoprotein filaments. Nature *423*, 309–312.

Velankar, S.S., Soultanas, P., Dillingham, M.S., Subramanya, H.S., and Wigley, D.B. (1999). Crystal structures of complexes of PcrA DNA helicase with a DNA substrate indicate an inchworm mechanism. Cell *97*, 75–84.

Walker, J.E., Saraste, M., Runswick, M.J., and Gay, N.J. (1982). Distantly related sequences in the alpha- and beta-subunits of ATP synthase, myosin, kinases and other ATP-requiring enzymes and a common nucleotide binding fold. EMBO J. *1*, 945–951.

Ward, J.D., Muzzini, D.M., Petalcorin, M.I.R., Martinez-Perez, E., Martin, J.S., Plevani, P., Cassata, G., Marini, F., and Boulton, S.J. (2010). Overlapping mechanisms promote postsynaptic RAD-51 filament disassembly during meiotic double-strand break repair. Mol. Cell *37*, 259–272.

Watanabe, R., Masui, R., Mikawa, T., Takamatsu, S., Kato, R., and Kuramitsu, S. (1994). Interaction of Escherichia coli RecA protein with ATP and its analogues. J. Biochem. *116*, 960–966.

Weinstock, G.M., McEntee, K., and Lehman, I.R. (1981). Interaction of the recA protein of Escherichia coli with adenosine 5'-O-(3-thiotriphosphate). J. Biol. Chem. *256*, 8850–8855.

Weiss, S. (1999). Fluorescence spectroscopy of single biomolecules. Science *283*, 1676–1683.

West, S.C. (1997). Processing of recombination intermediates by the RuvABC proteins. Annu. Rev. Genet. *31*, 213–244.

West, S.C., and Connolly, B. (1992). Biological roles of the Escherichia coli RuvA, RuvB and RuvC proteins revealed. Mol. Microbiol. *6*, 2755–2759.

West, S.C., Cassuto, E., and Howard-Flanders, P. (1981). recA protein promotes homologous-pairing and strand-exchange reactions between duplex DNA molecules. Proc. Natl. Acad. Sci. U.S.A. *78*, 2100–2104.

Williams, A., Güthlein, C., Beresford, N., Böttger, E.C., Springer, B., and Davis, E.O. (2011). UvrD2 is essential in Mycobacterium tuberculosis, but its helicase activity is not required. J. Bacteriol. *193*, 4487–4494.

Williams, A.B., and Michael, W.M. (2010). Eviction notice: new insights into Rad51 removal from DNA during homologous recombination. Mol. Cell *37*, 157–158.

Witkin, E.M. (1991). RecA protein in the SOS response: milestones and mysteries. Biochimie *73*, 133–141.

Wu, L., and Hickson, I.D. (2006). DNA helicases required for homologous recombination and repair of damaged replication forks. Annu. Rev. Genet. *40*, 279–306.

Xing, X., and Bell, C.E. (2004). Crystal structures of Escherichia coli RecA in complex with MgADP and MnAMP-PNP. Biochemistry *43*, 16142–16152.

Yang, Y., Dou, S.-X., Ren, H., Wang, P.-Y., Zhang, X.-D., Qian, M., Pan, B.-Y., and Xi, X.G. (2008). Evidence for a functional dimeric form of the PcrA helicase in DNA unwinding. Nucleic Acids Res. *36*, 1976–1989.

Yanowitz, J. (2010). Meiosis: making a break for it. Curr. Opin. Cell Biol. *22*, 744–751.

Yeruva, L., and Raney, K.D. (2010). Protein displacement by helicases. Methods Mol. Biol. *587*, 85–98.

Yu, J., Ha, T., and Schulten, K. (2007). How directional translocation is regulated in a DNA helicase motor. Biophys. J. *93*, 3783–3797.

Yu, X., and Egelman, E.H. (1992). Structural data suggest that the active and inactive forms of the RecA filament are not simply interconvertible. J. Mol. Biol. *227*, 334–346.

Yu, X., Jacobs, S.A., West, S.C., Ogawa, T., and Egelman, E.H. (2001). Domain structure and dynamics in the helical filaments formed by RecA and Rad51 on DNA. Proc. Natl. Acad. Sci. U.S.A. *98*, 8419–8424.

Zheng, H., Goldner, L.S., and Leuba, S.H. (2007). Homebuilt single-molecule scanning confocal fluorescence microscope studies of single DNA/protein interactions. Methods *41*, 342–352.